2014

A geochemical study of the Riddle Peaks gabbro, North Cascades: evidence for amphibole accumulation in the mid-crust of an arc

Angela C. Cota
Western Washington University

A GEOCHEMICAL STUDY OF THE RIDDLE PEAKS GABBRO, NORTH CASCADES: EVIDENCE FOR AMPHIBOLE ACCUMULATION IN THE MID CRUST OF AN ARC

By

Angela C. Cota

Submitted for Partial Completion
Of the Requirements for the Degree
Master of Science

Kathleen L. Kitto, Dean of the Graduate School

ADVISORY COMMITTEE

Chair, Dr. Susan DeBari

Dr. Elizabeth Schermer

Dr. Robert Miller

MASTER'S THESIS

In presenting this thesis in partial fulfillment of the requirements for a master's degree at Western Washington University, I grant to Western Washington University the nonexclusive royalty-free right to archive, reproduce, distribute, and display the thesis in any and all forms, including electronic format, via any digital library mechanisms maintained by WWU.

I represent and warrant this is my original work, and does not infringe or violate any rights of others. I warrant that I have obtained written permissions from the owner of any third party copyrighted material included in these files.

I acknowledge that I retain ownership rights to the copyright of this work, including but not limited to the right to use all or part of this work in future works, such as articles or books.

Library users are granted permission for individual, research and non-commercial reproduction of this work for educational purposes only. Any further digital posting of this document requires specific permission from the author.

Any copying or publication of this thesis for commercial purposes, or for financial gain, is not allowed without my written permission.

Angela C. Cota

July 22, 2014

A GEOCHEMICAL STUDY OF THE RIDDLE PEAKS GABBRO, NORTH CASCADES: EVIDENCE FOR AMPHIBOLE ACCUMULATION IN THE MID CRUST OF AN ARC

A Thesis
Presented to
The Faculty of
Western Washington University

In Partial Fulfillment
Of the Requirements for the Degree
Master of Science

By
Angela Cota
July 2014

Abstract

Mid-crustal arc rocks are not commonly exposed, hampering our understanding of magma differentiation processes and mineral crystallization in the mid-crust of arc systems. This thesis presents results of the study of one exposed mid-crustal arc pluton, which is a unique laboratory to understand the geochemical effects of crystallization in this type of system. I report on the major and trace element characteristics of amphibole, plagioclase, and apatite in hornblendite and hornblende gabbro cumulates from the ~44 km^2 Riddle Peaks pluton (~77 Ma) in the North Cascades Crystalline Core (NCCC), Washington. Electron microprobe and laser ablation-induced mass spectrometry (LA-ICP-MS), coupled with whole rock major and trace element data, show that the Riddle Peaks contains low Mg# cumulates with 40.7-47.2 wt.% SiO_2; Mg# 33-67, where Mg# is defined as $100*[(Mg/(Mg+Fe^{2+})]$. The two rock types present in the pluton are a rhythmically layered gabbro, consisting of hornblendite and hornblende gabbro layered with anorthite to plagioclase-rich gabbro, and a massive hornblende gabbro. The layered gabbro has higher Mg# amphibole (60-70, with the majority 66-70) than massive gabbro (60-63) and more anorthitic plagioclase (layered gabbro = An_{81-85}; massive gabbro = An_{71-77}), suggesting that it was formed by a more primitive liquid. This is supported by modeling that shows that equilibrium liquids from the massive gabbros could have been produced by 40% crystallization of a hornblende gabbro lithology from the parent, calculated liquids in equilibrium with the layered gabbros. Equilibrium liquid calculations also allow for calculation of new apatite partition coefficients for 16 trace elements and REE in a mid-crustal, basaltic andesite system. This study finds that cumulate amphiboles crystallized from a basaltic andesite parent are responsible for increasing La/Yb

ratios in derivative melts, such as arc magmas, continental crust and NCCC magmas (NCCC magmas approximated by liquid compositions from the Cardinal Peak and Tenpeak plutons). Amphibole crystallization decreases Dy/Yb in derivative melts; these results are in accordance with predictions from observed arc magmas. Other observed ratios in arc and crustal magmas, such as high Sr/Y (16-20), low Nb/Ta (10-17) and Ti/Zr (30) relative to primitive mantle/chondritic values (Sr/Y = 4.6; Nb/Ta = 18-20; Ti/Zr = 115) are not explained by amphibole crystallization. It has been suggested that amphibole-rich plutons could fractionate certain incompatible trace element pairs to explain the differing ratios in arc magmas and continental crust versus primitive mantle values. With the exception of REE, the Riddle Peaks pluton does not fractionate these ratios sufficiently to explain the differing ratios. If mineral fractionation is occurring, another mineral partitions these elements; or, another process occurs.

Acknowledgements

This research would not have been possible without the support of the Geological Society of America, Sigma Xi and the Western Washington University Geology Department. Additionally I personally would not have been able to complete this project without the support of many individuals. Many, many thanks to Susan DeBari for her invaluable guidance in the realm of igneous petrology. Committee members Dr. Liz Schermer and Dr. Bob Miller provided comments and input throughout the process. La-ICP-MS analysis would not have been possible without Dr. Brian Rusk's training and help with analyses and data interpretation. In the tradition of WWU graduate students, hearty thanks must go to George Mustoe for all his guidance in the sample preparation process and his friendship. Outside the department I thank the Whitman College Geology faculty for general support. Learning from my peers has been an important part of my graduate experience. To that end, I wish to thank all of my fellow graduate students. Julie Gross in particular was instrumental for her endless guidance and friendship and for obtaining my titanite analyses. Chelsea Mack provided help in the field. Zack McGuire also provided help in the field, and his personal support and contribution to this process went far beyond carrying rocks. And thank you to my ever-supportive family and friends, especially my wonderful and loving parents.

Table of Contents

List of Tables

List of Figures

Introduction

Magmatic arcs are thought to play an important role in crustal growth, because arcs and bulk continental crust share distinctive geochemical characteristics such as intermediate silica values, high concentrations of light rare earth elements (LREE), K, Rb, Cs, Sr, Ba and Pb, and low concentrations of Ti, Zr, Nb, Ta and Hf (Rudnick and Fountain, 1995). Over time, differentiation processes in arcs are thought to create an unsubductable mass of continental crust, which then provides a nucleus for additional continental growth. The exact processes by which this differentiation occurs are still debated (Tatsumi, 2000; Kelemen et al., 2003a).

Mantle-derived basalts are the dominant magmatic input at convergent margins today (Morgan et al. 2010), yet seismological and petrologic studies indicate a bulk andesitic (intermediate) composition for continental crust (Rudnick and Fountain, 1995). The derivation of intermediate crust from basaltic magma is of major concern to researchers studying crustal generation, because it implies that there are unseen processes at work to differentiate basaltic arc magmas and remove the more mafic residue. The geochemical affinities described above suggest that similar processes operate to form both arcs and continental crust. Intermediate rock types, which could serve as a link to understand how mantle-derived basalts differentiate to resemble geochemical traits of the continental crust, have been seismically imaged deep within the crust (Kodaira et al., 2007). However, they currently remain buried within the crust, inaccessible for sampling. Researchers have proposed exposed extinct arc crustal sections as a way to "view" the relationships between arc magmatic inputs, intermediate crustal rocks and bulk crustal compositions (DeBari and Greene, 2011; Jagoutz, 2010).

In rare cases, arc crustal sections preserve intermediate plutonic rocks equivalent to arc andesites, such as in the North Cascades Crystalline Core (NCCC). These plutonic rocks can then be used to elucidate processes responsible for their generation, and extrapolate to how this relates to the formation of continental crust. Studying arcs that preserve both intermediate plutonic rocks and cumulate rocks is an excellent way to test hypotheses for arc magma evolution. If plutonic roots are exposed in arc crustal sections, researchers may gain even more information about processes below arcs.

Current geochemical research on arc systems suggests that mid-to-lower crustal amphibole may be important in controlling compositions of derivative arc and crustal melts. Davidson and others (2007) suggested that amphibole may act as a "sponge" in the arc crust, in that crystallizing amphibole at the base of the crust could act as a reservoir for water from mantle-derived melts (Davidson et al., 2007). Further, amphibole as a sponge may be one way to explain differences between the geochemistry of chondrites (which are a proxy for Earth's mantle) and arc magmas, for ratios such as Nb/Ta, Ti/Zr, La/Yb and Dy/Yb. The elements in these ratios are expected to behave similarly during magmatic differentiation from the mantle to the crust. However, the ratios differ in mantle/chondrite from those of arc magmas and continental crust, so there must be some unseen process occurring to partition these elements. Amphibole can partition some of the elements in these poorly understood ratios; for example, low Mg# amphibole has a slightly higher affinity for Nb than Ta (Kd_{Nb}= 0.34; Kd_{Ta} = 0.32) (Foley et al., 2002). Trace element modeling shows that melt derived from low Mg# amphibolite (Mg# < 70) produces low Nb/Ta melt similar to early continental crust, approximated by tonalite-trondhjemite-granodiorite (TTG) compositions found on Archean terrains (Foley et al., 2002). Thus the existence of large amphibole-rich reservoirs could

explain subchondritic Nb/Ta ratios in derivative melts, which could include arc magmas or continental crust. As another example, models of low Mg# hornblendite crystallization in the Cretaceous Chelan Complex in the NCCC generate a high Sr and low Y concentration in resulting melts, which is a signature found most commonly in arc magmas, but is attributed to garnet crystallization rather than amphibole (Kay, 1978; Kelemen et al., 2003a; Dessimoz et al., 2011). Amphibole found within exposed crustal sections may be key to understanding some of the characteristics of arc and crust compositions.

The amphibole-rich Riddle Peaks pluton is located in the NCCC, one of the few exposed arc crustal sections in the world that can help researchers understand differentiation processes in the mid-continental crust. In the NCCC, numerous plutons and metamorphic rocks comprise a 35-km-thick section of the estimated >55 km-thick continental margin arc (Miller et al., 2009) (Fig. 1). Because the NCCC section is so thick, tilted, and deeply eroded, geologists are able to view and sample the "plumbing system" of this arc, revealing many elongated and tabular plutons that crystallized at depth (Miller et al., 2009). Because the Cretaceous arc was so thick (>55 km), the dominant rock types down to 35 km (the NCCC mid-crust) are intermediate to felsic, whereas other arcs expose mafic and ultramafic rocks at these depths (DeBari and Greene, 2011) (Fig. 2). Intermediate to felsic rock types include granodiorites and tonalites, and there is evidence that they formed by differentiation and mixing processes (DeBari and Greene, 2011; Miller et al., submitted manuscript.). The thick section of mid-crustal plutons in the NCCC is an excellent area to study hypotheses concerning arc differentiation processes.

The Riddle Peaks pluton is the largest mafic intrusion in the North Cascades (~40 km^2) (McPeek et al., 2002) (Fig. 3) and is composed entirely of cumulate hornblende gabbro

and hornblendite (Cater, 1982). It is little studied, and its role in geochemical differentiation in the NCCC is untested. Given its large volume and mafic composition, it may represent an end-member composition for mafic melts that mixed with felsic melts to form the tonalites in the NCCC (DeBari et al., 1998; Miller et al., submitted manuscript). More importantly, its abundance of amphibole can be used to test the role of amphibole in producing crustal signatures. Geochemical trends produced by amphibole fractionation are currently only predicted, based upon the chemistry of erupted arc volcanics and the presence of amphibole-bearing rocks in arc plutonics (Davidson et al., 2007). Geochemical data for amphiboles within these arc plutonics, which may control the trace element budgets of erupted products, are lacking.

The primary goals of this thesis are: 1) to provide a more complete geochemical data set than had previously existed for this distinctive pluton and 2) to evaluate the amphibole sponge hypothesis by providing real amphibole chemistry from a mid-crustal arc system. Results show that the Riddle Peaks' likely parent was a non-primitive, mantle-derived basaltic andesite. The gabbro itself is a low Mg# amphibole cumulate with trace element characteristics that are similar to other arc cumulates worldwide. I show that some predicted trends for amphibole crystallization (i.e., La/Yb and Dy/Yb ratios) are generated by amphibole crystallization in the Riddle Peaks pluton. However some ratios, such as Nb/Ta and Ti/Zr are not explained by the amphibole sponge hypothesis.

Geologic Setting

Regional Geology

The North Cascades Crystalline Core (NCCC) is a large igneous and metamorphic complex representing a thick crustal section of a Cretaceous continental margin magmatic arc (Miller et al., 2009). It is offset from its northern extension, the Coast Plutonic Complex, by the dextral strike-slip Straight Creek fault. It is separated from the sedimentary rocks of the Methow Basin to the east by the Ross Lake fault zone (Misch, 1966; Miller and Bowring, 1990). (Fig.1) The NCCC consists of batholithic rocks and metamorphic country rock such as the ophiolite of the Ingalls complex, metapelites and migmatitic gneiss of the Nason terrane; amphibolite, gneiss, schist, and calc-silicate of the Chelan Mountains terrane; and biotite gneiss of the Swakane terrane (Misch, 1966; Tabor et al., 1987; Tabor et al., 1989; Miller et al., 1994).

Broadly, the thick crust of the NCCC formed after the assembly of several terranes in the mid-late-Cretaceous. These terranes include oceanic arcs and oceanic crust, which form the country rock to the plutons (Miller et al., 2009). The NCCC experienced major regional shortening beginning in the Cretaceous. Metamorphic rocks record greenschist to sillimanite-zone amphibolite facies metamorphic conditions (Misch, 1966; Brown and Walker, 1993). The Cretaceous crust became extremely thick (possibly >55 km) due to both shortening and arc-related plutonism (Brown and Walker, 1993; Miller et al., 2009) (Fig.2). Most of the plutons formed during a magmatic peak around 96-88 Ma, but other pulses of plutonism may have occurred from 78-60 Ma, and 50-45 Ma (Miller et al., 1989; Miller et al., 2009; Gordon

et al., 2010) (Fig.3). These plutons are exposed in an oblique cross-section, such that deeper rocks are exposed in the northwest of the NCCC.

The Cretaceous and Eocene NCCC plutons are largely tonalite and granodiorite, but many are associated with minor mafic bodies (Misch, 1966; Cater, 1982). The Entiat, Seven-fingered Jack, Tenpeak, Mount Stuart, Black Peak, plutons are dominantly tonalitic but also contain mafic components, such as hornblende- or biotite-rich diorite, hornblendite, and pyroxene-bearing gabbro (Dawes, 1993; Matzel et al., 2006; Miller et al., 2009). Many of these mafic components are present as border complexes; for example, the Tenpeak pluton and the Cardinal Peak pluton have borders that contain hornblende gabbro to hornblendite (Cater, 1982; Parent, 1999; Miller et al. submitted manuscript). The early Cretaceous Chelan Complex (120-100 Ma), in the southeast portion of the NCCC, is also tonalitic but has significant mafic portions (Hopson and Mattinson, 1994). The Chelan Complex consists largely of metaplutonic migmatite and metatonalite, with lesser hornblendite, migmatitic amphibolite, and meta-ultramafic rocks (Hopson and Mattinson, 1994).

Riddle Peaks Geology

The Riddle Peaks pluton, preliminarily dated at ~77 Ma (McPeek et al., 2002), is one of the few mafic/ultramafic intrusive bodies in the NCCC. It intrudes into the Triassic Holden assemblage, part of the Chelan Mountains Terrane. The Holden assemblage is dominantly composed of amphibolite, hornblende gneiss, and hornblende-biotite schist, with lesser calc-silicate, leucocratic gneiss, plagioclase-biotite schist, pelitic schist, and metaconglomerate (Cater, 1982; Miller et al, 1994; Parent, 1999).

The Riddle Peaks pluton is intruded by the (~72) Cardinal Peak tonalitic pluton on its western and southern sides (Haugerud et al., 1991; Miller et al., 2009). However, the northern, mafic portions of the Cardinal Peak may have older zircon ages of ~76-77 Ma, closer to that of the Riddle Peaks (McPeek et al., 2002) and hence the relationship between the two plutons is not clear. The Cardinal Peak crystallization conditions (6-8 kbar; Parent, 1999) may then be a reasonable estimate for the Riddle Peaks. The Riddle Peaks pluton is also intruded by the 46 Ma Railroad Creek pluton to its north and east (Cater and Wright, 1967). The Cardinal Peak and Railroad Creek plutons contain many inclusions of the Riddle Peaks hornblende gabbro (Cater, 1982).

Field Relations and Rock Descriptions

The Riddle Peaks pluton is a medium to coarse-grained layered cumulate hornblende gabbro with some unlayered (massive) hornblende gabbro portions. Contacts between the zones of layered and massive gabbro are gradational; outcrops that appear between mapped zones of layered and massive gabbro are more similar to massive gabbro but with aligned hornblende crystals. In addition to the abundant hornblende and plagioclase, minor mineral phases include magnetite, apatite, zircon, ilmenite, pyrite, and titanite. Inclusions of the Holden assemblage and smaller inclusions of quartz diorite are common. At least two major granitoid dikes cut through the pluton (Cater, 1982). The pluton contains several types of structures including foliation, lineation, folds and ductile shear zones (McPeek et al., 2002). However, the pluton dominantly retains original igneous textures.

In this study, only the southern portion of the pluton was visited and sampled due to its greater accessibility, but this included both massive portions in addition to layered hornblende gabbros (Fig. 4). Layered gabbro comprises most of the pluton and are well exposed everywhere. Much of the massive gabbro is covered in vegetation, except for some steep cliffs, from the bases of which most of the massive samples were collected. Samples were not taken from weathered areas, ductile shear zones or other deformed areas.

Layered gabbro (hornblendite to hornblende gabbro to leucogabbro)

Layered hornblende gabbro is significantly more abundant than the massive gabbro in the pluton (Cater, 1982). Layering is composed of alternating hornblendite and hornblende gabbro layers with plagioclase-rich (leucogabbro) layers (Fig. 5). Layers are on the scale of centimeters to meters and are continuous laterally for 10's of meters (Cater, 1982). Layers range in thickness from 0.5 mm to at least 10 m. Some areas have bands that are folded or wrap around one another, but this was only seen in float. There is some variation in grain size throughout the layers, but most layers are medium or coarse-grained. Pegmatitic portions also occur.

Given the variability in layer thickness and mode in the layered hornblendite and hornblende gabbro, generalized rock descriptions are difficult. Layers composed of hornblendite are more common than layers composed of hornblende gabbro. Hornblendite may be described as containing largely black, subhedral to euhedral hornblende with 30% or less gray/white anhedral to euhedral plagioclase. Massive gabbro is dominantly hornblende but may have 15-45% plagioclase. There is generally a sharp transition at the border between

the two layers, except for occasional areas where there is a concentration of anhedral plagioclase that extends into the hornblendite or hornblende gabbro layer or vice-versa.

Modes for plagioclase-rich (leucogabbro) layers range between 70-95% plagioclase, 5-30% hornblende, and 0-2% epidote as a common alteration mineral. Plagioclase may appear granular on weathered surfaces. On fresh surfaces, plagioclase appears white to gray and anhedral, and crystals appear indistinct from one another. Occasional grains appear euhedral or show obvious cleavage. Hornblende is aligned or may occur in small clumps of crystals up to 1 cm across. Some groups of crystals have radiating aggregation. Crystals are black, subhedral to euhedral and 2-5 mm in length. Epidote appears in veins, not as distinct crystals, but covering the vein surface in mm-sized spots. Plagioclase-rich layers are relatively thin (<1 cm up to 30 cm) (Fig. 5).

In hornblende gabbro and hornblendite layers, samples are dominantly dark gray to black, but they are speckled due to visible plagioclase. In these layers, mineralogy includes hornblende (~70-100%), plagioclase (30-0%), pyrite (5-1%), magnetite (5-1%), apatite (0-1%), titanite (<1%), ilmenite (<1%) with minor chlorite and epidote (from alteration). Hornblende is black, euhedral with distinguishable cleavage, and grains range in size from medium to pegmatitic, sometimes within the same hand sample. In thin section, hornblende is brown to green and anhedral to euhedral. Grains may be as small as 0.2 mm and 4.0 mm in equant cross-sections. Elongate grains are 0.5 mm up to 1.0 cm. Very tiny inclusions exist within the cores of many hornblendes, giving these grains a “scratched-up” appearance under the petrographic microscope. Under highest power, the inclusions (10-100 μm) are too small to analyze chemically. However, they are high relief and given that the hornblende has

relatively high (0.39 to 4.6 wt%) TiO_2 content, they are probably rutile grains. At high power on the microscope, they appear to occur in amphibole's cleavage directions.

Plagioclase is generally white to gray, interstitial to amphibole and is anhedral, but it may appear as subhedral grains. Plagioclase grains are medium or coarse grained, generally equal in size or slightly smaller than hornblende grains. They may appear as localized blebs of white material, 1-5 mm long, sometimes displaying cleavage. In thin section, these "blebs" may be a 1-2 mm wide circular collection of crystals or one poikilitic grain. It may also have subhedral or euhedral amphibole within it. Pyrite is the most common accessory phase visible in hand sample; it is anhedral and present as tiny crystals surrounding plagioclase or hornblende grains, or occasionally within grains. Apatite may occur as individual grains or in clusters, and it is only visible in thin section (0.1-0.5 mm) and subhedral. Titanite occurs as inclusions within amphibole or between grains or along fractures; it is anhedral and quite small (<0.1 mm). Magnetite and ilmenite are <0.1 mm and anhedral.

Massive gabbro (hornblende gabbro)

In the massive gabbro, mineral modes are hornblende (45-85%), plagioclase (15-45%), ilmenite (1-5%), magnetite (1-5%), apatite (0-1%), zircon (0 to >1%), biotite (0 to >1%) and secondary titanite (1%) and pyrite (0-1%). Massive gabbro with subequal amounts of hornblende and plagioclase (45-65% hornblende, 50-35% plagioclase) is more common than massive gabbro with 65-85 % hornblende. A lack of distinct layering gives these rocks an overall gray appearance in the field (Fig. 6).

Hornblende is black, subhedral to euhedral, and 1-4 mm in length. Grains may be thin and elongate (<1mm thick, up to 5 mm long) or thicker (up to 2 mm) and stubbier. Textures

resemble hornblende from layered cumulate hornblende gabbro and hornblendite samples in thin section, including the many μm-sized inclusions.

Plagioclase is gray to white, 1-4 mm, subhedral, and has cleavage that may be visible in hand sample. Plagioclase is generally interstitial but may be euhedral in other areas, implying a cumulus origin. In thin section, interstitial plagioclase crystals are 0.2 to 3 mm in size, equant or elongate, and anhedral or subhedral. Plagioclase occasionally appears altered to sericite.

Ilmenite and magnetite together may make up as much as 10% of massive samples. These grains range in size from 0.1-1 mm. They are anhedral to subhedral, and they are clearly interstitial, except in some samples where they fill cracks <1 mm wide. Ilmenite and magnetite grains may appear dissolved, and they frequently exist intergrown with one another (Fig. 7). Using the Scanning Electron Microscope, it was determined that ilmenite (up to 5-8%) is more abundant than magnetite (2-5%) in thin sections that contain close to 10% of these minerals. Some of the magnetite could be hematite, but it is assumed to be mostly magnetite, because the rock is highly magnetic in hand sample.

Apatite does not occur in clusters as in layered samples but as individual grains and smaller (0.5 mm) than in layered samples. Apatite is generally subhedral but may be euhedral. Titanite is larger than in layered samples (<0.1 mm to 2 mm) but occurs more commonly near fractures and veins than as inclusions. Pyrite may be present as small, 0.2-2 mm anhedral crystals or as laths 2-4 mm long and ~1 mm wide. Rarely zircon is present as prismatic grains (<0.1 mm) within amphibole or plagioclase. Rare biotite (<1 mm) also exists, partially altered to chlorite.

Small fractures are fairly common (>1 mm thick) in the massive gabbro, but often do not permeate the whole sample. Fractures are sometimes filled with fine-grained anhedral epidote or are weathered to an orange-red. No magmatic epidote was identified, though it is commonly found in NCCC plutons, including the Cardinal Peak. Magmatic epidote would imply trapped melt (Dessimoz et al, 2011), and its absence supports the idea that this rock is a cumulate, in accordance with the textures described above.

Methods

Whole rock and mineral geochemical analyses were employed in this study for 10 layered gabbro and 28 massive gabbro samples. Powdered whole rock samples were analyzed for 29 major and trace elements at Washington State University's GeoAnalytical Laboratory. Mineral chemistry was obtained on Oregon State University's electron microprobe (10 major elements) and WWU's LA-ICP-MS (37 trace elements).

Whole Rock Chemical Analysis

Samples were prepared for whole rock analysis at WWU. In the first step, weathering rind was removed from the 1-2 kg samples by using a hammer on steel plates. Samples were then crushed and separated, so that 200 g of each rock sample were processed in the Sepor Chipmunk Jaw Crusher to coarse rock chips.

The resulting crushed samples were further processed for analysis by XRF (major elements) and ICP-MS (trace elements) by two different methods. A separate protocol for crushing ICP-MS samples is described, because the tungsten carbide chamber used to grind

XRF powders introduces Nb contamination. The two instruments also require different procedures for fusing powders into beads, so these are described separately below.

Massive samples had varying modes of plagioclase and hornblende. However, layered samples included only the hornblende-rich (hornblende gabbro or hornblendite) layers, as these are fairly thick layers and samples with both layers were difficult to obtain. No plagioclase-rich layers were analyzed, because layers were not wide enough to create an appropriate sample size for analysis. Additionally, obtaining hornblende chemistry was the main objective of this study.

Major Element Analysis

First, 200 g of crushed rock was run through a splitter, and half was then processed through the steel Disk Grinder to reduce size. Then the coarse powders were split again until 10 g remained. Remaining powders were ground in a tungsten carbide chamber using the Spex Mixer Mill ball mill to obtain a powder consisting of μm-size grains.

After rock powder was ground to -200 mesh, it was fused into a glass bead for analysis. After drying, 3.5 g of each powdered sample was weighed and mixed with 7.0 g of $Li_2B_4O_7$. These mixtures were transferred to a graphite crucible and heated in a 1000°C oven for 10 minutes. Upon removal, samples were poured into beads and then crushed again in the rock lab using a mortar and pestle. Then crushed glass was reground in the tungsten carbide chamber in the Spex Mixer Mill into a fine (μm-size) powder. Samples were re-fused in graphite crucibles. Many underwent several re-melts to get a wide, evenly sized, flat bead

free of bubbles. These beads were analyzed at WSU using the ThermoARL Advant'XP+ sequential X-ray fluorescence spectrometer.

Experiments run at WSU provide estimates of accuracy and precision of the XRF method. Accuracy of WSU's methods is measured by running nine USGS standards (and one other quartz standard) prepared at WSU and comparing with standard values. For major elements differences between the known values and WSU analysis are as follows: <0.60 wt.% for SiO_2,FeO; <0.40 wt.% for MgO; ≤ 0.20 wt.% for Al_2O_3, Na_2O; <0.10 wt.% for TiO_2, CaO, K_2O, P_2O_5; <0.01 wt% for MnO (Johnson et al., 1999). Trace elements Ni, Cr, Sc, Ba and V are only semi-quantitative at low concentrations (>30 ppm), but other trace elements are precise to 1-3 ppm. Full methods and discussion of accuracy and precision are detailed in Johnson et al., 1999.

Trace Element Analysis

Nine samples were analyzed at WSU for 14 rare earth elements and 13 other trace elements using Agilent 7700 ICP-MS. They were prepared at WWU by the same methods as for XRF analyses, but to avoid potential Nb contamination from the Mixer Mill's tungsten carbide chamber, samples were reduced to μm-size grains in an alumina-ceramic chamber in the SPEX Shatterbox. Samples were dried and mixed with lithium tetraborate flux in a 1:1 ratio. This mix was fused in a 1000°C oven for 10 minutes and then recrushed to μm-size powder. Resulting powders were mailed to WSU's laboratory. To assure dissolution of resistant mineral phases, the fluxed powders were dissolved in solution consisting of 2 ml HNO_3, 6 ml HF, and 2 ml $HClO_4$. This mixture was placed at 110° C and allowed to

evaporate. The mixture was diluted again in 2 ml $HClO_4$ at 160° C and evaporated. Finally samples were mixed with 10 ml H_2O, 3 ml HNO_3, 5 drops of H_2O_2, and 2 drops of HF. This mixture was heated to a hot plate and stored with 60 g of de-ionized water. The mixtures were further diluted upon analysis.

Accuracy of WSU's ICP-MS methods are measured by comparing trace element and REE compositions of samples prepared and analyzed at WSU's laboratory against published USGS known values. The maximum differences between the USGS values and the WSU analyses are as follows: <40 ppm for Ba; <30 ppm for Sr, Zr; 5< ppm for La, Ce, Pr, Nd, Sm, Dy, Hf, Th, Pb, Sc; <3 ppm for Rb, Y; <1 ppm for Gd, Eu, U, <0.5 ppm for Eu, Tm, Yb, Ho, Cs; and <0.1 ppm for Tb, Lu. Precision is better than 5% for the REE and better than 10% for the other analyzed trace elements. Full methods and discussion of error are detailed in Knaack et al. (1994).

Mineral Chemistry

Hornblende and plagioclase grains were analyzed from polished thick sections using the 100-SX Cameca electron microprobe at Oregon State University. Amphiboles were analyzed using a 30 nA beam current, and plagioclase was analyzed with a 20 nA beam current. Both used a 15 keV accelerating voltage and 1 μm beam diameter. Peak times were collected for 10-30 s. Standards included natural and synthetic crystals of anorthoclase, labradorite, hornblende, augite, k-feldspar, chromite, andradite and pyrope.

Titanite was analyzed by Julie Gross from polished thick sections on University of Washington's JEOL 733 Superprobe. Operating conditions were run with a 5 μm beam

diameter, 15 keV accelerating voltage, and a 15 nA beam current. It was calibrated for amphibole analyses to natural crystals of grunerite, albite, orthoclase, rutile, tremolite and spessartine as well as synthetic TiO_2.

Minerals were analyzed by LA-ICP-MS at Western Washington University on the Agilent 7500ce ICPMS with a New Wave UP213 laser. Trace element data was obtained for each location analyzed for major elements and some additional grains and locations. Samples were prepared on thick sections (100 μm) for laser ablation. Samples were analyzed in several sessions, and operating conditions were different for each. For sample Rg-36, the laser was set to 5 Hz, 55 μm-spot size at 90% energy. For all other analyses, conditions were 5 Hz, 55 μm-spot size at 80% energy. Standards were always NIST 610 and NIST 612. Data was reduced using SILLS reduction software with Al contents determined by microprobe as an internal standard for amphibole and plagioclase (Guillong et al., 2008). Apatite was the only mineral not analyzed by microprobe, and it was reduced using measured Ca contents for natural apatites found in Deer, Howie and Zussman (1996). NIST 612 was treated as an unknown during reduction; known contents were compared with NIST 612 concentrations gained from each day of analysis. Accuracy was better than 10% for all trace elements except for Li, V, Cr, Cu, Ni, Rb, Cs, and Ba, which were better than 25% for some analyses. Precision was better than 10% for all elements except for Cr and Cu (better than 25%). High-field strength elements and rare earth elements are most important for this study, and accuracy and precision were better than 5% for these elements.

Results

Whole Rock Major Element Data

Major element chemistry suggests that all rock samples are gabbroic cumulates, with silica values ranging from 40.7 to 47.2 wt% (Table 1). Within this range, samples collected from layered versus massive parts of the gabbro have a small range of silica values (42.9 to 44.0 wt%), probably reflecting the greater proportion of hornblende over plagioclase present in layered samples (Fig. 8). Figure 8 shows that silica is not as useful for discriminating between layered and massive samples as is Mg#, calculated as [100*[(Mg/(Mg+Fe^{2+})]. The Mg# for unlayered samples ranges from 33-60, whereas layered samples have higher Mg#, ranging from 57-67 (Fig. 8).

In Figure 9, major elements are plotted against Mg# to highlight trends between layered and unlayered gabbro. Two of the samples collected from layered outcrops plot within the same Mg# range as the unlayered samples. This is likely due to the fact that both of these samples contain higher plagioclase contents, and both of them were present on the border between massive and layered sections of the pluton.

In each of the plots in Fig. 9, the massive gabbro is separated by a lack of samples with Mg#s ~50, possibly because this section of the cumulate pile was not collected. Layered samples show higher TiO_2 and lower Al_2O_3 than massive samples. Both of these observations are explained by the higher abundance of hornblende (high in TiO_2) relative to plagioclase (high in Al_2O_3) in layered samples. MnO and K_2O exhibit very slight negative correlations with Mg#. FeO and MgO do not show a trend with Mg#, though MgO is notably higher in layered samples than in massive samples.

Due to the proximity of the Cardinal Peak pluton to the Riddle Peaks pluton, I hypothesize that the two are related by fractional crystallization. Figure 10 shows major oxide variation diagrams for the amphibole-rich cumulate rocks of the Riddle Peaks pluton compared to diorite and tonalite from the Cardinal Peak pluton. Some, but not all, of the trends are collinear. The elements FeO, CaO, TiO_2, MnO and MgO decrease with increasing SiO_2, whereas Na_2O and K_2O increase. These trends would be expected in a related suite of rocks containing both cumulates and liquid compositions. Removing cumulates from a parent magma will drive the liquid line of descent in the opposite direction. However crystallization of only a subset of the layered samples can produce the Al_2O_3 contents of the Cardinal Peak diorites and tonalites, and crystallization of only a subset of the massive gabbro can derive the Mg# of the Cardinal Peak rocks. Thus only a subset of each lithology from the Riddle Peaks pluton may be potential cumulate end-members to the Cardinal Peak pluton.

Whole Rock Trace Element Data

Nine samples that represent the range of whole rock compositions were chosen for trace element analysis, five layered gabbros and four massive gabbros (Table 1). One sample, Rlg-39, is clearly layered but has a higher percentage of plagioclase and generally exhibits trace element characteristics closer to the massive gabbro. Except for this sample, data for layered samples reflects mafic mineral characteristics, because only the hornblende gabbro/hornblendite rock types were analyzed from layered gabbro (no plagioclase layers included).

Plots of whole rock trace elements generally show some correlations to whole rock Mg# (Fig. 11). Compatible elements Ni and Cr show a weak positive correlation with Mg#. Ni and Cr are higher in layered cumulate rocks (61-143 ppm Ni, 40-340 ppm Cr) than the massive gabbro (2-96 ppm Ni; 5-67 ppm Cr), though there is scatter in the data. Sr and Sc show strong correlations with Mg#; Sr is negatively correlated while Sc is positively correlated. The low Sr concentrations in the layered gabbro reflect a lack of plagioclase.

Rare earth element (REE) data show typical convex upward patterns consistent with hornblende accumulation (Fig. 12). Layered gabbros have a very slight negative Eu anomaly, while massive gabbros have a very slight positive one. Other than this Eu difference, there is no distinction in REE abundances between layered and massive gabbro.

Plots of primitive mantle-normalized trace elements show that the Riddle Peaks gabbro samples have distinct enrichments in Cs, Ba, K, Pb and Sr relative to other elements, and depletions in Th, U, P, and Zr (Fig. 13). Ratios of these trace elements are used later as proxies for differentiation processes, and are compared to continental crust, arc lavas and high Mg# andesites. Zirconium is very depleted compared to Ti and Sm, which results in high Ti/Zr ratios (449 ±123) and low Zr/Sm ratios (6.94 ±0.95) in these cumulate rocks. Nb is more abundant than Ta, which results in high Nb/Ta (17.5 ± 0.98).

Comparison of trace element compositions from the cumulate rocks of the Riddle Peaks pluton with those of nearby tonalitic plutons (e.g., the Tenpeak and Cardinal Peak plutons) produces trends that are consistent with mineral fractionation (Figs. 14, 15). The concentrations of V, Cu, Zr, Y, Rb, Sc show a clear trend with SiO_2 in these three plutons (Fig. 14). If the Riddle Peaks gabbro represents cumulate compositions, differentiated liquid

compositions (the tonalitic plutons) should plot along a trend from a parent magma composition away from the cumulates.

Trace element ratios are even more useful than pure abundances to illustrate fractionation by mineral phases. As above, if the Riddle Peaks gabbro represents cumulates that are related to tonalitic plutons, then the tonalitic plutons (differentiated liquids) should plot as a line through the parent magma and away from the cumulates. Plotting Ti/Zr or V/Ti against SiO_2 produces straight lines with negative trends, suggesting that one or more Ti-rich phases (likely hornblende and Fe-Ti oxides) are removing Ti from the system (Fig. 15). Plotting Zr/Sm against SiO_2 produces a straight line with a positive slope. Increasing Zr/Sm in derivative melts suggests hornblende fractionation, because hornblende has a high Kd for moderately heavy REE such as Sm.

Mineral Major and Trace Element Data

The focus of this thesis is on amphibole trace element geochemistry. Amphiboles in many arc plutons are varieties of hornblende, and are addressed as such in the following discussion. Hornblende chemistry from the Riddle Peaks pluton is presented below. Mineral data for other phases in the Riddle Peaks gabbro with significant trace and REE concentrations (plagioclase, apatite and titanite) are also discussed. Their chemistry is also critical for understanding the Riddle Peaks' parental magma evolution, although apatite and titanite are only present in trace amounts.

Hornblende

Hornblende compositions range from pargasite to tschermakite, based on estimates of minimum and maximum ferric values (respectively) according to EPMA analysis and the procedure in Leake et al. (1997) (Table 2). Pargasite and tschermakite are calcic amphiboles and are considered varieties of hornblende (Leake et al., 1997). When discussing the Riddle Peaks pluton, the terms hornblendite and hornblende gabbro will still be used to maintain consistency with the previous discussion of the Riddle Peaks pluton. The term amphibole will be used when discussing the broad effects of amphibole crystallization on continental crust or arc andesites.

The Mg# of the hornblende (where Fe is taken as Fe^{2+}) ranges from 60 to 70, which is considered low-Mg# hornblende (Foley et al., 2002; Fig. 16, Table 2). Small variations in Si, calculated as atoms per formula unit (apfu), at similar Mg#s suggest minimal subsolidus reequilibration in hornblende grains (Dessimoz et al., 2011). Hornblende in layered gabbro generally shows higher Mg# (up to Mg# 70) than that in massive gabbro (Mg# 60-63) indicative of crystallization from a more Mg-rich magma. Other major elements in hornblende vary only slightly between layered and unlayered samples. TiO_2 and Cr_2O_3 are greater in layered samples, and MnO is elevated in massive hornblende but only by ~0.1 wt% (Fig. 17). Core to rim variations are not obvious in hornblende; the exceptions are slight increases in TiO_2 and Cr_2O_3 within hornblende cores relative to rims.

In plots of trace elements versus Mg#, hornblendes from massive sections of the pluton (Rg-36 and Rg-48) cluster together and are usually distinct from hornblendes from the layered samples (Fig. 17) (Table 3). For example, hornblende grains in layered samples have

higher concentrations of Ni, and most have higher Cr than hornblende in massive gabbro. Hornblende grains in layered gabbro also have lower concentrations of Zr and Y. These observations are consistent with the Mg# data described above, suggesting that hornblendes from the layered gabbro were crystallized from more primitive magmas than the massive gabbro. However, no systematic variation in V exists between hornblende in the two groups, though V is thought to be a tracer for amphibole-controlled magma evolution (Meurer and Claeson, 2002).

Hornblendes from the Riddle Peaks pluton may be compared to rocks of the Cretaceous Chelan Migmatic Complex in the North Cascades, which contains abundant hornblende in its ultramafic to tonalitic suite of rocks (Dessimoz et al., 2011). The Chelan Complex hornblendite contains hornblende with similar Mg#s (~64-82) as hornblende in the Riddle Peaks pluton (Fig. 16). Hornblende gabbros in both lithologies have lower Mg# hornblendes (Mg#s ~60-70 for Chelan Complex; 60-63 for Riddle Peaks pluton). However, hornblendes in the Chelan Complex hornblende gabbros and hornblendites are higher in average abundances of Ni (Chelan = 161, Riddle Peaks = 63) and Cr (Chelan = 802, Riddle Peaks = 184) but lower in Y (Chelan = 21, Riddle Peaks = 29) and Zr (Chelan = 22, Riddle Peaks = 34) (Fig. 17), suggesting that the Chelan Complex's parental melt was more Ni and Cr-rich than the Riddle Peaks pluton's parent, despite similar Mg#s for similar lithologies.

As expected for hornblende-rich cumulate rocks, hornblende trace element characteristics largely mimic whole rock trace element characteristics. Chondrite-normalized REE diagrams for hornblende show characteristic patterns, with abundances of MREE > HREE (Fig. 18) (Table 4). As in whole rock REE diagrams, Eu anomalies are slight.

However, while massive gabbros showed positive Eu anomalies, all hornblende Eu anomalies are negative. Whole rocks had indistinguishable REE abundances overall, but hornblendes from massive gabbro have higher REE concentrations than those from layered gabbro, which supports other evidence (lower Mg#, Ni, Cr) that massive gabbro hornblendes crystallized from a more differentiated melt than layered gabbro hornblendes. Differences in whole rock and mineral patterns are most likely due to effects of plagioclase and/or other trace minerals on the whole rock patterns.

Plagioclase

Plagioclase compositions range from $An_{70.9}$ to $An_{85.0}$ (Table 5). The highest An contents belong to plagioclase in the layered samples ($An_{81.2\text{-}85.0}$), and supports the conclusion from hornblende mineral chemistry that the layered gabbro represents crystallization from a more primitive magma than the massive gabbro. The Sr and Eu* ($Eu_{sample}/Eu_{chondrite}$) do not correlate with anorthite content, but some massive samples have anomalously high Eu* concentrations (Table 6,7). Plagioclase has lower REE abundances than hornblende. The plagioclase REE patterns are concave up and show positive Eu anomalies (Fig. 19).

Apatite

Apatite grains, which make up approximately 0-1% of mineral mode in any one sample, show steep chondrite-normalized REE patterns with very high abundances (Fig. 20) (Table 8). Some grains show a slight negative Eu anomaly. Only two apatite grains were analyzed from the layered samples, but they have a slightly lower abundance of REE than those from massive samples. Apatite grains from the layered apatite-bearing hornblendite,

Sample Rg-38, also show minor depletions in LREE, with La/Lu ~3.5, while other samples have apatites with La/Lu between 11.7-24.7.

Titanite

Titanite grains were analyzed in one sample (Rg-36) and their compositions are presented in Table 9. They were not analyzed for trace element chemistry, as the grains did not extend deep enough into the thick sections to get a good time-averaged analysis. Major element chemistry does not vary greatly between or within grains, even though some appeared to be inclusions within hornblende while others grew interstitially. TiO_2 contents had the greatest range, from 32.8 to 35.5 wt %, but this variation does not correlate with inclusion versus interstitial location.

Pressure and Temperature Constraints, Conditions of Emplacement and H_2O Estimates

Pressure and Temperature Constraints

Pressure and temperature estimates can be obtained using appropriate thermodynamic models based on composition of phases within the gabbro. The Anderson and Smith (1995) Al-in-hornblende barometer cannot be used, because it requires the assemblage Quartz + K-feldspar + $Plagioclase_{25-35}$ + Fe-Ti oxide + Hornblende + Biotite + Titanite + Melt + Fluid (Anderson and Smith, 1995). The empirical Al-in-hornblende barometer by Larocque and Canil (2010) was used instead, because it only requires hornblende. The Larocque and Canil barometer produces pressures that are widely variable within single samples. Calculated pressures show a range of 3-5 kbar within most samples but range as much as 6.65 kbar

(7.75-14.4 kbar) for massive gabbro Rg-48. This barometer was recalibrated by Krawczynski et al. (2012) based on a wider range of compositions (primitive magnesian andesites and primitive basaltic andesites). However the recalibrated calculation does no better at constraining pressure, yielding between ~2-5 kbar ranges for single samples. These barometers are based on the positive correlation between amphibole's Al^{VI} concentration and pressure. However, some experimental studies show variability in Al^{VI} at single pressures, so they are still poorly constrained (Krawczynski et al., 2012). Clearly the barometers perform poorly for hornblendes in the Riddle Peaks pluton, possibly due to the variable TiO_2 contents of the Riddle Peaks hornblendes or other stoichiometric effects (Krawczynski et al., 2012).

Use of the semi-quantitative calcic amphibole (hornblende) thermobarometer of Ernst and Liu (1998) only requires analyses for TiO_2 and Al_2O_3 in hornblende, and it also shows that all Riddle Peaks hornblendes fall between a large pressure range of 5-10 kbar. Analyzed core-rim pairs show that the Riddle Peaks hornblende followed a normal cooling progression from higher temperatures cores (~800-900°C) to cooler temperature rims (700-800°C) (Fig. 21). Very high core temperatures (900°C) only occur for layered cumulate samples. The centers of many hornblende grains contain abundant inclusions (likely rutile). Natural hornblendes that are slowly cooled from basaltic compositions tend to exsolve Ti and Fe minerals (titanite, rutile, ilmenite), so these inclusions may be evidence for protracted cooling (Ernst and Liu, 1998).

The Riddle Peaks pluton has higher temperature estimates than those estimated for the Cardinal Peak pluton by Parent (1999). The Cardinal Peak's temperature estimates range from 741 to 901°C, with the most reliable thermometer (hornblende-plagioclase

thermometry) producing a median of 860°C. The calculated emplacement pressures for the Riddle Peaks pluton are not reliable and cannot be compared to the Cardinal Peak pluton. The Cardinal Peak pluton has an estimated emplacement pressure of 6-7 kbar, constrained by experimental studies of magmatic epidote and Al-in-hornblende barometry (Parent, 1999). Thermobarometric estimates are hampered for the Riddle Peaks pluton due to lack of proper mineral assemblages and possible effects due to slow-cooling and reequilibration.

H_2O Estimates

Such large amounts of accumulated hornblende suggest that the parental magma to the Riddle Peaks was water-rich. In experimental studies, basaltic compositions crystallize hornblende only if H_2O contents are above 4 % (Baker and Eggler, 1983). Published hygrometers cannot be used for the Riddle Peaks gabbro, because these rely on knowing compositions of coexisting liquids. Sisson and Grove's (1993) phase experiments on lavas from the Aleutians, Fuego Volcano and the Lesser Antilles show a relationship between An content of plagioclase in lavas and H_2O content of melts. Comparing the Riddle Peaks' plagioclase compositions ($An_{70.9\text{-}84.5}$) to the lavas from Sisson and Grove's phase experiments shows that the Riddle Peaks pluton most likely had 4 wt% H_2O.

Discussion

The previous section presented new chemical data for the Riddle Peaks pluton, which is a potential amphibole reservoir in the mid-crust. The following sections use this data to explore how amphibole crystallization can affect the geochemistry of derivative magmas, with a focus on the sponge hypothesis and derivation of trace element characteristics in average continental crust, average arc magmas, and selected magmas from plutons in the North Cascades Crystalline Core (NCCC). Davidson and others (2007) suggested that amphibole acts as a sponge in the mid-crust of island arcs, such that amphibole cumulates should display anticorrelated chemical characteristics, such as depleted Ti and low Dy/Yb, with derivative arc magmas (and continental crust). However, it has been untested with real cumulate data until now, whether amphiboles show such geochemical characteristics. Because amphiboles in the Riddle Peaks pluton show enrichments of Nb/Ta, Ti/Zr, and depletions of Sm/Zr and Sr/Y relative to chondrites (Table 11), the Riddle Peaks pluton is a tangible example of an amphibole sponge. According to Davidson's predictions, crystallization of the Riddle Peaks should strongly affect compositions of Nb, Dy, Ti and Sm in derivative magmas such that some previously unexplained trace element ratios in continental crust and arc magmas (such as low Nb/Ta and Ti/Zr) can be produced by Riddle Peaks' amphibole crystallization.

Amphiboles in the Chelan Complex were shown to regulate the Dy/Yb and Y concentrations within the mafic igneous complex and in derivative liquids (Dessimoz et al., 2011). Amphiboles in the hornblende gabbros and hornblendites from the Chelan Complex have similar Mg#s to amphiboles in the gabbros and hornblendites from the Riddle Peaks

pluton (Fig. 16). These similarities suggest that Riddle Peaks amphiboles could deplete or enrich a derivative magma as did those in the Chelan Complex.

To test the amphibole sponge hypothesis, I model fractionation processes using the Riddle Peaks cumulates, to determine whether crystallization of amphibole-rich cumulate rocks such as these can produce geochemical characteristics of average arc magmas, average continental crust and nearby differentiated magmas. Nearby differentiated magmas included the Cardinal Peak and Tenpeak plutons in the NCCC. The Cardinal Peak pluton has been discussed previously; it exists in contact with the Riddle Peaks and its mafic rocks share a similar age and presumably P-T conditions of emplacement. The Tenpeak pluton (92.3-82.7 Ma) is not in contact with the Riddle Peaks pluton, but it is a dominantly tonalitic NCCC pluton with detailed trace element data (Miller et al., submitted manuscript). These two plutons show potentially comagmatic trends in major and trace element evolution when plotted with the Riddle Peaks pluton (Fig. 14, 15). Geochemical models presented below suggest that a derivative liquid produced by crystallizing the Riddle Peaks pluton from a parental basaltic andesite shares some similar trace element characteristics as arc magmas, continental crust and the Cardinal Peak and Tenpeak plutons' liquid compositions.

In the following sections, I start by addressing the cumulate origin for the Riddle Peaks pluton. Next, I discuss possible parental magmas to the Riddle Peaks pluton. Then, I present trace element models to show that amphibole in the Riddle Peaks pluton acts as a sponge for some trace elements that are depleted in arc and crustal lavas. Finally I present Kd values calculated for apatite in a high pressure, basaltic andesite system as in this study.

Cumulate Origin

Observed textures and whole rock and mineral geochemistry described above show that the Riddle Peaks pluton consists dominantly of cumulate rocks left behind after segregation of a parental magma. Whole rock data shows low SiO_2 contents (40.7 to 47.2 wt%), with REE patterns that largely reflect REE patterns of accumulated amphibole. These cumulates can therefore be used to model how segregation of amphibole-rich minerals from parental liquids affects magma evolution pathways.

To determine whether any trapped liquid remains as interstitial material in these cumulates, I have performed a simple mass balance test. This involves comparing *measured* whole rock REE abundances from two samples with *calculated* whole rock REE abundances using average mineral compositions and modes. Calculated REE abundances were obtained for each element by the equation:

$$Conc_{Calc} = [(Conc_{x1})(Mode_{X1}) + (Conc_{X2})(Mode_{X2}) + \dots]$$

where Conc represents the specific REE abundance, X represents the mineral, and $Conc_x$ is determined by LA-ICP-MS analyses. These tests show that calculated whole rock compositions are close to analyzed data (Fig. 22). There is no trapped liquid affecting REE patterns; these rocks are representative of accumulated hornblende and plagioclase.

Comparison to other amphibole cumulates

Amphiboles in the Riddle Peaks pluton have similar Mg#s and trace element concentrations to other amphiboles in cumulate plutons from arc settings, especially hornblendites or hornblende gabbros (Fig. 16, 23, 24). Arc-derived amphiboles worldwide show similarities in trace elements, and many of these suites have been shown to exhibit control on the evolution of trace elements during differentiation. For example, crystallization of amphiboles (Mg#s 60-82) in the Chelan Complex hornblendites and hornblende gabbros decreased Dy/Yb in derivative magmas and increased Sr/Y. Amphiboles from the Adamello Batholith, Italy (Tiepolo et al, 2011), Shikanoshima Island, Japan (Tiepolo et al, 2012), and Husky Ridge, Antarctica (Tiepolo and Tribuzio, 2008) are also shown to regulate trace elements such as La, Nb, Y within their respective systems (Fig. 24). Amphiboles in the Riddle Peaks pluton have comparable concentrations of these elements, and it may be assumed that crystallization of the Riddle Peaks pluton affected derivative magma composition similarly. I model this quantitatively below.

Parental Magmas

In this section, I investigate the nature of the parental magma to the Riddle Peaks pluton. First, I discuss geochemical evidence that the Riddle Peaks pluton formed from a mafic, but not primitive (close to mantle equilibrium), parent magma. Then I calculate compositions of equilibrium liquids for the Riddle Peaks pluton, which are proxies for liquids that were in equilibrium with the Riddle Peaks' minerals as they crystallized. Equilibrium liquids are compared to liquid compositions in the Cardinal Peak (McCrady, 2013) and

Tenpeak plutons (Miller et al., submitted manuscript) to better understand the nature of the Riddle Peaks' magmatic parent.

Geochemical evidence for mafic parental liquid

Geochemical data suggests that the Riddle Peaks cumulates probably formed from a parental magma that was not primitive. Average Ni (63 ppm) and Cr (181 ppm) contents in amphibole are low compared to Ni (410 ppm) and Cr (1100 ppm) in amphiboles from Husky Ridge, Antarctica, which are interpreted to have crystallized from a mantle-derived magma (with a melted sediment component) (Tiepolo and Tribuizio, 2008). The Riddle Peaks amphiboles lack clinopyroxene inclusions, which are commonly found in primitive arc amphiboles (Tiepolo et al., 2011; Tiepolo et al., 2012; Tiepolo and Tribuzio, 2008; El-Rahman, et al., 2012; Dessimoz et al., 2011). Finally, Mg#s similar to the Riddle Peaks amphiboles are found in amphiboles in the hornblende gabbros and hornblendites in the Chelan Complex, which crystallized from a parent with 52-57 wt.% SiO_2 (Dessimoz et al., 2011). This is in contrast to olivine websterites and pyroxenites from the Chelan Complex that have amphiboles with much higher Mg#s (68-88). The Riddle Peaks pluton likely has a similar basaltic andesitic parent, and more mafic cumulates are below the level of exposure. Although the Chelan Complex basaltic andesites underwent some differentiation, cumulate rocks are shown to continue to affect trace elements throughout evolution of the complex (Dessimoz et al., 2011).

Calculation of Equilibrium Liquids

Equilibrium liquids are calculated using amphibole trace element concentrations and experimental partition coefficients. Major element partition coefficients are poorly

constrained, while trace element partition coefficients are well characterized (Tiepolo et al., 2007). Here I calculate trace element concentrations of the equilibrium liquids.

Trace elements of these calculated equilibrium liquids can be determined using the relationship:

$$Cl = \frac{Cs}{Kd}$$

where Kd is the published partition coefficient, C_s is the measured concentration of a trace element in the solid crystal (e.g., the amphibole cumulate), and C_l is the calculated concentration of that trace element in the equilibrium liquid. Trace elements were measured in amphibole crystals (C_s) using LA-ICP-MS as shown in tables 3 and 4, and liquids were calculated using partition coefficients for calcic amphiboles in a basaltic andesite composition (Tiepolo et al., 2007) (Table 10).

Calculated REE patterns of equilibrium liquids have slightly sloping REE patterns with very slight positive Eu anomalies (Fig. 25). Calculated liquids match REE concentrations of three samples of quartz diorite and diorite of the Cardinal Peak pluton (McCrady, 2013). Calculated liquid patterns also match some of the mafic end-member magma compositions within the Tenpeak pluton (Miller et al., submitted manuscript) (Fig. 25). These similarities suggest that the Riddle Peaks cumulate rocks may be representative of the types of cumulate lithologies created by early fractionation of Tenpeak parental magmas (high-Al basalt) or Cardinal Peak parental magmas (hydrous mantle-derived melt).

Relationship of Hornblendite to Hornblende Gabbro Lithologies

It is necessary to understand how hornblende gabbro from the massive part of the pluton and hornblende gabbro/hornblendite lithologies from the layered part of the pluton are related for purposes of modeling liquid evolution in the pluton. Whole rock compositional data, such as REE patterns, show that both lithologies are cumulates, but lower Mg#s in amphibole from hornblende gabbro from the massive areas show that these must be derived from more differentiated liquids. It is possible then that these two domains of the pluton can be related by very small degrees of crystal fractionation. This can be tested by modeling fractionation of trace elements, such as the REE from equilibrium liquids associated with amphiboles from layered hornblende gabbro/hornblendite to equilibrium liquids associated with amphiboles from massive hornblende gabbro.

The REE concentrations were modeled using the Rayleigh fractionation equation for fractional crystallization:

$$C_L = F^{(D-1)} \cdot C_0^L$$

where C_L is the concentration in the daughter liquid; F is the fraction of melt remaining, and D is the bulk distribution coefficient. C_0^L is the concentration in the initial liquid. Partition coefficients are from Tiepolo et al. (2007) (Table 10).

This model is done in two steps, where the first step represents fractionation of the layered hornblende gabbro/hornblendite lithology from a parental magma, and the second step represents fractionation of the massive hornblende gabbro lithology from the result of step 1. In step 1, C_0^L is the most primitive equilibrium liquid, where primitiveness was

determined by Mg# of the amphibole analyses from which the equilibrium liquid was calculated. In this model, C_0^L is an equilibrium liquid from amphibole with Mg# 70. Crystallizing proportions were 90% amphibole and 10% plagioclase, as hornblendites are more common than hornblende gabbro lithologies in the layered part of the pluton. The model's output is the daughter composition (C_L), calculated at varying percentages of crystallization and compared with an intermediate equilibrium liquid (from amphibole with Mg# 65).

The second step is fractionation of the hornblende gabbro lithology, where C_0^L is the daughter composition from step 1, the modeled composition that matches an intermediate equilibrium liquid with Mg# 65. Crystallizing proportions were 40% amphibole, 45% plagioclase and 5% each of ilmenite and magnetite. Crystallizing proportions were chosen according to observations of the sample from which the most differentiated liquid (Mg# 60) was calculated. This liquid is compared to the model's output (C_L) at varying percentages of crystallization.

The models are successful and show that fractionation from one starting parental magma is a viable, unique model to produce the range of cumulate compositions in the Riddle Peaks pluton. Calculated daughter products do match equilibrium liquids at reasonable crystallization fractions. Step 1 required 40% crystallization from the most primitive equilibrium liquid to generate the intermediate liquid (Fig. 26a). In step 2, 25% crystallization from the intermediate generated the most differentiated equilibrium liquid (Fig. 26b). Slight mismatch for some REE in the models is reasonable given the potential

error involved in using experimental Kd values to calculate equilibrium liquids. Amount of crystallization is reasonable, and this model shows that hornblendite in the layered gabbro could have crystallized from the same parental liquid that ultimately crystallized the hornblende gabbro in the massive gabbro.

The Riddle Peaks Pluton as an Amphibole Sponge

There are discrepancies between chondritic ratios of certain trace elements (which presumably represent the mantle source) and average compositions of arc magmas. This has been noted for ratios such as Nb/Ta and Ti/Zr, where both elements in the ratios are incompatible and should not change during typical closed-system igneous processes. Something must cause these ratios to change from those found in the mantle (Nb/Ta = ~18-20; Ti/Zr = ~115) to those in arc magmas (Nb/Ta = ~10-17; Ti/Zr = ~30) (Sun and McDonough, 1989; McDonough and Sun, 1995; Rudnick and Fountain, 1995; Taylor and McLennan, 1995; Rudnick and Gao, 2003). Amphibole has been proposed as one mineral that can appreciably fractionate some of these elements (Foley et al., 2002; Garrido and Bodinier, 2005; Müntener et al, 2009). Based on geochemistry of arc lavas, Beard (1986) predicted that amphibole can accumulate beneath arcs but does not erupt due to the high density of the accumulated minerals. If amphibole exists in large quantities below arcs, it may act as a sponge for water and various trace elements, holding on to these elements and depleting them in derivative liquids (Davidson et al., 2007). However, the amphibole sponge hypothesis is only predicted and requires real amphibole cumulate data to substantiate. This section addresses whether or not the Riddle Peaks acts an amphibole sponge, based on

geochemical evidence and trace element modeling. I test whether three types of liquids could have been derived from a basaltic andesite parental magma by crystallization of the Riddle Peaks pluton as a sponge: average arc lavas, NCCC magmas (the Cardinal Peak pluton and the Tenpeak pluton) and average continental crust, which shows similar discrepancies with mantle/chondrite ratios as arc magmas.

Geochemical evidence for an amphibole sponge

Geochemical data show that the Riddle Peaks pluton could indeed have acted as a sponge, given its high ratios of Nb/Ta and Ti/Zr, and low values of Zr/Sm, Sr/Y, and La/Yb relative to chondritic values (as a proxy for mantle) (Table 11). Arc lavas and continental crust have depleted Nb/Ta ratios (~10-17) relative to chondrites (~18-20) (Sun and McDonough, 1989; McDonough and Sun, 1995; Rudnick and Fountain, 1995; Taylor and McLennan, 1995; Rudnick and Gao, 2003). The Riddle Peaks amphiboles have Nb/Ta ratios ranging from 17.0 to 33.1 (average = 22.3). Thus the Riddle Peaks pluton (and most of its constituent amphibole) took in more Nb than Ta during amphibole growth, which should deplete residual liquids in Nb/Ta.

Similarly, arc lavas and continental crust have depleted Ti/Zr ratios (~30) relative to the mantle/chondrite value of 115 (Sun and McDonough, 1989; McDonough and Sun, 1995; Rudnick and Fountain, 1995; Taylor and McLennan, 1995; Rudnick and Gao, 2003) (Table 11). In contrast Riddle Peaks amphiboles have much higher Ti/Zr ratios (average = 364), so that the Riddle Peaks pluton could be a Ti-enriched reservoir. Other ratios (Zr/Sm, La/Yb) have the opposite relationship with arc lavas or crust, where these ratios are elevated in arcs and crust (Zr/Sm ~ 30, La/Yb = ~ 8-10) compared to chondrites (Sun and McDonough, 1989;

McDonough and Sun, 1995; Rudnick and Fountain, 1995; Taylor and McLennan, 1995; Rudnick and Gao, 2003), and consonantly, the Riddle Peaks cumulates have lower ratios than arcs, crust or chondrites (Zr/Sm = 8.7, La/Yb = 0.94).

The ratios Sr/Y and Dy/Yb are also thought to change via amphibole fractionation, but these ratios have more complicated relationships to arcs, crust and chondrites. Ratios of Sr/Y and Dy/Yb are enriched in arcs and crust (Sr/Y ~ 16-20, Dy/Yb ~ 1.8) relative to chondrites (Sr/Y = 4.6, Dy/Yb = 1.52) (Sun and McDonough, 1989; McDonough and Sun, 1995; Rudnick and Fountain, 1995; Taylor and McLennan, 1995; Rudnick and Gao, 2003). However the Riddle Peaks' Sr/Y ratio is low (7.6), but not lower than chondrites as in the case of Zr/Sm or La/Yb. The Riddle Peaks' Dy/Yb ratio is higher than in continental crust or chondrites. These two ratios will be included in the following modeling section to better understand their change with amphibole crystallization. I next test hypotheses about the effects of this elemental storage on Riddle Peaks' liquid evolution with a Rayleigh fractionation model for trace element ratios.

Liquid evolution of trace element ratios in the Riddle Peaks pluton

This section of the discussion models the evolution of trace element ratios in calculated equilibrium liquids, and the results will be compared to ratios for arc magmas, continental crust and NCCC magmas. The model is the fractional crystallization model described above, and the two lithologies from layered and massive gabbros are used in two steps. In step 1, hornblendite (in layered gabbro) is crystallized from the most primitive calculated equilibrium liquid (Mg#70), which was chosen based on the Mg# of its associated amphibole analysis. Crystallizing proportions are 90% amphibole and 10% plagioclase.

Trend lines for fractionation are produced for increments of 5, 10, 15, 20, and 25% fractionation (Fig. 27). The trend lines are compared to ratios from equilibrium liquids calculated from amphiboles with intermediate Mg#s (68-63). The ratios Nb/Ta, Ti/Zr, Sr/Y, La/Yb and Dy/Yb are examined. Some ratios are plotted against Zr as a measure of differentiation, because typical indicators for differentiation (Si, Mg#) have poorly constrained partition coefficients, preventing their use in this type of modeling.

Results of step 1 show that crystallizing hornblendite decreases Ti/Zr and Dy/Yb ratios in derivative liquids, shown by the negative slope of the fractionation trend line (Fig. 27). Crystallizing hornblendite increases Sr/Y and La/Yb ratios, shown by the positive slope of the fractionation trend line. The Nb/Ta ratio changes little by fractionating small amounts of hornblendite. Fractionation trend lines do not intersect all of the plotted intermediate equilibrium liquids. Most of the trend lines intersect Rg-45, but it has Mg# 68, which is too similar to the starting point of the step 1 model (Mg# 70). Most of the trend lines also intersect equilibrium liquid Rg-39, which has a more intermediate Mg# 64, so it is taken as the best fit to be used in the second step of modeling (below) (Fig. 28, 29).

The second step models fractionation of hornblende gabbro lithology (in the massive gabbro) from the second best-fit intermediate liquid from the previous step (Fig. 27). Crystallizing proportions are 50% amphibole, 45% plagioclase, 2.5% ilmenite, and 2.5% magnetite, to represent a typical massive hornblende gabbro. Fractionation trend lines are shown for every 20% of the crystallization process and extrapolated to 100% (to F=0) to show how these liquids might continue to evolve. The trend lines are compared in Figure 27 to the most differentiated equilibrium liquids (Mg# 60). Equilibrium liquids from sample Rg-48 show a relationship with Mg# that is indicative of a magmatic trend, while liquids from

sample Rg-36 do not (Appendix A). Thus three liquids representing the range of Mg#s (60-63) from amphiboles in Rg-48 are shown, but only an average composition is shown for sample Rg-36. The second step also compares fractionation trend lines to average continental crust (Rudnick and Gao, 2003), Cardinal Peak (McCrady, 2013) and Tenpeak liquids (Miller et al., submitted manuscript).

Modeled liquid evolution lines (fractionated trend lines) for different ratios in step 2 show mostly poor fits to derivative compositions (including arc lavas, continental crust, and nearby Cardinal Peak and Tenpeak plutons), but some discernable trends emerge, including important La/Yb and Dy/Yb trends (Fig. 28, 29). The fractionation trend lines for La/Yb and Dy/Yb match those predicted by Davidson et al. (2007), whose predictions were based upon plotting these ratios from worldwide arc magmas against SiO_2 to understand differentiation trends for amphibole versus garnet (Fig 29). Thus the Riddle Peaks pluton is a tangible example of an amphibole sponge whose modeled liquid evolution matches predicted amphibole differentiation trends for La/Yb and Dy/Yb ratios. The ability of amphibole to produce such trends is important, as this can distinguish between contrasting hypotheses involving garnet, such as lower crustal melting or melting of the subducting slab.

Within the Riddle Peaks pluton, liquid evolution proceeds following the expected trend for amphibole fractionation, except for Nb/Ta ratios. Differentiated equilibrium liquids for the Riddle Peaks pluton generally follow the fractionation trend line modeled in these graphs and require less than 20% fractionation to produce the most differentiated equilibrium liquids. Only the Nb/Ta fractionation trend line does not come close to intersecting the most differentiated equilibrium liquids in the pluton. The reason for this is unclear; hornblende gabbro from the massive portion of the pluton had noticeably more ilmenite and magnetite,

which strongly partition Ta over Nb. Perhaps these differentiated liquids involved a prior phase of accumulated oxide minerals, unobserved in this study. More likely, given that abundances of Nb and Ta in amphibole are so low, analytical error (uncertainty of 2.14-8.12% for Nb and 1.87-4.87% for Ta) will have a larger effect on these ratios.

Except for Dy/Yb and La/Yb, the average continental crust compositions generally do not intersect with the fractionation lines from Riddle Peaks' amphibole fractionation. Modeled Dy/Yb produces a good fit for continental crust at 40% fractionation, and La/Yb requires 60% fractionation. Continental crustal Ti/Zr, Nb/Ta and Sr/Y concentrations are not produced from Riddle Peaks crystallization. This is surprising given the high values of Riddle Peaks amphiboles' Ti/Zr and Nb/Ta discussed in the section above. It appears that amphibole (with trace ilmenite, magnetite) fractionates Ti/Zr too effectively and Nb/Ta not effectively enough. There must be another process to explain these depleted ratios in continental crust. However, the crustal Sr/Y concentration is already similar to that of the intermediate Riddle Peaks equilibrium liquid. This suggests that crustal Sr/Y could instead be derived in a situation more similar to step 1, with crystallization of hornblendite.

Nearby plutons are also compared to the modeled fractionation lines in Figure 28, but only Ti/Zr is successful. The Ti/Zr of the Cardinal Peak tonalites lie along the fractionation trend line with 20-40% fractionation. This is consistent with observations of fractionation trends with the Riddle Peaks pluton (Fig. 14, 15). However despite these trends, no other trace element ratios for the Cardinal Peaks pluton are derived by crystallization of the Riddle Peaks pluton. The Tenpeak's felsic end-members are not produced in any model, which is

consistent with a more complicated origin, involving mixing with garnet-bearing crustal melt (Miller et al., submitted manuscript).

Some of the Tenpeak pluton's mafic end-member compositions have similar Sr/Y and Nb/Ta compositions as the Riddle Peaks' intermediate equilibrium liquid. Based on experimental partition coefficients, the elements Sr, Y, Nb, and Ta will be more affected by amphibole or garnet fractionation than by olivine or pyroxene. Thus a parental magma could undergo olivine and pyroxene crystallization, leaving Sr/Y and Nb/Ta ratios relatively unchanged until amphibole joined the crystallization sequence. The Riddle Peak's intermediate equilibrium liquid was produced via hornblendite fractionation, so similar Sr/Y and Nb/Ta ratios in the Tenpeak mafic end-members suggests that they were also generated by hornblendite fractionation. This hornblendite signature is more typical of sub-arc crystallization processes than a garnet signature, which requires melt of the subducting slab or lower crust. However, generating the Tenpeak's more differentiated liquids (felsic end-members) clearly involved more complex, open-system processes involving crustal melt (Miller et al., submitted manuscript).

The Sr/Y ratio is of particular concern to the question of arc magma generation, because adakites (Sr/Y>50 and Y<20 ppm; Kelemen et al., 2003b), which are almost exclusively found in arc settings, are thought to be produced by garnet fractionation. However, Dessimoz et al. (2011) showed that high, adakitic Sr/Y ratios in the Chelan Complex were produced by amphibole crystallization from a hydrous magma at high pressure (10 kbar) in absence of early plagioclase crystallization. The Sr/Y ratios generated in this model of Riddle Peaks equilibrium liquid evolution are not sufficiently high to

produce the high Sr/Y ratios generated by garnet fractionation. Because the Riddle Peaks' parental magmas are already more differentiated than the Chelan Complex parental magmas, plagioclase was already crystallizing and depleting Sr; thus adakitic signatures are not produced here.

In summary, projected liquid evolution paths show that the Riddle Peaks pluton acts an amphibole sponge for the elements La and Dy in arc lavas and continental crust. Fractionation of the Riddle Peaks pluton does not explain crustal Nb/Ta or Ti/Zr ratios. The crust's Sr/Y ratio may be explained by fractionation of hornblendites but not plagioclase-bearing rocks such as hornblende gabbro. High Sr/Y ratios resembling those of adakites are not produced in this model, because plagioclase is present early in crystallization of this pluton as thin layers between hornblendite. Some concentrations of trace elements in NCCC magmas, such as Ti and Zr, can be explained for the Cardinal Peak pluton, and some ratios (Sr/Y, Nb/Ta) in the Tenpeak pluton's mafic end-members could have been produced via hornblendite fractionation. Amphibole cumulates such as the Riddle Peaks pluton have a complicated role in producing various potential liquid compositions, and if these cumulates are involved in producing arc and crustal signatures, they are only part of the process.

Calculated Apatite Partition Coefficients

Apatite is a very important accessory mineral in igneous rocks, as its structure can easily accommodate REE and other incompatible elements that are important to arc rock evolution. Though apatite partition coefficient (Kd) values exist in the literature, information on apatite in cumulates from a mid-crustal, high-pressure basaltic andesite system are not

available. Because the partition coefficients for amphibole in this type of system are fairly well-known, the calculated equilibrium liquids from amphibole analyses presented above may be used in conjunction with LA-ICP-MS analyses on Riddle Peaks' apatite to derive their Kd values for basaltic andesite.

Mineral analyses from this study are used to calculate Kd values according to the equation:

$$Kd = \frac{Cs}{Cl}$$

where Kd is the partition coefficient, C_s is the concentration in the solid (the apatite analysis), and C_l is the calculated equilibrium liquid from amphibole analyses. Kd values are presented as averages for each sample (Table 12, 13). LREE including La (averages 6.4-9.7) and Ce (averages 6.05 – 9.86) have the highest Kd values, but all Kd_{REE} >1 and are comparable to published values for basalt compositions (Table 13). Since most published Kd values are for REE, here we present values for other trace elements. Large ion lithophiles Rb (0.004 – 0.04) and Ba (0.002 – 0.02) act incompatibly, while Sr is compatible (1.81 – 2.87) (Table 12). The HFSE including Th, Zr, Hf, Nb, and Ta are also incompatible (< 0.05), except for Y (2.96 – 3.62) and U (0.9-1.6).

Conclusions

The Riddle Peaks pluton is a gabbroic cumulate, and it most likely crystallized from a basaltic andesite that was ultimately derived by fractionation from mantle melt beneath the NCCC. Riddle Peaks' cumulates have low Mg#s (33-67), and its hornblende has low Mg#s (60-70). Geochemical and modeling results suggest that hornblende gabbro from the massive part of the pluton crystallized from a more differentiated liquid than hornblendite/hornblende gabbro from the layered part.

Calculated equilibrium liquid evolution shows that the Riddle Peaks pluton is an amphibole sponge for certain elements, such as REE. Fractionation of the Riddle Peaks pluton is shown to produce predicted amphibole fractionation trends in arc magmas and crust for ratios La/Yb and Dy/Yb. This is an important finding, because the Riddle Peaks is now a physical example of a rock type that can produce such trends. These trends contrast with those of garnet fractionation, which is involved in other arc processes, such as slab melting. The presence of this pluton in an ancient exhumed arc, and its modeled liquid evolution, suggests that amphibole does play a role in generating part of arc signatures.

However amphibole fractionation in the Riddle Peaks cannot produce arc/crustal ratios such as Sr/Y, Ti/Zr and Nb/Ta. Though amphibole has been shown to produce adakitic Sr/Y ratios elsewhere, the inclusion of plagioclase in the crystallization processes prevents this in the Riddle Peaks pluton. Most ratios in selected NCCC plutons are not produced via fractionation of the Riddle Peaks pluton, though the Tenpeak pluton's mafic end-members were likely generated in part by hornblendite cumulate crystallization. The nearby Cardinal Peak pluton may be related to the Riddle Peaks pluton for the following reasons: close

proximity with ambiguous contact relationships; observed major-element fractionation trends between the two plutons; similarity in Riddle Peaks' equilibrium liquid REE patterns to observed REE patterns in Cardinal Peak diorite and quartz diorites; and trace element models showing derivation of the Cardinal Peak pluton's Ti/Zr ratio by fractionation of Riddle Peaks amphibole.

The Riddle Peaks pluton shows that amphibole cumulates do exist beneath arcs as potential reservoirs for water and trace elements. However this study finds that this particular reservoir only explains part of the geochemical anomalies present in arcs and continental crust. Other mechanisms are still needed to understand the depleted Nb/Ta and Ti/Zr ratios in arcs and continental crust.

References

Anderson, J. L. and Smith, D. R., 1995, The effect of temperature and oxygen fugacity on Al-in-hornblende barometry, American Mineralogist, vol. 80, p. 549-859.

Baker, D.R. and Eggler, D.H., 1983, Fractionation paths of Atka (Aleutians) high alumina basalts: Constraints from phase relations, Journal of Volcanology and Geothermal Research, vol. 18, p. 387-404.

Beard, J.S., 1986, Characteristic mineralogy of arc-related cumulate gabbros: implications for the tectonic setting of gabbroic plutons and for andesite genesis: Geology, vol. 14, no. 10, p. 848-851.

Brown, E.H. and Walker, N.W., 1993, A magma-loading model for Barrovian metamorphism in the southeast Coast plutonic complex, British Columbia and Washington: Geological Society of America Bulletin, vol. 105, no. 4, p. 479-500.

Cater, F.W., 1982, Intrusive rocks of the Holden and Lucerne quadrangles, Washington; the relation of depth zones, composition, textures, and emplacement of plutons: U.S. Geological Survey Professional Paper, no. 1220, p. 1-115.

Cater, F.W., and Crowder, D.F., 1967, Geologic map of the Holden Quadrangle, Snohomish and Chelan Counties, Washington, U.S. Geologic Survey Quadrangle Map GQ-646.

Cater, F.W. and Wright, T.L., 1967, Geologic map of the Lucerne Quadrangle, Chelan County, Washington: U.S. Geologic Survey Geologic Quadrangle Map GQ-647.

Dawes, R.L., 1993, Mid-crustal, Late Cretaceous plutons of the North Cascades; petrogenesis and implications for the growth of continental crust [Ph.D. thesis]: University of Washington. 272 p.

Davidson, J., Turner, S., Handley, H., Macpherson, C., and Dosseto, A., 2007, Amphibole "sponge" in arc crust?: Geology, vol. 35, no. 9, p. 787-790.

DeBari, S.M., Miller, R.B., and Paterson, S.R., 1998, Genesis of Tonalitic Plutons in the Cretaceous Magmatic Arc of the North Cascades: mixing of mantle derived magmas and melting of garnet-bearing lower crust, *in* Geological Society of America, Abstracts with Programs, p. A257-A258.

DeBari, S.M. and Greene, A.R., 2011, Vertical stratification of composition, density, and inferred magmatic processes in exposed arc crustal sections *in* D. Brown and P.D. Ryan (eds.) Arc-Continent Collision, Frontiers in Earth Sciences, Springer-Verlag, Berlin, Heidelberg, 2011.

Deer, W.A., Howie, R.A., Zussman, J., 1996, An Introduction to the Rock-Forming Minerals, 2nd edition, Prentice Hall, 172 p.

Dessimoz, M., Müntener, O., and Ulmer, P., 2011, A case of hornblende dominated fractionation of arc magmas: The Chelan Complex (North Cascades, Washington), Contributions to Mineralogy and Petrology, vol. 157, p. 541-558.

Dunn, T. and Sen, C., 1994, Mineral/matrix Partition coefficients for orthopyroxene, plagioclase, and olivine in basaltic to andesitic systems: A combined analytical and experimental study, Geochimica et Cosmochimica Acta, vol. 58, p. 717-733.

El-Rahman, Y.A., Helmy, H.M, Shibata, T., Yoshikawa, M., Arai, S., Tamura, A., 2012, Mineral chemistry of the Neoproterozoic Alaskan-type Akarem Intrusion with special emphasis on amphibole: Implications for the pluton origin and evolution of subduction-related magma, Lithos, vol. 155, p. 410-425.

Ernst, W.G. and Liu, J., 1998, Experimental phase-equilibrium study of Al-and Ti contents of calcic amphibole in MORBS: A semiquantitative thermobarometer, American Mineralogist, vol. 83, p. 952-969.

Foley, S., Tiepolo, M., and Vannucci, R., 2002, Growth of early continental crust controlled by melting of amphibolite in subduction zones, Nature, vol. 417, p. 837-840.

Garrido, C.J. and Bodinier, J.L., 2005, Intracrustal Nb/Ta fractionation in island arcs due to dehydration melting of hornblende-bearing plutonics: Evidence from the Kohistan Paleo-island Arc Complex (N. Pakistan), Geophysical Research Abstracts, vol. 7, 2 pp.

Gordon, S.M., Bowring, S.A., Whitney, D.L., Miller, R.B., and McLean, N., 2010, Time scales of metamorphism, deformation, and crustal melting in a continental arc, North Cascades USA: Geological Society of America Bulletin, v. 122, no. 7,8, p. 1308-1330.

Green, T.H., and Pearson, N.J., 1987, An experimental study of Nb and Ta partitioning between Ti-rich minerals and silicate liquids at high pressure and temperature. Geochimica et Cosmochimica Acta, vol. 51, p. 55-62.

Guillong, M., Meier, D.L., Allan, M.M., Heinrich, C.A., Yardley, B.W.D., 2008, Appendix A6: SILLS: A MATLAB-based program for the reduction of laser ablation ICP-MS data of homogeneous materials and inclusions *in* Mineralogical Society of Canada short course: Laser ablation in the Earth Sciences: Current practices and outstanding issues, vol. 40, p. 328-333.

Haugerud, R.A., van der Heyden, P., Tabor, R.W., Stacey, J.S., and Zartman, R.E., 1991, Late Cretaceous and Early Tertiary plutonism and deformation in the Skagit Gneiss Complex, North Cascade Range, Washington and British Columbia: Geological Society of America Field Guide 4, p. 251-265.

Hopson, C.A. and Mattinson, J.M., 1994, Chelan Migmatite Complex, Washington: Field evidence for mafic magmatism, crustal anatexis, mixing and protodiapiric emplacement, *in* D.A. Swanson and R.A. Haugerud (eds.) Guides to Field Trips, 1994, Geological Society of America Annual Meeting, Seattle, Washington, Ch. 2K, p. 1-23.

Jagoutz, O.E., 2010, Construction of the granitoid crust of an island arc; Part II: a quantitative petrogenetic model, Contributions to Mineralogy and Petrology, vol. 160, p. 359-381.

Johnson, D. M., Hooper, P. R., and Conrey, R. M., 1999, XRF analysis of rocks and minerals for major and trace elements on a single low dilution Li-tetraborate fused bead: Advances in X-Ray Analysis, v. 41, p. 843-867.

Kay, R.W., 1978, Aleutian magnesian andesites: melts from subducted Pacific ocean crust, Journal of Volcanology and Geothermal Research, vol. 4, no. 1-2, p. 117 132.

Kelemen, P.B., Yogodzinski, G.M., Scholl, D.W., 2003a, Along-strike variation in the Aleutian Island Arc: Genesis of high Mg# andesite and implications for continental crust *in* American Geophysical Union Monograph Series, no. 138.

Kelemen, P.B., Hanghoj, K., Greene, A.R., 2003b, One view of the geochemistry of subduction-related magmatic arcs with an emphasis on primitive andesite and lower crust, Treatise on Geochemistry, vol. 3, p. 593-659.

Knaack, C., Cornelius, S.B., and Hooper, P.R., 1994, Trace element analyses of rocks and minerals by ICP-MS, March 2, 2009, <http://www.sees.wsu.edu/Geolab/note/icpms.html>.

Kodaira, S., Sato, T., Takahashi, N., Miura, S., Tamura, Y., Tatsumi, Y., and Kaneda, Y., 2007, New seismological constraints on growth of continental crust in the Izu Bonin intra-oceanic arc: Geology, vol. 35, no. 11, p. 1031-1034.

Krawczynski, M.J., Grove, T.L., Behrens, H., 2012, Amphibole stability in primitive arc magmas: effects of temperature, H_2O content, and oxygen fugacity, Contributions to Mineralogy and Petrology, vol. 164, no. 2, p. 1-27.

Larocque, J., and Canil, D., 2010, The role of amphibole in the evolution of arc magmas and crust: the case from the Jurassic Bonanaza arc section, Vancouver Island, Canada, Contributions to Mineralogy and Petrology, vol. 159, p. .475-492.

Leake, B.E., Woolley, A.R., and 20 others, 1997, Nomenclature of amphiboles: Report of the Subcommittee on Amphiboles of the International Mineralogical Association, Commission on New Minerals and Mineral Names, The Canadian Mineralogist, Vol. 35, p. 219-246.

Matzel, J.E.P., Bowring, S.A., and Miller, R.B., 2006, Time scales of pluton construction at differing crustal levels: Examples from the Mount Stuart and Tenpeak intrusions, North Cascades, Washington, Geological Society of America Bulletin: vol. 118, no. 11/12, p.1412-1430.

McCrady, K., 2013, Petrology of the Cardinal Peak pluton in the North Cascades, Washington [B.Sc. thesis]: Bellingham, Western Washington University.

McDonough, W.F. and Sun, S., 1995, The composition of the Earth, Chemical Geology, vol. 120, p. 223-254.

McPeek, S.L., Miller, R.B., Miller, J.S., and Matzel, J., 2002, Significance of fabric development in the gabbroic Riddle Peaks Pluton, North Cascades, Washington *in* Geological Society of America, Abstracts with Programs, vol. 34, no. 5, p. 96.

Miller, R.B., Bowring, S.A., and Hoppe, W.J., 1989, Paleocene plutonism and its tectonic implications, North Cascades, Washington, Geology, vol. 17, p. 846-849.

Miller, R.B. and Bowring, S.A., 1990, Structure and chronology of the Oval Peak Batholith and adjacent rocks: Implications for the Ross Lake fault zone, North Cascades, Washington: Geological Society of America Bulletin, v. 102, no. 10, p. 1361-1377.

Miller, R.B., 1994, The transitions from magmatic to high-temperature solid-state deformation: Implications from the Mount Stuart Batholith, Washington, Journal of Structural Geology, vol. 16, p. 853-865.

Miller, R.B., Haugerud, R.A., Murphy, F., and Nicholson, L.S., 1994, Tectonostratigraphic framework of the northeastern Cascades: Washington Division of Geology and Earth Resources Bulletin, vol. 80, p. 73-92.

Miller, R.G., DeBari, S.M., Paterson, S.R., Submitted Manuscript, Construction, emplacement, and geochemical evolution of deep-crustal intrusions: Tenpeak and Dirtyface plutons, North Cascades, 49 pp.

Miller, R.B., Paterson, S.R., and Matzel, J.P., 2009, Plutonism at different crustal levels: Insights from the approximately 5-40 km (paleodepth) North Cascades crustal section, Washington: Special Paper - Geological Society of America, vol. 456, p. 125-149.

Misch, P.H., 1964, Tectonic evolution of the Northern Cascades of Washington State- A west cordilleran case history, *in* A symposium on the tectonic history and mineral deposits of the western Cordillera, Vancouver, B.C.: Canadian Institute of Mining and Metallurgy Special Volume 8, p. 101-148.

Morgan, J., Abers, G., and 19 others, 2010. GeoPRISMS Draft Science Plan, <http://www.nsf-margins.org/Planning_and_review/DSP_final.html>.

Meurer, W.M., and Claeson, D.T., 2002, Evolution of crystallizing interstitial liquid in an arc-related cumulate determined by LA ICP-MS mapping of a large amphibole oikocryst, Journal of Petrology, vol. 43, no. 4, p. 607-629.

Müntener, O, Ulmer, P., Alonso-Perez, R., 2009, Experimental garnet and hornblende trace element partitioning on andesitic magmas in the deep arc crust, Geochemica et Cosmochimica Acta, vol. 73 (12S), A919.

Nielsen, R.L., Gallahan, W.E. and Newberger, F.,1992, Experimentally determined mineral-melt partition coefficients for Sc, Y and REE for olivine, orthopyroxene, pigeonite, magnetite and ilmenite, Contributions to Mineralogy and Petrology, vol.110, p. 488-499.

Parent, L.A., 1999, Petrology and Petrogenesis of the Cardinal Peak Pluton, North Cascades, Washington [M.Sc. thesis]: San Jose State University. 146 p.

Rollinson, H., 1993, Using geochemical data: evaluation, presentation, interpretation: Longman, London, ch. 4

Rudnick, R.L., and Fountain, D.M., 1995, Nature and composition of the continental crust; a lower crustal perspective: Reviews of Geophysics, vol. 33, no. 3, p. 267 309.

Rudnick, R.L., and Gao, S., 2003, Composition of the continental crust, Treatise On Geochemistry, vol. 3, p. 1-64.

Sisson, T.W., and Grove, T.L., 1993, Experimental investigations of the role of H_2O in calc alkaline differentiation and subduction zone magmatism, Contributions to Mineralogy and Petrology, vol. 113, p. 143-166.

Sun, S. and McDonough, W.F., 1989, Chemical and isotopic systematics of oceanic basalts: implications for mantle composition and processes, Geological Society, London, Special Publications, vol. 42, p. 313-345.

Tabor, R.W. Frizzell, V.A., Jr., Whetten, J.T., Waitt, R.B., Jr. Swanson, D.A., Byerly, G.R., Booth, D.B., Hetherington, M.J., and Zartman, R.E., 1987, Geologic map of the Chelan 30- by 60-minute Quadrangle, Washington: U.S. Geological Survey, scale: 1:100,00.

Tabor, R.W., Haugerud, R.A., and Miller, R.B., 1989, Overview of the geology of the North Cascades, Internationl Geologic Congress Trip T307: Washington, American Geophysical Union, 62 p.

Tatsumi, Y., 2000, Continental crust formation by delamination in subduction zones and complementary accumulation of the enriched mantle I component in the mantle, Geochemistry, Geophysics,Geosystems, vol. 1, p. 1-17.

Taylor, S.R. and McLennan, S.M., 1995, The geochemical evolution of the continental crust, Reviews in Geophysics, vol. 33, p. 241-265.

Tiepolo, M., Oberti, R., Zanetti, A., Vannucci, R., Foley, S.F., 2007, Trace-element partitioning between amphibole and silicate melt, In: Hawthrone, F.C., Oberti, R., Della Ventura, G., Mottana, A. (eds), *Amphiboles: Crystal Chemistry, Occurrence and Health Issues. Mineralogical Society of American and Geochemical Society, Reviews in Mineralogy and Geochemistry,* vol., 67, p. 417-452.

Tiepolo, M. and Tribuzio, R., 2008, Petrology and U-Pb zircon geochronology of amphibole-rich cumulates with sanukitic affinity from Husky Ridge (Northern Victoria Land, Antarctica): Insights into the role of amphibole in the petrogenesis of subduction-related magmas, Journal of Petrology, vol. 49, p. 937-970.

Tiepolo, M., Tribuzio, R., Langone, A., 2011, High-Mg andesite petrogenesis by amphibole crystallization and ultramafic crust assimilation: Evidence from the Adamello hornblendites (Central Alps, Italy), Journal of Petrology, vol. 52, no. 5, p. 1011-1045.

Tiepolo, M., Langone, A., Morishita, T., Yuhara, M., 2012, On the recycling of amphibole-rich ultramafic intrusive rocks in the arc crust: Evidence from Shikanoshima Island (Kyushu, Japan), Journal of Petrology, vol. 53, no. 6, p. 1255-1285

Table 1. Whole rock major and trace element compositions.

Layered Gabbro										
Sample	Rlg-2	Rlg-38	Rlg-39	Rlg-40	Rlg-41	Rlg-42	Rlg-43	Rlg-44	Rlg-45	Rlg-46
Major element oxides (wt%) analyzed by XRF										
SiO_2	43.72	43.15	43.21	42.86	42.67	42.74	44.77	43.66	42.75	42.35
TiO_2	1.773	2.411	1.696	2.322	2.391	2.283	1.490	2.254	2.235	2.417
Al_2O_3	19.26	11.88	20.01	15.67	15.09	14.96	23.51	14.86	14.73	13.04
FeO	11.15	14.05	10.32	12.12	12.32	11.99	10.82	12.78	11.66	12.90
MnO	0.132	0.181	0.114	0.138	0.134	0.140	0.138	0.153	0.141	0.155
MgO	8.60	12.97	8.05	12.03	12.63	12.53	4.28	12.18	13.67	13.95
CaO	11.95	11.96	12.26	11.37	11.29	11.39	12.04	10.97	11.20	11.12
Na_2O	2.31	1.66	2.28	2.38	2.32	2.37	2.18	2.47	2.41	2.30
K_2O	0.30	0.32	0.24	0.39	0.40	0.35	0.53	0.52	0.41	0.37
P_2O_5	0.033	0.203	0.040	0.021	0.024	0.022	0.092	0.043	0.022	0.026
Total	99.23	98.79	98.21	99.32	99.27	98.78	99.85	99.88	99.23	98.64
Mg#	57.9	62.2	58.2	63.9	64.6	65.2	65.7	62.9	67.6	65.8
Trace elements (ppm) analyzed by XRF										
Ni	61.18	133.16	66.33	82.86	89.99	96.23	122.56	94.35	142.66	103.85
Cr	45.24	339.77	40.29	48.91	70.09	134.84	258.89	44.15	276.01	110.98
Sc	50.89	74.84	48.11	73.95	76.03	71.38	86.92	68.11	81.28	84.74
V	342.84	464.90	359.87	535.49	568.95	538.16	536.68	462.53	514.11	552.62
Cu	60.69	81.77	55.94	92.37	67.91	61.88	63.56	58.31	50.99	37.62
Zn	77.62	108.21	67.62	80.49	80.59	86.23	90.88	95.83	69.89	82.76
Trace elements (ppm) analyzed by ICP-MS										
La		3.71	2.45	2.32			2.24		2.03	
Ce		12.86	7.04	8.31			8.78		7.86	
Pr		2.44	1.26	1.79			1.84		1.68	
Nd		14.39	7.52	11.45			11.33		10.66	
Sm		4.94	2.75	4.49			4.44		4.11	
Eu		1.65	1.14	1.60			1.53		1.50	
Gd		5.94	3.51	5.80			5.62		5.45	
Tb		0.94	0.58	0.97			0.95		0.92	
Dy		5.53	3.49	5.82			5.78		5.69	
Ho		1.05	0.69	1.13			1.16		1.16	
Er		2.65	1.71	2.80			2.96		2.95	
Yb		2.04	1.31	2.07			2.24		2.20	
Lu		0.30	0.19	0.30			0.32		0.32	
Ba		70.50	69.69	150.27			85.52		133.51	
Th		0.12	0.08	0.06			0.08		0.06	
Nb		1.95	1.10	1.93			2.50		2.07	
Y		24.82	16.04	26.58			27.45		26.80	
Hf		1.54	0.84	1.34			1.34		1.33	
Ta		0.10	0.07	0.10			0.16		0.11	
U		0.05	0.03	0.02			0.03		0.02	
Pb		0.73	1.13	0.73			0.75		0.72	
Rb		1.27	1.59	2.80			1.54		2.43	
Cs		0.03	0.25	0.05			0.02		0.07	
Sr		145.96	687.35	345.59			242.92		367.03	
Zr		37.42	20.69	27.42			29.70		29.50	

All analyses performed at WSU's GeoAnalytical Lab. Fe is reported as FeO. Mg# is calculated by $Mg\#=Mg/(Mg+Fe^{2+})*100$. Full discussion of precision and accuracy are presented in Methods section.

Table 1. (Cont.). Whole rock major and trace element compositions.

Massive Gabbro										
Sample	Rg-8	Rg-9	Rg-10	Rg-12	Rg-13	Rg-14	Rg-15	Rg-	Rg-	Rg-19
Major element oxides (wt%) analyzed by XRF										
SiO_2	42.95	42.55	42.18	41.84	40.18	42.26	44.03	44.96	44.60	45.69
TiO_2	1.756	1.689	1.491	1.764	2.200	1.774	1.520	1.606	1.540	1.425
Al_2O_3	21.25	21.48	22.71	21.04	18.92	21.19	22.75	20.62	21.85	22.21
FeO	14.41	14.43	13.93	13.08	16.13	14.64	11.41	10.66	9.01	9.17
MnO	0.118	0.112	0.091	0.110	0.135	0.120	0.086	0.117	0.104	0.094
MgO	4.93	4.29	4.20	5.80	7.37	5.87	4.08	7.01	7.11	6.66
CaO	10.80	11.21	12.15	11.48	11.28	11.62	11.30	11.64	12.71	12.59
Na_2O	2.75	2.74	2.45	2.42	2.17	2.44	2.93	2.72	2.34	2.50
K_2O	0.29	0.19	0.28	0.18	0.22	0.19	0.14	0.21	0.25	0.27
P_2O_5	0.146	0.399	0.024	0.024	0.023	0.026	0.029	0.027	0.026	0.020
Total	99.41	99.09	99.52	97.73	98.62	100.1	98.27	99.58	99.54	100.6
Mg#	37.90	34.62	34.97	44.16	44.88	41.66	38.95	53.96	58.44	56.41
Trace elements (ppm) analyzed by XRF										
Ni	12.77	2.28	13.56	2.38	13.17	15.84	7.23	13.07	19.70	24.35
Cr	17.92	5.25	23.76	6.24	7.13	25.94	5.64	21.78	28.02	66.92
Sc	24.26	21.48	22.47	32.97	40.10	33.17	24.55	40.00	44.35	43.36
V	323.3	312.25	416.0	418.87	587.5	428.27	382.83	326.0	332.0	325.7
Cu	24.26	39.70	93.06	69.10	74.55	83.85	37.32	54.35	34.75	58.41
Zn	117.7	100.39	75.83	99.59	112.6	100.88	79.99	78.90	63.56	64.15
Trace elements (ppm) analyzed by ICP-MS										
La				2.40						
Ce				6.40						
Pr				1.10						
Nd				6.36						
Sm				2.34						
Eu				1.01						
Gd				2.89						
Tb				0.48						
Dy				2.91						
Ho				0.58						
Er				1.47						
Yb				1.15						
Lu				0.16						
Ba				109.81						
Th				0.10						
Nb				1.04						
Y				13.63						
Hf				0.68						
Ta				0.06						
U				0.06						
Pb				1.82						
Rb				4.35						
Cs				0.25						
Sr				832.60						
Zr				16.73						

All analyses performed at WSU's GeoAnalytical Lab. Fe is reported as FeO. Mg# is calculated by $Mg\#=Mg/(Mg+Fe^{2+})*100$. Full discussion of precision and accuracy are presented in Methods section.

Table 1. (Cont.) Whole rock major and trace element compositions.

Massive Gabbro										
Sample	Rg-20	Rg-21	Rg-26	Rg-27	Rg-28	Rg-29	Rg-30	Rg-31	Rg-32	Rg-33
Major element oxides (wt%) analyzed by XRF										
SiO_2	45.66	46.48	43.08	42.88	45.46	42.94	43.99	46.77	44.45	47.02
TiO_2	1.545	1.591	1.811	2.382	1.568	1.834	2.016	1.188	1.268	1.138
Al_2O_3	21.75	21.12	19.19	13.20	21.63	20.82	21.50	22.76	22.34	22.83
FeO	9.92	8.82	10.19	13.03	9.38	13.86	12.32	8.56	12.25	9.86
MnO	0.099	0.102	0.128	0.156	0.119	0.141	0.125	0.096	0.107	0.095
MgO	6.40	6.52	8.73	14.03	6.79	5.18	5.83	5.31	3.83	3.40
CaO	12.28	11.73	12.04	11.35	12.38	10.72	11.77	12.15	10.93	11.01
Na_2O	2.46	2.69	2.28	2.28	2.13	2.15	2.41	2.67	3.09	3.50
K_2O	0.29	0.30	0.24	0.39	0.49	0.74	0.31	0.35	0.22	0.26
P_2O_5	0.068	0.124	0.026	0.022	0.037	0.048	0.118	0.034	0.094	0.416
Total	100.48	99.49	97.73	99.71	99.97	98.43	100.38	99.89	98.58	99.52
Mg#	53.49	56.85	60.43	41.36	56.34	39.95	45.77	52.52	35.78	38.08
Trace elements (ppm) analyzed by XRF										
Ni	24.85	23.17	15.74	16.14	44.15	20.89	10.89	17.92	86.72	38.91
Cr	27.42	18.91	18.41	24.55	58.11	11.98	16.34	39.60	30.00	16.53
Sc	34.55	36.43	49.80	21.09	39.60	26.53	31.38	24.35	15.84	16.93
V	322.15	302.15	339.97	200.97	318.98	352.14	340.16	232.95	282.25	239.28
Cu	69.10	40.59	50.89	74.35	22.67	103.95	68.11	36.63	36.33	48.61
Zn	78.01	69.80	74.25	95.83	89.20	122.36	106.82	66.13	100.09	89.99
Trace elements (ppm) analyzed by ICP-MS										

All analyses performed at WSU's GeoAnalytical Lab. Fe is reported as FeO. Mg# is calculated by $Mg\#=Mg/(Mg+Fe^{2+})*100$. Full discussion of precision and accuracy are presented in Methods section.

Table 1. (Cont.) Whole rock major and trace element compositions.

Massive Gabbro								
Sample	Rg-34	Rg-35	Rg-36	Rg-47	Rg-48	Rg-49	Rg-50	Rg-51
Major element oxides (wt%) analyzed by XRF								
SiO_2	44.70	44.45	45.83	44.43	44.27	43.00	42.56	44.77
TiO_2	1.720	1.255	1.375	1.710	1.358	2.081	1.877	1.505
Al_2O_3	19.42	22.36	20.73	19.52	22.49	18.30	20.37	22.09
FeO	14.30	12.78	11.07	10.43	8.80	14.30	14.88	8.76
MnO	0.140	0.109	0.136	0.117	0.099	0.147	0.134	0.094
MgO	5.85	3.58	6.63	8.16	5.65	8.60	6.83	7.48
CaO	10.61	11.06	11.89	12.04	12.59	11.33	11.54	12.96
Na_2O	2.85	3.11	2.63	2.38	2.44	2.39	2.32	2.18
K_2O	0.34	0.28	0.34	0.28	0.25	0.28	0.27	0.26
P_2O_5	0.233	0.341	0.081	0.034	0.050	0.029	0.028	0.020
Total	100.16	99.33	100.71	99.11	98.00	100.46	100.82	100.12
Mg#	42.18	33.31	51.61	58.23	53.36	51.74	44.99	60.33
Trace elements (ppm) analyzed by XRF								
Ni	51.48	95.54	65.93	61.28	40.79	42.77	35.94	69.00
Cr	19.60	34.55	38.12	31.88	24.75	21.68	23.96	61.48
Sc	29.40	17.13	31.88	46.33	33.26	47.82	37.22	45.34
V	328.88	286.21	243.54	360.06	288.39	475.50	448.07	327.99
Cu	42.57	40.79	77.81	61.78	43.96	75.14	68.61	67.62
Zn	126.72	102.37	92.17	73.26	62.37	96.23	94.15	56.83
Trace elements (ppm) analyzed by ICP-MS								
La		4.17	3.89		2.75			
Ce		11.13	12.11		8.20			
Pr		1.93	2.27		1.47			
Nd		10.73	13.29		8.73			
Sm		3.44	4.77		3.16			
Eu		1.35	1.59		1.28			
Gd		4.10	5.62		4.15			
Tb		0.65	0.92		0.69			
Dy		3.85	5.48		4.19			
Ho		0.76	1.06		0.85			
Er		1.95	2.74		2.11			
Yb		1.46	2.11		1.66			
Lu		0.21	0.31		0.23			
Ba		116.75	103.51		84.70			
Th		0.27	0.24		0.11			
Nb		1.44	2.45		1.28			
Y		17.93	25.46		19.74			
Hf		1.11	1.50		0.92			
Ta		0.09	0.14		0.07			
U		0.14	0.13		0.05			
Pb		1.53	1.99		1.41			
Rb		3.16	3.18		2.19			
Cs		0.10	0.31		0.13			
Sr		1067	707.3		643.5			
Zr		28.71	34.16		15.25			

All analyses performed at WSU's GeoAnalytical Lab. Fe is reported as FeO. Mg# is calculated by $Mg\#=Mg/(Mg+Fe^{2+})*100$. Full discussion of precision and accuracy are presented in Methods section.

Table 2. Amphibole major element analyses by electron microprobe.

Layered Gabbro												
Sample	SiO_2	TiO_2	Al_2O_3	FeO	MnO	MgO	CaO	Na_2O	K_2O	Cr_2O_3	Total	Mg#
Rg-38-2-1	41.84	4.61	12.01	12.49	0.17	13.35	11.06	1.90	0.32	0.05	97.81	65.59
Rg-38-2-2	45.04	1.01	13.16	12.98	0.17	13.47	11.64	2.04	0.37	0.09	99.96	64.91
Rg-38-2-3	45.03	0.95	12.90	12.94	0.17	13.50	11.50	1.99	0.37	0.09	99.44	65.04
Rg-38-4-1	45.62	1.01	12.00	12.60	0.13	14.14	11.71	1.85	0.31	0.02	99.39	66.67
Rg-38-4-2	43.09	3.73	12.33	12.92	0.16	13.26	11.05	1.86	0.29	0.00	98.69	64.65
Rg-38-4-3	44.31	1.43	13.15	12.89	0.13	13.36	11.52	2.17	0.38	0.02	99.37	64.88
Rg-38-5-1	46.06	0.94	12.26	13.28	0.19	13.79	11.69	1.88	0.32	0.11	100.52	64.93
Rg-38-5-2	45.52	1.00	12.22	13.12	0.17	13.85	11.64	1.82	0.29	0.05	99.69	65.29
Rg-38-5-3	43.75	1.22	13.41	13.81	0.18	13.09	11.55	1.99	0.41	0.05	99.46	62.82
Rg-38-6-1	45.01	1.48	11.43	13.45	0.18	13.57	11.83	1.78	0.36	0.02	99.11	64.26
Rg-38-6-3	42.30	4.11	12.44	13.15	0.15	12.58	11.13	1.86	0.36	0.05	98.12	63.02
Rg-40-1-1	43.22	1.95	13.87	12.44	0.17	13.73	11.15	2.62	0.41	0.00	99.56	66.30
Rg-40-1-2	43.53	2.16	13.61	12.46	0.15	13.76	11.05	2.56	0.36	0.03	99.66	66.31
Rg-40-1-3	43.31	2.15	13.75	12.47	0.17	13.77	11.10	2.66	0.38	0.00	99.77	66.31
Rg-40-1-4	43.87	2.38	13.80	12.08	0.11	13.78	11.15	2.43	0.35	0.01	99.96	67.04
Rg-40-2-1	43.27	1.84	14.03	12.67	0.11	13.70	11.16	2.55	0.44	0.03	99.79	65.85
Rg-40-2-2	43.68	1.81	13.99	12.98	0.17	13.19	11.15	2.45	0.37	0.00	99.79	64.44
Rg-40-2-3	43.50	1.04	14.88	12.28	0.15	13.56	11.41	2.39	0.31	0.00	99.51	66.32
Rg-40-3-1	43.80	2.23	13.51	12.36	0.17	13.84	10.91	2.62	0.43	0.00	99.87	66.62
Rg-40-3-2	43.69	2.27	13.42	12.20	0.16	13.75	10.97	2.53	0.42	0.04	99.44	66.75
Rg-40-3-3	43.72	1.84	14.06	11.87	0.15	13.83	11.22	2.45	0.37	0.00	99.52	67.51
Rg-40-4-1	43.75	2.28	13.62	12.10	0.14	13.85	11.05	2.57	0.38	0.00	99.72	67.11
Rg-40-4-2	42.90	2.03	13.72	11.86	0.10	14.01	11.10	2.52	0.40	0.01	98.66	67.80
Rg-40-4-3	43.74	2.10	13.78	12.03	0.14	13.98	11.08	2.64	0.39	0.00	99.87	67.46
Rg-40-4-4	43.21	2.28	13.76	12.36	0.13	13.82	10.97	2.67	0.42	0.00	99.61	66.61
Rg-40-4-5	43.33	2.27	13.58	11.87	0.13	13.88	11.13	2.65	0.39	0.00	99.22	67.56
Rg-40-5-1	43.40	1.52	14.30	12.23	0.12	13.83	11.34	2.57	0.44	0.01	99.75	66.84
Rg-40-5-2	43.36	1.93	14.08	12.03	0.14	13.82	11.36	2.53	0.41	0.01	99.67	67.18
Rg-40-5-3	42.73	4.44	12.44	12.36	0.19	14.10	10.88	2.35	0.36	0.00	99.84	67.05
Rg-40-5-4	44.34	1.64	13.63	11.71	0.16	14.18	11.30	2.37	0.38	0.00	99.71	68.34
Rg-40-6-1	43.50	2.22	13.79	12.66	0.19	13.40	11.09	2.64	0.36	0.00	99.85	65.36
Rg-40-7-1	43.39	1.56	13.77	12.26	0.16	13.86	11.09	2.43	0.35	0.00	98.87	66.85
Rg-40-7-2	43.63	2.24	13.79	11.58	0.10	14.03	11.28	2.37	0.39	0.00	99.43	68.35
Rg-40-7-3	43.29	1.71	13.96	12.15	0.16	13.92	11.23	2.52	0.39	0.00	99.32	67.13
Rg-40-7-4	43.02	2.25	13.93	12.06	0.17	13.84	11.17	2.72	0.39	0.02	99.55	67.17
Rg-43-1-1	45.03	1.63	13.07	11.88	0.13	14.12	11.03	2.20	0.45	0.11	99.63	67.94
Rg-43-1-2	43.67	2.18	13.43	12.17	0.18	13.97	10.96	2.32	0.51	0.00	99.38	67.17
Rg-43-1-3	43.64	2.03	13.48	11.98	0.16	13.93	10.93	2.31	0.51	0.07	99.05	67.46
Rg-43-1-4	44.44	2.04	13.02	11.89	0.13	14.12	10.85	2.42	0.57	0.07	99.55	67.91
Rg-43-1-5	44.25	2.11	13.40	12.08	0.15	13.96	10.78	2.36	0.44	0.09	99.63	67.32
Rg-43-2-1	43.15	1.79	12.39	12.76	0.13	13.39	10.26	2.13	0.46	0.02	96.48	65.17
Rg-43-2-2	44.45	1.35	13.69	11.68	0.14	14.19	11.22	2.29	0.44	0.07	99.52	68.40
Rg-43-2-3	45.71	1.88	12.56	11.92	0.13	14.26	10.95	2.20	0.49	0.00	100.10	68.07
Rg-43-2-4	43.77	1.97	13.44	12.53	0.16	13.80	11.25	2.30	0.52	0.05	99.79	66.25
Rg-43-3-1	44.36	1.83	12.67	11.98	0.16	14.47	10.99	2.31	0.38	0.13	99.27	68.29
Rg-43-3-2	44.10	1.99	13.09	12.38	0.14	14.22	10.90	2.41	0.44	0.04	99.70	67.19
Rg-43-3-3	44.16	2.68	13.08	12.10	0.14	14.08	10.90	2.38	0.56	0.01	100.10	67.48
Rg-43-4-1	44.10	1.85	13.55	12.27	0.15	13.97	11.10	2.36	0.46	0.04	99.84	67.00
Rg-43-4-2	44.01	1.41	13.59	12.02	0.17	14.24	11.26	2.35	0.41	0.04	99.51	67.85
Rg-43-4-3	43.68	1.89	13.62	12.27	0.17	14.02	11.12	2.37	0.51	0.05	99.71	67.07
Rg-43-5-1	44.18	1.17	13.63	12.04	0.16	14.18	11.31	2.30	0.42	0.18	99.59	67.73
Rg-43-5-2	43.67	1.74	13.57	12.22	0.13	13.95	11.11	2.40	0.40	0.05	99.24	67.05
Rg-43-5-3	44.74	1.93	12.57	11.90	0.15	14.40	10.93	2.32	0.41	0.01	99.36	68.32
Rg-43-6-1	43.58	1.62	13.63	12.35	0.17	13.92	11.12	2.40	0.35	0.15	99.28	66.77
Rg-43-6-2	43.60	1.46	13.76	12.10	0.09	14.01	11.09	2.42	0.47	0.12	99.12	67.36
Rg-43-6-3	45.26	1.19	13.24	11.49	0.12	14.77	11.32	2.36	0.42	0.16	100.33	69.61
Rg-45-1-1	43.67	1.99	13.71	11.36	0.15	14.63	11.20	2.32	0.38	0.03	99.45	69.65
Rg-45-1-2	43.76	2.02	13.74	11.50	0.14	14.72	11.22	2.39	0.38	0.02	99.89	69.54
Rg-45-1-3	43.70	1.97	13.77	11.32	0.10	14.66	11.15	2.54	0.42	0.05	99.66	69.77
Rg-45-1-4	43.63	2.01	13.82	11.48	0.09	14.64	11.16	2.42	0.38	0.05	99.69	69.46
Rg-45-2-1	43.16	2.02	13.80	11.42	0.16	14.58	11.05	2.40	0.40	0.08	99.08	69.47

All analyses performed at OSU's Electron Microprobe Lab. Fe is reported as FeO. Mg# is calculated by $Mg\#=Mg/(Mg+Fe^{2+})*100$.

Table 2. (Cont.) Amphibole major element analyses by electron microprobe.

Sample	SiO_2	TiO_2	Al_2O_3	FeO	MnO	MgO	CaO	Na_2O	K_2O	Cr_2O_3	Total	Mg#
Rg-45-2-3	43.34	1.96	13.79	11.54	0.13	14.61	11.07	2.44	0.44	0.09	99.39	69.29
Rg-45-3-1	42.94	1.97	13.78	11.44	0.12	14.68	11.06	2.43	0.40	0.10	98.92	69.57
Rg-45-3-2	43.83	2.02	13.81	11.41	0.12	14.64	11.12	2.55	0.38	0.04	99.93	69.58
Rg-45-3-3	43.58	2.04	13.83	11.25	0.12	14.61	11.11	2.47	0.36	0.05	99.41	69.85
Rg-45-3-4	43.00	2.02	13.98	11.36	0.16	14.42	11.17	2.51	0.42	0.11	99.14	69.35
Rg-45-3-5	43.75	2.02	13.70	11.45	0.14	14.47	11.11	2.42	0.45	0.11	99.61	69.25
Rg-45-3-6	43.79	1.98	13.85	11.37	0.14	14.56	11.23	2.54	0.34	0.01	99.81	69.54
Rg-45-4-1	43.69	1.63	14.32	11.34	0.15	13.99	11.32	2.44	0.40	0.07	99.36	68.74
Rg-45-4-2	44.17	1.94	14.13	11.70	0.13	14.08	11.17	2.46	0.42	0.11	100.30	68.20
Rg-45-5-1	43.38	1.99	13.71	11.49	0.16	14.55	11.00	2.54	0.42	0.05	99.30	69.29
Rg-45-5-2	44.03	1.45	13.90	11.59	0.17	14.66	11.03	2.45	0.41	0.03	99.70	69.28
Rg-45-5-3	43.72	2.06	13.55	11.66	0.10	14.52	11.05	2.60	0.36	0.07	99.68	68.94
Rg-45-5-4	43.15	1.78	13.80	11.63	0.15	14.57	11.18	2.52	0.42	0.05	99.25	69.06
Massive Gabbro												
Rg-36-1-1	45.13	1.02	13.29	14.58	0.22	12.82	11.41	1.67	0.34	0.02	100.48	61.05
Rg-36-1-2	44.99	1.01	13.10	14.33	0.21	12.77	11.45	1.63	0.42	0.06	99.98	61.37
Rg-36-1-3	45.59	0.97	12.58	14.27	0.16	13.22	11.38	1.57	0.42	0.00	100.15	62.28
Rg-36-2-1	44.58	1.05	13.49	14.51	0.17	12.41	11.31	1.68	0.33	0.00	99.55	60.40
Rg-36-2-2	43.43	2.29	12.72	13.71	0.18	12.11	12.11	1.47	0.30	0.00	98.31	61.16
Rg-36-2-3	44.96	0.89	13.04	13.90	0.14	13.09	11.17	1.68	0.42	0.00	99.29	62.67
Rg-36-3-1	43.98	1.00	13.94	14.74	0.26	12.34	11.20	1.78	0.36	0.00	99.59	59.88
Rg-36-3-2	44.21	0.90	13.85	13.77	0.24	13.17	10.56	1.59	1.04	0.00	99.33	63.03
Rg-36-3-3	45.41	0.87	13.26	14.03	0.20	12.99	11.37	1.65	0.39	0.02	100.19	62.27
Rg-36-4-1	45.06	0.97	13.13	14.62	0.24	12.73	11.37	1.66	0.47	0.01	100.26	60.82
Rg-36-4-2	44.54	1.25	13.34	14.66	0.22	12.47	11.26	1.71	0.56	0.01	100.00	60.24
Rg-36-4-3	42.84	0.90	14.78	14.61	0.20	12.13	11.56	1.85	0.40	0.01	99.27	59.66
Rg-36-4-4	45.42	0.71	12.61	14.11	0.20	13.15	11.60	1.61	0.39	0.00	99.81	62.43
Rg-36-5-1	44.84	0.91	13.49	14.59	0.19	12.67	11.42	1.67	0.40	0.00	100.18	60.75
Rg-36-5-2	44.76	1.21	13.56	14.52	0.16	12.65	11.50	1.65	0.46	0.01	100.48	60.83
Rg-36-5-3	44.85	1.10	13.59	14.28	0.16	12.64	11.48	1.63	0.55	0.02	100.30	61.20
Rg-36-5-4	44.22	0.91	13.39	14.04	0.20	12.77	11.47	1.68	0.49	0.00	99.17	61.85
Rg-36-5-5	44.92	0.86	13.29	14.19	0.17	12.71	11.33	1.56	0.35	0.00	99.38	61.48
Rg-36-5-6	45.05	0.85	13.29	13.93	0.20	12.99	11.59	1.69	0.36	0.00	99.93	62.44
Rg-39-1-1	45.28	0.90	13.83	12.99	0.15	13.28	11.45	2.12	0.30	0.00	100.29	64.57
Rg-39-1-2	44.03	0.75	14.55	13.66	0.14	12.91	11.31	2.31	0.35	0.03	100.05	62.75
Rg-39-1-3	44.33	1.38	15.08	12.81	0.16	12.91	11.38	2.25	0.43	0.01	100.75	64.25
Rg-39-2-1	43.60	1.37	14.13	13.38	0.15	12.79	11.08	2.21	0.35	0.00	99.06	63.02
Rg-39-2-2	44.43	0.80	14.25	13.11	0.16	13.35	11.19	2.17	0.37	0.00	99.83	64.48
Rg-39-2-3	43.99	1.04	14.06	13.43	0.16	12.91	11.22	2.25	0.32	0.03	99.41	63.16
Rg-39-2-4	44.01	1.89	13.93	13.51	0.13	12.53	10.98	2.21	0.33	0.02	99.54	62.33
Rg-39-2-5	44.48	0.99	14.26	12.77	0.16	13.31	11.20	2.12	0.34	0.02	99.65	65.00
Rg-39-3-1	43.83	0.94	14.37	13.24	0.15	13.17	11.33	2.12	0.31	0.04	99.49	63.94
Rg-39-3-2	43.34	2.44	13.43	14.30	0.16	12.69	10.86	2.09	0.27	0.01	99.59	61.26
Rg-39-3-3	44.45	1.20	13.89	13.31	0.16	13.17	11.25	2.23	0.30	0.00	99.95	63.81
Rg-39-4-1	43.37	0.97	14.53	13.19	0.16	13.10	11.24	2.23	0.36	0.02	99.18	63.91
Rg-39-4-2	43.42	1.21	14.43	13.52	0.13	12.84	11.34	2.23	0.41	0.01	99.52	62.87
Rg-39-4-3	44.64	1.12	13.73	12.98	0.15	13.40	11.31	2.12	0.34	0.01	99.79	64.78
Rg-39-5-1	44.70	1.80	13.65	13.15	0.10	13.25	11.33	2.09	0.32	0.00	100.38	64.23
Rg-39-5-2	44.33	0.97	14.39	13.44	0.12	13.04	11.32	2.18	0.37	0.00	100.16	63.36
Rg-39-5-3	43.92	2.41	13.64	13.01	0.17	13.18	11.05	2.15	0.34	0.00	99.89	64.37
Rg-39-5-4	42.60	2.30	14.42	13.84	0.17	12.42	10.92	2.52	0.39	0.01	99.60	61.55
Rg-48-1-1	43.88	1.54	13.88	14.28	0.21	12.47	11.11	2.17	0.47	0.08	100.09	60.88
Rg-48-1-2	44.38	0.95	13.67	13.84	0.22	13.01	11.36	2.03	0.37	0.00	99.84	62.61
Rg-48-1-3	43.30	1.67	14.28	14.44	0.21	12.40	11.30	2.15	0.45	0.00	100.20	60.50
Rg-48-2-1	43.56	1.16	14.31	13.54	0.14	13.03	11.66	2.07	0.47	0.00	99.93	63.17
Rg-48-2-2	43.01	1.34	14.36	13.66	0.17	12.87	11.65	2.15	0.35	0.05	99.61	62.68
Rg-48-2-3	42.93	0.84	15.18	13.84	0.18	12.58	11.60	2.19	0.45	0.00	99.79	61.84
Rg-48-2-4	42.02	0.39	16.66	14.56	0.16	12.16	11.57	2.42	0.36	0.00	100.29	59.81
Rg-48-3-1	41.38	0.64	17.32	14.02	0.18	11.66	11.68	2.24	0.44	0.03	99.60	59.71
Rg-48-3-2	43.43	1.29	14.25	13.68	0.20	12.79	11.37	2.11	0.41	0.00	99.52	62.50
Rg-48-3-3	42.59	2.26	13.26	15.08	0.23	12.75	10.98	1.93	0.35	0.00	99.44	60.12
Rg-48-3-4	43.69	0.90	14.39	14.25	0.17	12.64	11.37	2.12	0.43	0.00	99.97	61.25
Rg-48-4-1	43.68	0.93	14.45	14.52	0.18	12.42	11.23	2.14	0.39	0.00	99.92	60.39
Rg-48-4-2	44.18	0.98	14.25	14.55	0.18	12.58	11.27	2.18	0.37	0.00	100.54	60.66
Rg-48-4-3	43.94	1.01	14.09	13.99	0.20	12.72	11.21	2.05	0.37	0.03	99.62	61.84

Table 3. Amphibole trace element data determined by LA-ICP-MS.

Layered Gabbro																					
Sample	Li	P	Sc	V	Cr	Co	Ni	Cu	Zn	Ga	Rb	Sr	Y	Zr	Nb	Cs	Ba	Hf	Ta	Pb	U	Th
Rg-38-2-1	4.54	86.5	74.1	501	362	50.6	113	89.4	128	19.7	2.05	122	23.0	29.2	2.13	0.04	80.8	1.54	0.10	0.80	0.02	-
Rg-38-2-2	3.78	124	75.9	545	339	55.4	108	3.3	129	19.3	1.26	179	25.6	38.8	2.95	0.02	93.3	1.80	0.13	0.62	0.02	-
Rg-38-2-3	8.86	63.1	82.4	709	775	53.3	107	1.3	115	17.1	1.52	216	18.6	20.7	1.58	0.02	91.7	0.85	0.08	0.56	0.03	-
Rg-38-4-1	5.72	68.3	69.8	520	443	54.8	111	19.0	127	18.7	1.39	133	21.3	26.7	2.05	0.02	68.6	1.23	0.09	0.64	0.02	-
Rg-38-4-2	9.25	142	72.1	654	317	53.5	96.5	21.8	117	18.6	1.16	196	24.5	30.4	2.29	0.03	94.1	1.47	0.10	0.72	0.04	-
Rg-38-4-3	14.9	113	74.9	588	290	65.7	112	33.7	143	21.6	1.44	221	26.6	34.9	2.83	0.03	99.3	1.45	0.13	0.70	0.03	-
Rg-38-5-1	3.53	122	73.3	515	392	62.9	121	74.3	118	20.0	1.42	152	22.8	26.8	2.33	0.02	78.5	1.35	0.10	0.74	0.08	-
Rg-38-5-2	3.31	90.1	69.2	537	337	61.5	11	40.5	121	18.9	1.58	167	22.6	29.3	2.26	0.02	85	1.24	0.08	0.82	0.29	-
Rg-38-5-3	6.69	72.5	78.3	585	572	56.7	93.4	6.4	121	19.6	1.45	203	22.4	29.1	1.96	0.02	96.6	1.22	0.12	0.67	0.03	-
Rg-38-6-1	3.24	132	68.1	472	291	66.7	131	111	125	19.7	3.07	145	22.1	36.6	2.14	0.10	94.2	1.62	0.08	0.99	0.04	-
Rg-38-6-2	4.25	86.4	67.5	478	310	62.4	119	65.6	115	18.6	1.63	127	19.4	24.4	1.80	0.06	84	1.11	0.08	0.62	0.02	-
Rg-38-6-3	6.79	80.8	67.3	522	387	56.5	94.8	6.2	111	18.9	1.25	141	20.7	27.8	2.01	0.02	82.3	1.07	0.09	0.68	0.03	-
Rg-40-1-1	5.42	105	74.5	588	38.0	53.9	46.3	1.6	86.5	19.2	2.17	232	27.0	29.3	2.80	0.35	95.5	1.96	0.43	1.12	0.47	0.50
Rg-40-1-2	4.12	80.1	83.2	655	177	57.8	51.3	2.1	87.7	18.8	1.74	264	23.7	25.4	2.35	0.36	92.4	1.36	0.61	3.28	0.59	0.59
Rg-40-2-1	4.46	130	85.1	690	41.6	63.2	53.4	1.0	98.4	21.5	1.85	257	28.5	34.6	2.34	0.11	102	1.66	0.13	0.60	0.08	0.12
Rg-40-2-3	3.85	94.3	79.3	629	45.4	52.0	71.6	5.6	96.9	19.5	1.82	245	27.2	30.2	2.15	0.16	95.8	1.47	0.10	0.72	1.69	0.24
Rg-40-3-1	4.52	111	76.6	603	33.9	50.5	49.0	2.9	89.4	19.5	3.40	243	26.5	37.1	2.10	0.17	116	1.43	0.36	1.01	0.10	0.13
Rg-40-3-2	4.25	122	81.1	655	52.0	56.7	47.0	0.7	89.9	19.5	1.45	248	26.1	30.6	2.28	0.11	93.8	1.35	0.11	0.49	0.17	0.04
Rg-40-4-4	4.47	95.0	78.3	636	40.3	48.0	43.2	0.9	89.9	19.6	1.52	242	26.1	29.9	2.32	0.05	96.9	1.33	0.12	0.52	0.08	0.09
Rg-40-4-5	5.04	110	80.6	642	36.9	51.8	47.5	0.8	86.8	17.9	1.72	238	25.5	29.6	2.25	0.08	91.3	1.31	0.14	0.44	0.04	0.05
Rg-40-4-6	3.48	102	78.7	632	54.6	52.4	45.1	5.5	86.2	18.3	2.00	243	25.6	29.6	2.23	0.06	94.5	1.42	0.11	0.54	0.09	0.05
Rg-43-1-1	5.33	164	83.8	644	252	56.2	100	17.3	116	18.1	2.34	276	26.4	27.2	3.16	0.04	119	1.26	0.16	0.91	0.05	-
Rg-43-1-2	5.69	93.3	79.7	633	575	56.5	92.0	10.7	115	18.5	2.37	273	25.3	35.0	2.75	0.04	105	1.33	0.13	0.92	0.07	-
Rg-43-1-3	4.35	75.3	79.6	638	291	57.9	91.4	8.6	118	18.9	2.19	285	26.5	37.8	3.19	0.03	111	1.36	0.15	1.01	0.04	-
Rg-43-1-4	4.47	142	76.2	612	195	55.1	84.2	5.4	113	18.4	2.02	266	28.0	37.4	3.40	0.02	114	1.49	0.17	0.89	0.05	-
Rg-43-2-1	6.53	138	68.0	623	163	56.9	91.6	10.9	121	18.7	2.47	256	23.9	29.9	3.38	0.03	109	1.18	0.13	1.04	0.08	-

Table 3. (Cont.) Amphibole trace element data determined by LA-ICP-MS.

Sample	Li	P	Sc	V	Cr	Co	Ni	Cu	Zn	Ga	Rb	Sr	Y	Zr	Nb	Cs	Ba	Hf	Ta	Pb	U	Th
Rg-43-2-3	8.39	178	59.5	507	89.2	59.1	77.9	3.39	135	19.0	3.92	198	23.7	47.5	4.32	0.04	145	1.79	0.20	0.87	0.12	-
Rg-43-2-4	6.83	93.5	73.9	655	201	58.0	91	9.41	129	19.0	3.54	282	22.0	27.7	3.11	0.02	106	0.98	0.14	1.12	0.07	-
Rg-43-3-1	4.38	134	71.0	633	205	54.4	81.4	0.65	112	18.4	1.61	267	25.9	31.4	3.51	0.02	110	1.40	0.15	0.88	0.03	-
Rg-43-3-2	4.70	167	73.5	649	380	57.9	87.9	0.74	120	19.5	2.14	249	25.9	36.3	3.81	0.03	131	1.47	0.20	0.85	0.05	-
Rg-43-3-3	4.88	153	73.9	665	175	58.9	87.3	1.02	122	19.6	1.78	273	26.1	33.6	3.69	0.02	120	1.44	0.15	0.95	0.05	-
Rg-43-3-4	4.87	162	72.6	664	165	58.5	88.5	0.66	120	19.9	1.85	282	28.2	34.7	3.93	0.03	126	1.39	0.16	0.95	0.05	-
Rg-43-4-1	5.30	87	83.7	616	168	51.4	80	3.22	107	18.5	1.64	288	27.5	34.6	3.13	0.02	106	1.34	0.15	0.85	0.03	-
Rg-43-4-2	4.94	174	83.4	602	255	52.4	76.9	0.56	108	17.3	1.60	284	30.5	32.8	3.44	0.03	119	1.52	0.18	0.78	0.04	-
Rg-43-4-3	5.73	162	80.7	636	202	55.0	86.4	11.4	111	18.2	1.94	275	28.0	32.0	3.29	0.02	118	1.56	0.15	0.78	0.03	-
Rg-43-4-4	5.14	76.1	84.3	608	99.6	49.2	83.7	10.7	110	17.9	1.71	289	24.2	27.5	2.53	0.02	99	1.12	0.12	0.80	0.03	-
Rg-43-5-1	5.06	94.7	80.8	648	596	58.0	109	33.1	123	19.7	1.90	279	20.3	25.7	2.33	0.04	95	1.16	0.10	0.90	0.02	-
Rg-43-5-2	5.23	174	79.6	650	229	55.1	96.4	10.9	123	19.0	1.96	279	27.5	32.8	3.82	0.02	117	1.42	0.18	0.88	0.02	-
Rg-43-5-3	4.50	175	73.0	603	215	52.1	87	0.85	115	17.7	1.54	253	24.2	29.3	3.41	0.03	107	1.26	0.16	0.87	0.03	-
Rg-43-6-1	4.54	102	89.0	668	922	56.4	91.5	4.44	125	18.8	1.80	304	20.7	22.5	2.32	0.03	112	1.23	0.12	0.78	0.02	-
Rg-43-6-2	4.48	75.7	84.7	663	644	57.0	91.8	1.23	121	19.6	1.70	300	23.0	28.8	2.87	0.03	108	1.21	0.14	0.98	0.03	-
Rg-43-6-3	4.59	177	77.0	630	312	54.4	91.9	0.88	119	18.8	1.70	261	25.7	29.0	3.36	0.03	109	1.28	0.16	0.79	0.02	-
Rg-45-1-1	2.56	93.8	78.9	556	315	54.7	110	0.54	79.3	17.7	1.57	245	25.6	28.4	2.41	0.17	88	1.30	0.11	0.56	0.09	0.05
Rg-45-1-2	2.50	98.1	78.4	557	294	55.1	107	0.46	76.8	17.3	1.56	249	24.9	28.3	2.34	0.12	90	1.34	0.18	0.52	0.09	0.10
Rg-45-1-3	2.95	87.6	80.7	557	299	54.2	108	0.39	76.2	16.6	1.81	254	25.7	29.2	2.17	0.09	87	1.38	0.29	0.53	0.06	0.12
Rg-45-1-4	3.84	83.8	82.1	564	334	55.4	112	11.1	77.5	17.2	1.71	251	26.5	29.0	2.38	0.07	91	1.43	0.11	0.57	0.18	0.08
Rg-45-2-1	1.82	79.1	81.6	569	292	58.6	116	2.97	75.8	17.7	1.61	258	26.4	28.6	2.29	0.07	94	1.17	0.14	0.55	0.05	0.08
Rg-45-2-2	2.10	95.6	82.0	570	295	57.7	115	0.74	71	17.3	1.71	256	26.2	28.5	2.31	0.09	90	1.42	0.14	0.49	0.03	0.08
Rg-45-2-3	2.14	87.9	83.3	578	348	58.1	116	0.67	75.7	18.5	1.59	261	27.1	30.5	2.33	0.10	94	1.27	0.12	0.45	0.11	0.05
Rg-45-2-4	1.97	95.5	80.0	556	317	55.3	110	0.51	75.2	17.9	1.75	254	26.3	29.3	2.35	0.06	95	1.39	0.10	0.46	0.03	0.04
Rg-45-3-1	2.51	117	81.0	570	270	56.6	114	0.53	72.5	18.4	1.86	280	27.9	31.2	2.43	0.04	102	1.56	0.13	0.63	0.03	0.05
Rg-45-3-2	2.15	89.4	77.8	537	257	51.9	108	0.49	67.9	16.5	1.43	247	25.7	28.0	2.12	0.09	85	1.11	0.12	0.45	0.04	0.03
Rg-45-3-3	4.00	97.9	80.2	561	319	53.7	116	4.93	75.3	18.0	1.63	254	26.4	29.9	2.48	0.05	91	1.34	0.15	0.50	0.03	0.04

Table 3. (Cont.) Amphibole trace element data determined by LA-ICP-MS.

Massive Gabbro																					
Sample	Li	P	Sc	V	Cr	Co	Ni	Cu	Zn	Ga	Rb	Sr	Y	Zr	Nb	Cs	Ba	Hf	Ta	Pb	U	Th
Rg-36-1-1	7.37	114	56.2	340	5.22	42.0	15.8	0.99	127	21.2	2.63	102	36.3	43.1	3.32	0.04	119	1.71	0.14	0.62	0.14	-
Rg-36-1-2	6.84	142	61.6	302	4.19	41.4	14.6	0.81	131	20.9	1.28	136	44.9	50.5	3.87	0.01	91	2.29	0.14	0.56	0.10	-
Rg-36-1-3	4.59	27	33.8	289	4.68	26.9	11.2	15.2	91	17.5	0.72	184	27.2	9.2	0.66	0.05	35	0.52	0.03	0.70	0.03	-
Rg-36-2-1	6.27	106	54.9	437	19.4	47.1	19.1	1.42	159	25.5	2.08	148	29.2	39.8	2.95	0.04	97	1.50	0.13	0.86	0.18	-
Rg-36-2-2	8.15	138	52.1	247	3.84	45.0	16.0	6.23	156	22.5	1.98	109	51.6	54.2	4.32	0.15	100	2.28	0.14	0.51	0.17	-
Rg-36-2-3	5.41	86	55.7	401	12.3	45.7	19.9	6.92	163	23.3	1.90	62	37.3	43.1	2.44	0.04	62	1.92	0.12	0.64	0.19	-
Rg-36-2-4	13.1	113	45.5	344	4.57	44.9	20.0	25.9	170	23.9	1.68	80	35.9	35.4	3.55	0.14	102	1.80	0.11	0.65	0.10	-
Rg-36-2-5	6.66	158	54.0	348	3.05	48.1	17.8	2.85	172	23.7	2.74	90	42.4	45.9	4.42	0.04	101	2.10	0.19	0.50	0.10	-
Rg-36-3-1	6.52	184	65.9	387	9.01	45.8	15.3	3.73	138	23.0	1.42	188	40.8	46.2	4.38	0.18	94	2.36	0.17	0.42	0.11	-
Rg-36-3-2	8.64	137	65.0	429	22.7	44.4	15.1	7.75	138	21.1	2.01	141	37.1	42.6	3.65	0.03	89	1.87	0.17	0.68	0.10	-
Rg-36-3-3	7.44	150	62.8	342	4.88	42.9	15.1	3.95	139	20.7	1.44	127	44.5	47.8	4.04	0.04	90	2.16	0.19	0.67	0.10	-
Rg-36-4-1	6.03	106	49.0	315	5.93	42.7	17.3	1.51	142	21.5	2.08	96	43.0	57.2	4.38	0.02	92	2.36	0.17	0.76	0.30	-
Rg-36-4-2	7.14	129	52.9	387	10.0	43.6	18.0	1.07	151	23.5	1.59	133	40.8	52.2	4.13	0.01	98	2.15	0.17	0.69	0.10	-
Rg-36-4-3	11.5	80	45.6	355	8.80	46.1	21.4	9.54	162	22.7	1.44	75	30.7	31.6	2.10	0.03	58	1.33	0.09	0.69	0.09	-
Rg-36-4-4	6.11	129	49.9	366	8.57	42.5	16.5	0.85	146	21.9	1.94	112	35.5	48.6	4.89	0.02	94	2.17	0.25	0.62	0.07	-
Rg-36-5-1	13.6	107	44.9	360	8.98	43.4	22.3	43.1	149	22.7	2.38	119	30.5	43.8	4.01	0.05	88	2.11	0.22	0.48	0.06	-
Rg-36-5-2	7.23	117	52.2	383	15.4	45.3	26.5	22.4	142	23.7	2.19	133	34.1	46.4	3.89	0.03	91	1.81	0.17	0.70	0.08	-
Rg-39-1-1	8.70	78	78.6	546	19.0	48.2	38.4	12.0	91	20.1	1.47	153	23.0	27.1	1.23	0.13	69	1.10	0.07	0.43	0.03	0.06
Rg-39-2-1	8.42	120	69.7	542	17.6	46.7	32.9	4.25	96	20.3	1.30	165	24.8	30.0	1.59	0.05	77	1.09	0.09	0.49	0.06	0.09
Rg-39-2-2	6.95	133	77.5	613	16.7	57.4	33.6	6.79	105	19.2	1.22	170	25.2	27.6	1.66	0.05	78	1.37	0.08	0.41	0.04	0.07
Rg-39-2-3	10.9	222	67.4	529	14.2	55.5	34.0	18.0	105	18.3	1.14	120	27.2	33.9	2.17	0.10	76	1.67	0.10	0.26	0.06	0.09
Rg-48-1-1	5.78	184	72.8	500	20.2	49.2	14.3	0.99	109	19.6	1.93	94	31.9	38.2	2.32	0.04	93	1.54	0.09	0.42	0.02	0.08
Rg-48-1-2	6.72	122	69.3	528	12.5	48.0	12.4	1.12	113	19.1	1.14	95	31.9	29.5	1.89	0.04	71	1.17	0.10	0.39	0.06	0.09
Rg-48-2-1	5.92	111	66.7	510	33.2	47.9	12.8	2.94	119	18.5	2.22	81	27.3	31.6	1.90	0.15	80	1.10	0.08	0.46	0.06	0.12
Rg-48-2-2	6.52	168	74.0	580	10.1	51.2	15.3	3.15	128	19.5	2.80	82.0	30.7	35.7	2.22	0.18	86.4	1.55	0.10	0.48	0.11	0.11
Rg-48-2-3	6.27	147	66.8	454	39.6	45.3	11.8	1.12	106	18.2	2.62	80.9	30.2	33.1	1.39	0.07	85.5	1.47	0.08	0.35	0.02	0.08

Table 3. (Cont.) Amphibole trace element data determined by LA-ICP-MS.

Sample	Li	P	Sc	V	Cr	Co	Ni	Cu	Zn	Ga	Rb	Sr	Y	Zr	Nb	Cs	Ba	Hf	Ta	Pb	U	Th
Rg-48-2-3	6.27	147	66.8	454	39.6	45.3	11.8	1.12	106	18.2	2.62	80.9	30.2	33.1	1.39	0.07	85.5	1.47	0.08	0.35	0.02	0.08
Rg-48-3-1	6.94	21	75.3	54	15.	52.9	12.8	1.06	108	19.4	2.71	87.8	33.0	32.6	2.15	0.05	97.0	1.58	0.10	0.31	0.05	0.07
Rg-48-3-2	9.11	227	89.8	622	23.3	59.8	16.8	1.58	126	23.7	1.89	176	43.8	51.7	2.91	0.05	112	2.17	0.14	0.57	0.22	0.10
Rg-48-3-3	5.85	173	80.5	561	38.4	57.2	13.2	1.31	123	23.4	1.67	124	40.7	46.4	2.50	0.05	93.9	1.77	0.11	1.02	0.10	0.15
Rg-48-3-4	5.91	75	41.5	391	12.1	38.7	9.7	1.28	85	17.0	1.18	56.3	20.7	16.4	0.58	0.03	42.7	0.60	0.03	0.40	0.04	0.04
Rg-48-4-1	9.79	116	80.8	1273	69.4	66.4	15.6	2.88	160	26.5	1.73	116	30.5	31.3	3.44	0.09	99.8	1.39	0.14	0.61	0.05	0.15
Rg-48-4-2	6.79	116	72.6	671	51.3	53.8	10.6	6.09	131	22.2	2.20	138	32.5	33.2	2.11	0.14	87.7	1.31	0.08	1.02	0.07	0.12
Rg-48-4-3	6.59	194	67.9	549	30.0	49.5	11.3	2.69	125	21.1	2.72	134	31.9	42.2	2.32	0.11	101	1.57	0.09	0.68	0.06	0.12
Rg-48-5-1	6.29	65	67.7	969	73.5	49.6	13.0	1.50	125	21.1	0.75	35.9	29.7	13.1	1.00	0.06	42.9	0.85	0.04	0.33	0.02	0.05
Rg-48-5-2	7.02	246	83.7	608	18.1	57.0	14.9	1.54	125	23.6	1.71	142	43.1	51.4	3.07	0.06	106	2.19	0.14	0.66	0.08	0.09
Rg-48-5-3	5.00	138	68.3	518	27.1	48.3	14.5	1.19	101	20.4	1.20	128	32.0	37.9	1.82	0.04	83.2	1.26	0.09	0.43	0.03	0.10

Table 4. Rare-earth element concentrations of amphiboles by LA-ICP-MS.

Layered Gabbro														
REE	La	Ce	Pr	Nd	Sm	Eu	Gd	Tb	Dy	Ho	Er	Tm	Yb	Lu
Rg-38-2-1	2.50	10.68	2.14	13.41	4.28	1.57	5.89	0.80	4.97	1.01	2.68	0.28	2.23	0.32
Rg-38-2-2	2.35	12.72	2.80	18.40	6.13	1.75	6.85	0.95	5.64	1.07	2.82	0.35	2.24	0.29
Rg-38-2-3	1.69	7.77	1.49	9.66	3.54	1.49	4.52	0.67	4.16	0.75	2.09	0.24	1.57	0.20
Rg-38-4-1	1.95	10.30	2.17	13.56	4.61	1.57	5.36	0.75	4.63	0.82	2.33	0.28	1.84	0.28
Rg-38-4-2	2.20	10.47	2.26	14.70	5.81	1.80	6.26	0.89	5.44	1.03	2.70	0.35	2.17	0.27
Rg-38-4-3	2.45	12.40	2.57	15.91	6.21	1.91	6.42	1.04	6.51	1.11	3.22	0.37	2.19	0.29
Rg-38-5-1	2.11	9.81	2.24	13.90	5.21	1.64	5.64	0.89	5.09	0.96	2.72	0.32	1.90	0.30
Rg-38-5-2	2.73	11.65	2.30	13.96	4.77	1.64	5.34	0.77	4.42	0.99	2.52	0.32	2.61	0.39
Rg-38-5-3	1.97	9.35	2.07	13.00	4.31	1.76	5.00	0.79	5.09	0.96	2.66	0.32	1.97	0.29
Rg-38-6-1	3.35	10.23	2.33	13.97	4.67	1.58	5.82	0.76	4.69	0.93	2.29	0.30	1.95	0.28
Rg-38-6-2	1.61	7.06	1.58	11.32	4.01	1.49	4.43	0.66	4.19	0.82	2.14	0.22	1.53	0.26
Rg-38-6-3	1.54	8.76	1.90	11.81	4.62	1.46	4.79	0.72	4.62	0.80	2.20	0.27	2.08	0.28
Rg-40-1-1	2.06	8.21	2.06	12.22	5.20	1.82	5.93	1.38	5.92	1.33	2.93	0.68	2.46	0.80
Rg-40-1-2	2.16	7.70	1.63	10.11	4.50	1.75	5.41	1.44	5.79	1.71	2.84	<0.86	2.22	0.57
Rg-40-2-1	4.59	19.18	4.26	24.06	10.4	3.71	11.0	2.00	11.57	2.23	6.45	0.86	4.54	0.70
Rg-40-2-2	1.52	6.73	1.25	8.69	3.15	1.47	4.22	0.64	3.38	0.79	1.64	0.27	1.83	0.27
Rg-40-2-3	2.15	9.13	2.00	12.91	5.06	1.82	6.45	1.08	6.14	1.09	3.04	0.53	2.43	0.34
Rg-40-3-1	1.86	8.44	1.81	12.52	5.22	1.47	6.15	0.97	5.48	1.18	3.04	<0.53	2.32	<0.42
Rg-40-3-2	2.02	8.50	1.87	12.44	4.32	1.79	5.68	0.93	5.57	1.12	3.12	0.42	1.99	0.32
Rg-40-4-1	1.99	8.25	1.85	11.89	5.05	1.50	5.67	0.92	5.51	1.07	2.83	0.33	2.21	0.30
Rg-40-4-4	1.94	8.37	1.76	12.05	4.35	1.46	5.62	0.97	5.64	0.98	2.78	0.35	2.13	0.33
Rg-40-4-5	1.87	8.13	1.60	11.65	4.79	1.63	6.08	0.87	5.45	1.08	2.97	0.36	2.06	<0.41
Rg-40-4-6	1.95	8.20	1.73	11.59	4.41	1.47	5.65	0.92	5.50	1.07	2.94	0.32	2.14	0.24
Rg-43-1-1	2.45	10.46	2.10	13.51	5.33	1.63	5.98	0.93	5.69	1.07	2.90	0.35	2.25	0.28
Rg-43-1-2	2.66	10.86	1.90	11.22	4.49	1.57	5.20	0.79	5.27	1.04	2.89	0.33	2.26	0.35
Rg-43-1-3	2.70	11.38	2.05	12.59	4.58	1.64	5.31	0.85	5.52	1.05	3.09	0.37	2.54	0.33
Rg-43-1-4	2.88	11.95	2.33	14.49	5.08	1.70	6.12	0.94	5.92	1.17	3.07	0.40	2.49	0.37
Rg-43-2-1	2.60	11.79	2.09	12.71	4.30	1.69	5.34	0.77	5.27	0.99	2.71	0.33	2.37	0.31
Rg-43-2-2	1.94	8.76	1.63	10.00	3.85	1.48	3.82	0.65	4.04	0.79	2.37	0.28	1.83	0.25
Rg-43-2-3	3.74	15.19	2.75	14.84	4.91	1.72	5.28	0.86	4.80	0.94	2.77	0.34	2.29	0.29
Rg-43-2-4	2.56	10.71	1.92	11.44	4.28	1.57	4.67	0.73	4.58	0.88	2.38	0.30	2.25	0.28
Rg-43-3-1	2.60	12.46	2.41	14.49	5.15	1.66	5.74	0.85	5.53	1.06	3.04	0.37	2.52	0.33
Rg-43-3-2	3.25	14.54	2.65	15.11	5.84	1.89	5.81	0.89	5.86	1.06	2.86	0.37	2.48	0.34
Rg-43-3-3	2.84	12.69	2.47	14.92	5.84	1.81	5.87	0.91	5.67	1.06	3.00	0.37	2.27	0.31
Rg-43-3-4	2.91	13.47	2.56	15.82	5.63	1.85	6.60	0.97	6.14	1.15	3.12	0.39	2.72	0.36
Rg-43-4-1	2.56	10.58	2.04	12.13	4.78	1.61	5.89	0.87	5.70	1.09	3.01	0.37	2.71	0.34
Rg-43-4-2	2.39	11.04	2.32	15.67	5.59	1.71	7.49	1.11	6.79	1.29	3.53	0.37	2.69	0.37
Rg-43-4-3	2.62	11.01	2.19	14.32	5.39	1.86	5.88	0.98	6.07	1.14	3.12	0.38	2.63	0.34
Rg-43-4-4	1.80	7.83	1.56	10.28	3.93	1.46	4.90	0.77	5.09	1.05	2.76	0.35	2.43	0.30
Rg-43-5-1	1.90	8.27	1.54	9.66	3.52	1.37	4.54	0.70	4.11	0.81	2.36	0.26	1.94	0.29
Rg-43-5-2	2.54	12.43	2.47	14.44	5.39	1.88	6.40	0.89	5.99	1.15	3.26	0.37	2.49	0.34
Rg-43-5-3	2.56	11.33	2.30	13.02	4.95	1.56	5.29	0.84	4.72	1.01	2.71	0.34	2.29	0.30
Rg-43-6-1	1.63	7.77	1.53	9.79	3.83	1.40	4.45	0.71	4.55	0.85	2.34	0.29	1.86	0.26
Rg-43-6-2	2.24	9.76	1.82	11.32	4.14	1.58	5.01	0.73	4.71	0.97	2.74	0.33	2.21	0.28
Rg-43-6-3	2.44	11.27	2.28	13.89	5.10	1.64	5.90	0.87	5.39	1.01	2.90	0.36	2.33	0.33
Rg-45-1-1	1.73	7.86	1.64	10.80	3.87	1.53	5.07	0.82	5.34	1.01	2.77	0.39	2.54	0.34
Rg-45-1-2	1.83	7.69	1.62	10.59	4.28	1.43	5.15	0.82	5.55	1.03	2.91	0.47	2.40	0.33
Rg-45-1-3	1.92	7.46	1.59	11.36	4.10	1.34	5.09	0.87	5.52	1.03	3.05	0.40	2.26	0.24
Rg-45-1-4	1.88	8.00	1.69	11.93	4.35	1.48	5.36	0.84	5.37	1.10	3.32	0.42	2.46	0.29
Rg-45-2-1	1.93	7.81	1.62	11.14	4.44	1.40	5.69	0.90	5.26	1.07	2.81	0.35	2.40	0.35
Rg-45-2-2	1.84	7.76	1.66	10.61	4.13	1.43	5.29	0.86	5.43	1.02	2.74	0.38	2.29	0.32
Rg-45-2-3	1.83	7.92	1.66	10.76	4.29	1.38	5.61	0.92	5.62	1.08	2.97	0.39	2.42	0.31
Rg-45-2-4	1.96	7.97	1.75	11.26	3.96	1.44	5.43	0.79	5.21	1.10	3.02	0.36	2.32	0.37
Rg-45-3-1	1.90	8.28	1.70	11.68	4.28	1.43	5.93	0.90	5.90	1.16	3.06	0.44	2.50	0.35
Rg-45-3-2	1.71	7.38	1.57	10.18	3.99	1.32	5.60	0.86	4.80	1.00	2.82	0.40	2.26	0.31
Rg-45-3-3	1.81	7.57	1.66	10.51	4.38	1.37	5.04	0.82	5.55	1.04	2.93	0.34	2.37	0.33
Rg-45-4-1	1.75	7.55	1.69	10.69	4.25	1.49	5.34	0.87	5.49	1.05	3.03	0.39	2.28	0.32

Table 4 (Cont.). Rare-earth element concentrations of amphiboles by LA-ICP-MS.

Massive Gabbro														
REE	La	Ce	Pr	Nd	Sm	Eu	Gd	Tb	Dy	Ho	Er	Tm	Yb	Lu
Rg-36-1-1	3.24	14.13	2.90	19.40	7.16	2.15	7.96	1.27	7.46	1.35	3.97	0.49	3.06	0.45
Rg-36-1-2	3.50	16.09	3.50	24.56	8.71	2.62	10.6	1.55	9.72	1.88	4.88	0.58	3.55	0.53
Rg-36-1-3	2.47	10.83	2.26	14.58	4.94	1.72	6.12	0.94	5.60	1.12	3.00	0.40	2.67	0.32
Rg-36-2-1	3.18	14.67	2.67	15.96	5.71	1.97	6.28	0.91	5.84	1.16	3.30	0.45	3.22	0.39
Rg-36-2-2	3.71	20.83	4.54	29.17	10.2	3.04	10.9	1.78	10.83	2.01	5.38	0.69	4.72	0.64
Rg-36-2-3	3.60	19.70	3.98	24.33	8.59	2.77	9.24	1.30	7.93	1.47	4.01	0.48	3.37	0.48
Rg-36-2-4	3.10	16.37	3.35	21.25	8.02	2.28	8.90	1.34	7.60	1.40	3.98	0.47	3.33	0.38
Rg-36-2-5	3.29	18.89	3.91	25.51	9.40	2.55	9.83	1.51	8.86	1.70	4.92	0.58	3.91	0.52
Rg-36-3-1	3.02	14.95	3.25	21.55	8.05	2.66	10.0	1.45	7.67	1.56	3.87	0.62	3.80	0.54
Rg-36-3-2	2.85	13.03	2.97	19.84	7.59	2.37	8.58	1.29	7.91	1.50	4.13	0.53	3.29	0.43
Rg-36-3-3	3.18	15.61	3.57	24.25	8.93	2.49	10.6	1.56	9.18	1.79	5.01	0.62	3.94	0.50
Rg-36-4-1	3.53	17.46	3.64	23.07	8.25	2.42	9.98	1.44	9.10	1.72	4.69	0.62	4.10	0.55
Rg-36-4-2	3.44	16.97	3.54	22.91	8.20	2.42	9.20	1.34	8.61	1.57	4.56	0.56	3.66	0.47
Rg-36-4-3	2.22	10.59	2.19	13.80	5.11	1.71	6.24	0.97	6.13	1.29	3.49	0.47	3.01	0.40
Rg-36-4-4	3.15	16.31	3.33	21.08	7.27	2.10	8.22	1.26	7.52	1.34	3.89	0.47	3.20	0.42
Rg-36-5-1	3.10	16.85	3.22	19.37	7.23	2.06	7.42	1.02	6.32	1.22	3.42	0.43	2.63	0.38
Rg-36-5-2	2.98	15.21	3.11	18.77	6.44	2.13	7.79	1.16	7.19	1.29	3.69	0.48	3.18	0.44
Rg-39-1-1	1.67	6.78	1.48	9.25	3.93	1.32	4.65	0.76	4.57	0.96	2.35	0.32	2.04	0.26
Rg-39-2-1	2.03	8.38	1.73	11.18	4.51	1.46	5.26	0.80	4.93	0.92	2.62	0.35	2.07	0.31
Rg-39-2-2	1.59	7.29	1.61	10.74	4.28	1.44	5.67	0.80	5.27	1.01	2.85	0.35	2.20	0.31
Rg-39-2-3	1.91	9.20	2.16	13.20	4.75	1.59	6.25	0.92	5.69	1.08	2.89	0.36	2.36	0.34
Rg-48-1-1	2.25	10.61	2.28	14.33	5.61	1.84	7.29	1.04	6.50	1.32	3.81	0.46	2.97	0.41
Rg-48-1-2	2.19	9.80	1.98	14.17	5.03	1.72	6.50	1.06	6.35	1.22	3.66	0.44	2.92	0.40
Rg-48-2-1	2.33	9.55	1.84	11.85	4.45	1.84	6.15	0.86	6.19	1.19	2.89	0.38	2.77	0.33
Rg-48-2-2	2.65	10.68	2.19	14.27	5.59	1.72	6.63	1.08	6.27	1.25	3.47	0.46	2.54	0.38
Rg-48-2-3	2.17	10.36	2.21	14.07	5.52	1.88	6.43	0.95	6.57	1.19	3.52	0.42	2.84	0.41
Rg-48-3-1	1.74	8.03	1.78	12.70	5.61	1.78	6.68	1.06	6.60	1.37	3.57	0.47	2.81	0.39
Rg-48-3-2	3.20	12.20	2.50	17.81	7.22	2.17	9.20	1.45	9.30	1.74	4.98	0.68	3.92	0.55
Rg-48-3-3	4.54	15.15	2.83	17.20	5.99	2.23	8.19	1.26	8.36	1.64	4.40	0.60	3.59	0.49
Rg-48-3-4	1.24	5.11	1.08	6.84	3.10	1.28	4.24	0.66	4.16	0.81	2.23	0.34	1.95	0.29
Rg-48-4-1	2.04	9.19	1.94	12.35	4.92	2.02	6.35	1.05	6.47	1.24	3.17	0.51	2.75	0.39
Rg-48-4-2	2.64	10.14	2.08	12.79	4.89	1.75	7.01	1.05	7.19	1.34	3.36	0.43	2.78	0.46
Rg-48-4-3	3.10	12.42	2.54	16.61	5.92	1.94	6.35	1.07	6.70	1.38	3.52	0.41	3.03	0.40
Rg-48-5-1	2.37	10.84	2.22	14.94	4.95	1.97	5.88	0.98	5.97	1.19	3.08	0.37	2.77	0.37
Rg-48-5-2	3.48	15.70	3.26	20.28	7.31	2.28	8.81	1.27	8.63	1.77	4.90	0.59	3.96	0.54
Rg-48-5-3	2.56	11.24	2.20	14.40	4.98	1.70	6.16	1.05	6.32	1.37	3.43	0.44	3.14	0.43

Table 5. Plagioclase major element concentrations determined by electron microprobe.

Layered Gabbros											
Sample	SiO_2	TiO_2	Al_2O_3	FeO	MgO	CaO	Na_2O	K_2O	SrO	Total	An
Rg-39-1-1	47.97	0.00	33.95	0.07	0.00	16.75	1.93	0.00	0.21	100.88	82.8
Rg-39-1-2	48.30	0.00	33.57	0.06	0.00	16.14	2.06	0.00	0.25	100.37	81.2
Rg-39-1-3	49.70	0.02	32.86	0.08	0.00	15.31	2.63	0.02	0.14	100.74	76.2
Rg-40-1-1	49.50	0.00	33.31	0.02	0.00	15.73	2.53	0.00	0.15	101.25	77.4
Rg-40-2-1	50.23	0.00	32.94	0.07	0.00	15.22	2.62	0.01	0.16	101.25	76.2
Rg-40-2-2	50.76	0.00	31.91	0.05	0.00	14.42	3.26	0.01	0.15	100.56	70.9
Rg-40-2-3	46.78	0.00	33.11	0.09	0.00	16.09	2.00	0.02	0.18	98.27	81.5
Rg40-7-1	48.78	0.00	33.19	0.05	0.00	16.11	2.21	0.00	0.16	100.50	80.1
Rg40-7-2	47.96	0.00	33.60	0.15	0.00	16.69	1.88	0.02	0.27	100.57	83.0
Rg40-7-3	50.41	0.01	31.70	0.11	0.00	14.77	2.99	0.00	0.15	100.14	73.2
Rg-45-4-1	47.66	0.01	33.76	0.11	0.00	17.40	1.69	0.00	0.15	100.78	85.1
Rg-45-5-1	47.51	0.02	34.03	0.14	0.00	17.05	1.72	0.01	0.16	100.64	84.5
Massive Gabbros											
Rg-36-1-1	49.60	0.01	32.75	0.08	0.00	15.80	2.45	0.02	0.17	100.87	78.0
Rg-36-1-2	49.41	0.00	32.66	0.09	0.00	15.44	2.40	0.02	0.14	100.17	78.0
Rg-36-1-3	49.74	0.00	32.43	0.10	0.00	15.59	2.58	0.01	0.13	100.57	76.9
Rg-36-1-4	49.43	0.00	32.81	0.14	0.00	15.45	2.44	0.01	0.18	100.47	77.7
Rg-48-2-1	50.14	0.01	32.82	0.11	0.00	15.40	2.69	0.00	0.19	101.36	76.0
Rg-48-2-2	51.47	0.01	31.98	0.15	0.00	14.31	3.13	0.02	0.17	101.24	71.6
Rg-48-2-3	51.16	0.00	31.45	0.13	0.00	14.29	3.22	0.02	0.26	100.52	70.9
Rg-48-2-4	49.58	0.01	32.47	0.05	0.00	15.63	2.50	0.00	0.16	100.41	77.6

All analyses performed at OSU's Electron Microprobe Lab. Fe is reported as FeO. An =Ca/(Ca+Na)*100.

Table 6. Plagioclase trace element concentrations determined by LA-ICP-MS.

Layered Gabbro																	
Sample	Li	P	Sc	V	Cr	Co	Ni	Cu	Zn	Ga	Rb	Sr	Y	Zr	Nb	Cs	Ba
Rg-40-2-1	0.97	68.6	1.73	0.52	2.11	0.39	0.61	1.24	1.91	22.8	0.31	1293	0.50	0.87	0.16	0.27	51.4
Rg-40-2-5	0.94	45.8	1.69	2.97	1.85	14.4	59.9	260	4.20	22.6	17.0	1512	0.18	0.43	0.22	0.38	210
Rg-45-4-3	0.50	36.8	3.28	14.1	8.57	1.80	10.7	15.6	2.63	19.3	0.69	1630	0.71	0.86	0.05	0.21	54.8
Rg-45-4-4	1.39	37.8	2.71	10.8	4.57	1.76	22.8	45.4	3.10	20.7	6.85	1745	0.28	0.82	0.05	0.23	76.0
Massive Gabbro																	
Rg-36-1-4	3.63	65.4	13.3	92.6	2.69	8.32	3.33	69.3	24.2	25.9	2.07	1496	6.58	4.16	0.29	0.33	140
Rg-36-1-5	0.30	109	2.90	0.25	2.46	0.04	0.20	0.58	1.21	25.6	0.05	1544	0.04	0.03	0.02	0.01	49.8
Rg-36-3-5	0.26	98.8	2.95	0.98	3.54	0.14	0.22	0.89	1.17	26.0	0.04	1492	0.15	0.11	0.03	0.03	52.7
Rg-36-4-5	0.51	84.0	3.37	3.01	3.62	0.50	0.76	1.88	4.59	23.2	0.23	1673	0.20	0.87	0.11	0.06	59.6
Rg-36-5-4	0.20	99.4	3.09	0.55	3.35	0.20	0.36	1.20	1.19	34.2	14.7	1625	0.04	0.09	0.04	0.37	666
Rg-39-1-2	0.50	106	1.50	0.44	1.90	0.13	0.48	1.01	1.18	24.1	0.23	1306	0.11	0.16	0.03	0.09	48.0
Rg-29-2-4	0.42	83.9	1.34	2.42	2.35	0.25	0.66	1.73	2.28	20.8	0.21	1495	0.12	0.12	0.07	0.16	59.5
Rg-39-2-5	0.44	101	1.27	0.33	1.30	0.12	0.16	0.76	1.20	22.1	0.15	1475	0.06	0.07	0.03	0.07	55.3
Rg-48-2-3	1.89	98.5	3.79	18.7	5.32	4.08	3.98	3.16	15.4	22.3	1.31	1358	1.99	2.12	0.69	0.19	66.3
Rg-48-2-4	0.81	85.6	1.71	9.52	4.84	2.30	1.73	2.24	6.78	21.2	0.56	1164	0.43	0.86	0.13	0.15	56.3
Rg-48-3-5	1.14	113	1.30	2.92	2.47	0.38	0.43	1.39	2.19	22.4	4.16	1299	0.19	0.36	0.06	1.95	64.5

Table 7. Plagioclase REE concentrations determined by LA-ICP-MS.

Layered Gabbro															
Sample	La	Ce	Pr	Nd	Sm	Eu	Eu*	Gd	Tb	Dy	Ho	Er	Tm	Yb	Lu
Rg-40-2-1	1.33	2.09	0.41	0.87	0.93	0.60	10.59	0.20	0.79	0.53	0.14	1.03	0.52	0.47	0.11
Rg-40-2-5	1.27	2.04	0.16	0.74	0.34	0.15	2.72	0.11	0.12	0.22	0.09	0.15	0.17	0.36	0.20
Rg-45-4-3	1.22	2.05	0.25	0.83	0.15	0.33	5.78	0.25	0.03	0.33	0.04	0.07	0.02	0.12	0.02
Rg-45-4-4	1.24	1.71	0.15	0.48	0.08	0.15	2.70	0.11	0.05	0.07	0.01	0.04	0.27	0.07	0.02
Massive Gabbro															
Rg-36-1-4	2.62	6.13	0.78	4.59	0.98	0.63	11.11	1.48	0.18	1.33	0.23	0.74	0.09	0.58	0.10
Rg36-1-5	2.39	3.61	0.32	0.96	0.08	0.26	4.57	0.07	0.01	0.04	0.01	0.03	0.01	0.05	0.01
Rg-36-3-5	2.16	3.23	0.34	1.25	0.13	0.30	5.36	0.11	0.02	0.06	0.02	0.05	0.01	0.07	0.02
Rg36-4-5	2.23	3.39	0.25	1.48	0.36	0.42	7.51	0.37	0.05	0.21	0.05	0.16	0.05	0.23	0.05
Rg36-5-4	2.02	3.33	0.23	0.61	0.10	0.11	1.94	0.09	0.01	0.05	0.01	0.04	0.03	0.06	0.01
Rg-39-1-2	1.71	3.20	0.26	1.03	0.14	0.26	4.54	0.15	0.02	0.07	0.02	0.06	0.02	0.08	0.02
Rg-29-2-4	1.85	2.67	0.23	0.89	0.14	0.21	3.73	0.13	0.02	0.11	0.03	0.06	0.02	0.09	0.02
Rg-39-2-5	1.91	2.64	0.25	0.76	0.09	0.19	3.36	0.08	0.01	0.04	0.01	0.05	0.01	0.05	0.01
Rg-48-2-3	1.60	1.89	0.38	2.65	1.62	0.45	7.95	1.73	0.33	1.40	0.26	0.89	0.20	0.89	0.19
Rg-48-2-4	1.80	3.11	0.24	0.83	0.82	0.29	5.14	0.45	0.10	0.27	0.17	0.20	0.05	0.30	0.05
Rg-48-3-5	2.11	2.77	0.23	0.71	0.20	0.12	2.05	0.19	0.02	0.19	0.04	0.06	0.03	0.07	0.02

Eu* = $Eu_{sample}/Eu_{chodnrite}$, where chondrite compositions are from McDonough and Sun, 1995.

Table 8. Apatite REE analyses determined by LA-ICP-MS

Layered Gabbro														
Sample	La	Ce	Pr	Nd	Sm	Eu	Gd	Tb	Dy	Ho	Er	Tm	Yb	Lu
Rg-38-5-4	21.1	84.0	15.3	89.1	23.9	7.28	24.9	3.10	15.4	2.67	7.14	0.79	4.09	0.66
Rg-38-5-5	29.3	117.7	22.2	134	32.6	9.57	34.6	4.20	21.6	3.80	9.37	1.04	6.44	0.84
Massive Gabbro														
Rg-36-1-1	111.1	282.7	37.9	173	37.1	9.95	33.4	4.08	21.4	3.66	9.32	1.14	5.98	0.88
Rg-36-1-2	102.8	272.7	36.9	169	34.3	9.90	31.9	3.94	20.6	3.76	9.62	1.06	6.36	0.87
Rg-36-2-1	109.9	323.7	46.6	225	40.9	8.32	33.8	3.39	17.2	2.98	6.37	0.66	4.03	0.46
Rg-39-1-1	100.0	246.6	28.5	115	21.2	6.21	19.3	2.18	11.4	1.97	4.75	0.49	2.88	0.38
Rg-39-1-2	97.5	246.1	29.8	125	23.3	6.60	21.0	2.25	11.2	1.94	5.09	0.56	3.14	0.43
Rg-48-2-1	89.3	226.5	30.8	137	28.9	7.53	28.6	3.89	16.4	3.25	9.36	0.92	4.02	0.73
Rg-48-2-2	79.1	185.4	23.4	109	25.9	7.20	26.7	3.08	16.3	2.90	6.99	0.81	4.10	0.66
Rg-48-2-3	80.8	194.2	25.2	118	27.1	6.87	26.9	3.27	18.9	3.31	8.39	0.81	5.04	0.72
Rg-48-2-4	74.7	170.3	21.6	105	20.9	6.90	23.9	3.27	16.9	3.25	8.33	0.86	5.23	0.65

Table 9. Titanite major element concentrations determined by electron microprobe.

Name	SiO_2	TiO_2	Al_2O_3	FeO	MnO	MgO	CaO	Na_2O	K_2O	Total
Rg-36-1-1	31.02	34.22	2.981	1.401	0.047	0	28.92	0.054	0.004	98.64
Rg-36-1-2	29.86	35.52	2.317	0.855	0.035	0.004	28.53	0	0	97.12
Rg-36-1-3	30.68	32.75	3.780	1.370	0.022	0	28.42	0.0242	0.001	97.06
Rg-36-1-4	30.40	33.55	3.080	1.464	0.015	0.004	28.56	0.0034	0.018	97.09

All analyses performed at UW's Electron Microprobe Facility by Julie Gross. Fe is reported as FeO.

Table 10. Partition coefficients used in modeling. All values were taken from studies using basaltic andesite compositions.

	Ilmenite	Magnetite	Plagioclase	Hornblende
Ta	2.700	2.000	0.027	0.32
La	0.007	1.500	0.180	0.18
Ce	0.008	1.300	0.140	0.3
Pr	0.008	1.300	0.130	0.45
Nd	0.009	1.000	0.120	0.64
Sm	0.009	1.100	0.083	1.06
Eu	0.009	0.600	0.700	0.96
Gd	0.008	1.100	0.067	1.32
Tb	0.009	1.000	0.061	1.37
Dy	0.010	1.000	0.031	1.42
Ho	0.012	1.000	0.020	1.34
Er	0.014	1.000	0.016	1.32
Yb	0.017	1.800	0.011	1.16
Y	0.0045	0.200	0.0380	1.390
Nb	2.300	0.400	0.022	0.340
Sr	-	0.010	1.700	0.71
Ti	9	7.500	0.050	2.900
Zr	0.28	0.1	0.003	0.450
Source	Green and Pearson, 1987; Nielsen et al., 1992	Rollinson, 1993	Dunn and Sen, 1994	Tiepolo et al., 2007

Table 11. Comparison of Trace Element Ratios

Ratio	Chondrites[1]	Average Continental Arcs[2]	Average Island Arcs[3]	Average Bulk Continental Crust[4]	Average Riddle Peaks Amphibole
Nb/Ta	17.6	10.0	-	11.4	21.1
Ti/Zr	115.2	43.2	28.8	31.8	364
Zr/Sm	25.8	30.0	27.0	33.8	6.38
Sr/Y	4.62	17.9	18.2	16.8	7.31
La/Yb	1.47	8.42	8.64	10.5	0.94
Dy/Yb	1.53	1.79	1.68	1.89	2.33

References (1) McDonough and Sun, 1995 (2) Rudnick and Fountain, 1995 (3) Taylor and McLennan, 1995 (4) Rudnick and Gao, 2003

Table 12. Calculated Apatite Partition Coefficients for Trace Elements

Sample	Sc	V	Cr	Rb	Sr	Y	Zr	Nb	Cs	Ba	Hf	Ta	Pb	U	Th	Ti
Rg-38	0.017	0.036	0.019	0.002	7.959	4.133	0.001	0.004	-	0.002	0.025	0.050	0.116	0.378	-	0.004
Rg-38	0.028	0.068	0.042	0.002	7.478	5.715	0.005	0.004	-	0.003	0.024	0.059	0.108	0.191	-	0.004
Average	**0.023**	**0.052**	**0.031**	**0.002**	**7.719**	**4.924**	**0.003**	**0.004**	-	**0.003**	**0.025**	**0.054**	**0.112**	**0.284**	-	**0.004**
Rg-36	0.013	0.098	0.000	0.038	1.600	3.452	0.002	0.001	0.000	0.043	0.009	0.020	0.156	1.680	-	0.010
Rg-36	0.018	0.069	0.372	0.007	2.102	3.775	0.002	0.001	0.014	0.017	0.009	0.019	0.114	1.746	-	0.002
Rg-36	0.000	0.050	1.420	0.004	2.440	2.435	0.001	0.002	0.013	0.002	0.012	0.020	0.104	1.307	-	0.002
Average	**0.010**	**0.072**	**0.597**	**0.017**	**2.047**	**3.220**	**0.002**	**0.001**	**0.009**	**0.021**	**0.010**	**0.020**	**0.124**	**1.577**	-	**0.005**
Rg-39	0.010	0.044	0.563	0.002	1.907	2.914	0.001	0.003	0.002	0.001	0.015	0.035	0.105	1.567	1.244	0.005
Rg-39	0.030	0.051	0.319	0.007	1.713	3.013	0.003	0.002	0.000	0.004	0.014	0.027	0.079	0.363	0.653	0.002
Average	**0.020**	**0.047**	**0.441**	**0.005**	**1.810**	**2.964**	**0.002**	**0.003**	**0.001**	**0.002**	**0.014**	**0.031**	**0.092**	**0.965**	**0.948**	**0.003**
Rg-48	0.194	0.054	4.463	0.053	2.766	3.307	0.004	0.032	-	0.005	0.188	0.433	0.334	2.479	1.425	0.008
Rg-48	0.016	0.035	0.389	0.004	1.552	2.454	0.001	0.003	-	0.001	0.017	0.027	0.138	0.474	0.896	0.001
Rg-48	0.034	0.029	0.440	0.012	2.155	2.831	0.001	0.006	-	0.001	0.038	0.121	0.096	0.945	0.644	0.002
Rg-48	0.352	0.030	7.226	0.077	5.026	5.880	0.008	0.115	-	0.024	0.480	1.728	0.168	2.598	2.466	0.019
Average	**0.149**	**0.037**	**3.129**	**0.036**	**2.875**	**3.618**	**0.003**	**0.039**	-	**0.008**	**0.180**	**0.577**	**0.184**	**1.624**	**1.358**	**0.008**

Table 13. Calculated Apatite Partition Coefficients for REE

Sample	La	Ce	Pr	Nd	Sm	Eu	Gd	Tb	Dy	Ho	Er	Yb
Rg-38	1.728	2.465	3.286	3.938	4.672	4.082	5.600	4.615	4.128	3.674	3.378	2.399
Rg-38	1.856	2.910	4.624	5.907	6.955	5.390	8.215	7.230	6.650	5.090	4.790	2.746
Average	**1.792**	**2.688**	**3.955**	**4.922**	**5.814**	**4.736**	**6.908**	**5.922**	**5.389**	**4.382**	**4.084**	**2.572**
Rg-36	6.625	5.674	5.832	5.139	4.891	3.589	4.365	3.870	3.958	3.244	1.826	
Rg-36	6.496	6.277	6.215	5.445	4.784	4.010	4.909	4.204	3.705	3.468	2.242	
Rg-36	6.226	6.222	6.512	5.937	4.847	3.205	4.218	2.991	2.662	2.302	1.184	
Average	**6.449**	**6.058**	**6.186**	**5.507**	**4.841**	**3.601**	**4.497**	**3.688**	**3.441**	**3.004**	**1.751**	
Rg-39	10.780	10.918	9.621	7.968	5.708	4.510	5.473	3.958	3.530	2.818	2.711	1.635
Rg-39	8.658	8.811	8.612	7.161	5.473	4.351	5.267	3.850	3.217	2.892	2.604	1.756
Average	**9.719**	**9.864**	**9.116**	**7.564**	**5.590**	**4.430**	**5.370**	**3.904**	**3.373**	**2.855**	**2.657**	**1.696**
Rg-48	9.217	8.469	8.684	6.893	5.468	4.069	5.659	5.056	3.516	3.274	3.512	1.660
Rg-48	4.445	4.559	4.691	3.902	3.800	3.180	3.835	2.922	2.489	2.298	1.881	1.213
Rg-48	3.202	3.846	4.450	4.390	4.793	2.956	4.343	3.565	3.218	2.789	2.553	1.630
Rg-48	10.861	9.989	9.954	9.840	7.137	5.189	7.432	6.843	5.759	5.546	5.000	3.113
Average	**6.931**	**6.716**	**6.945**	**6.256**	**5.299**	**3.848**	**5.317**	**4.596**	**3.745**	**3.477**	**3.236**	**1.904**

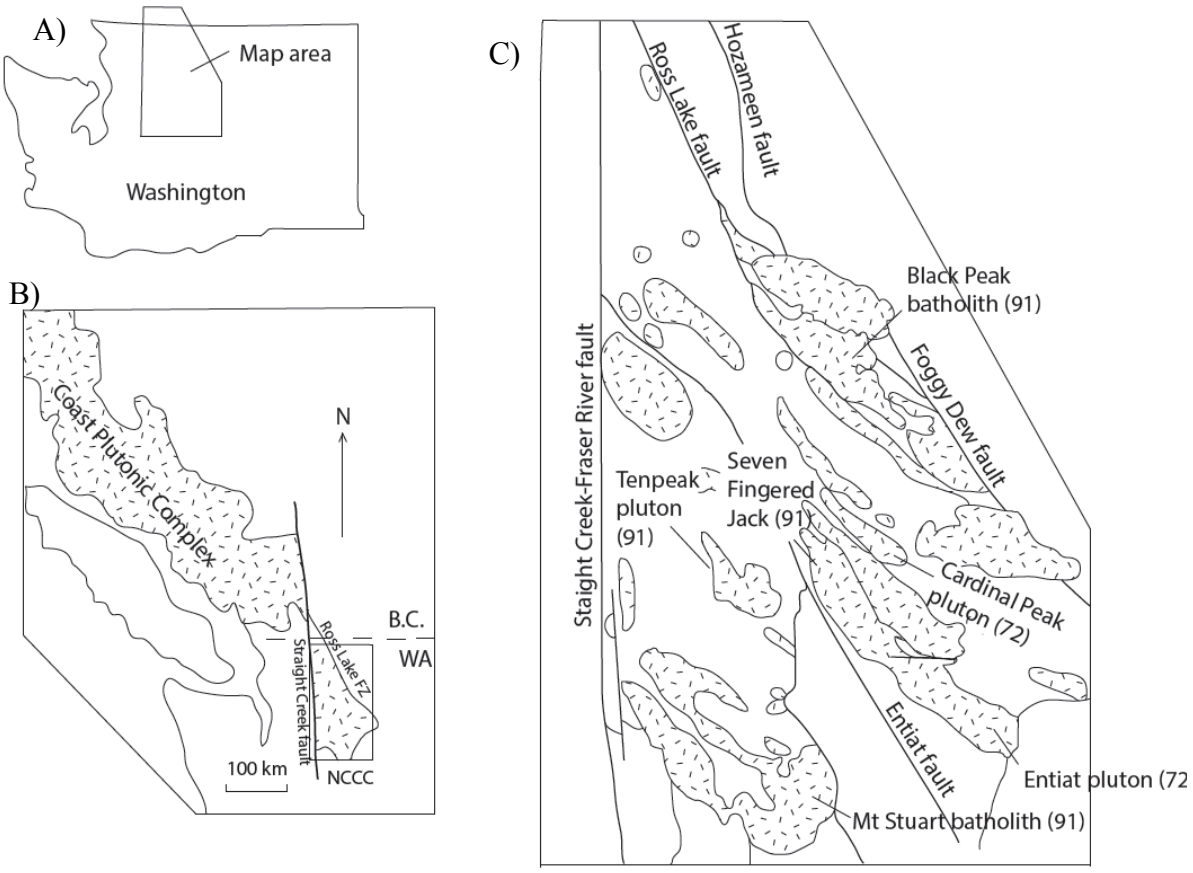

Figure 1. Generalized geologic maps of the NCCC. The NCCC is located in the northern part of Washington State and southwest British Columbia (A). The NCCC is separated from the Coast Plutonic Complex by the Straight Creek Fault (B). Some of the major plutons in the area are outlined above, with their crystallization ages in parentheses (Miller et al., 2009) (C). (Modified from DeBari and Greene, 2011).

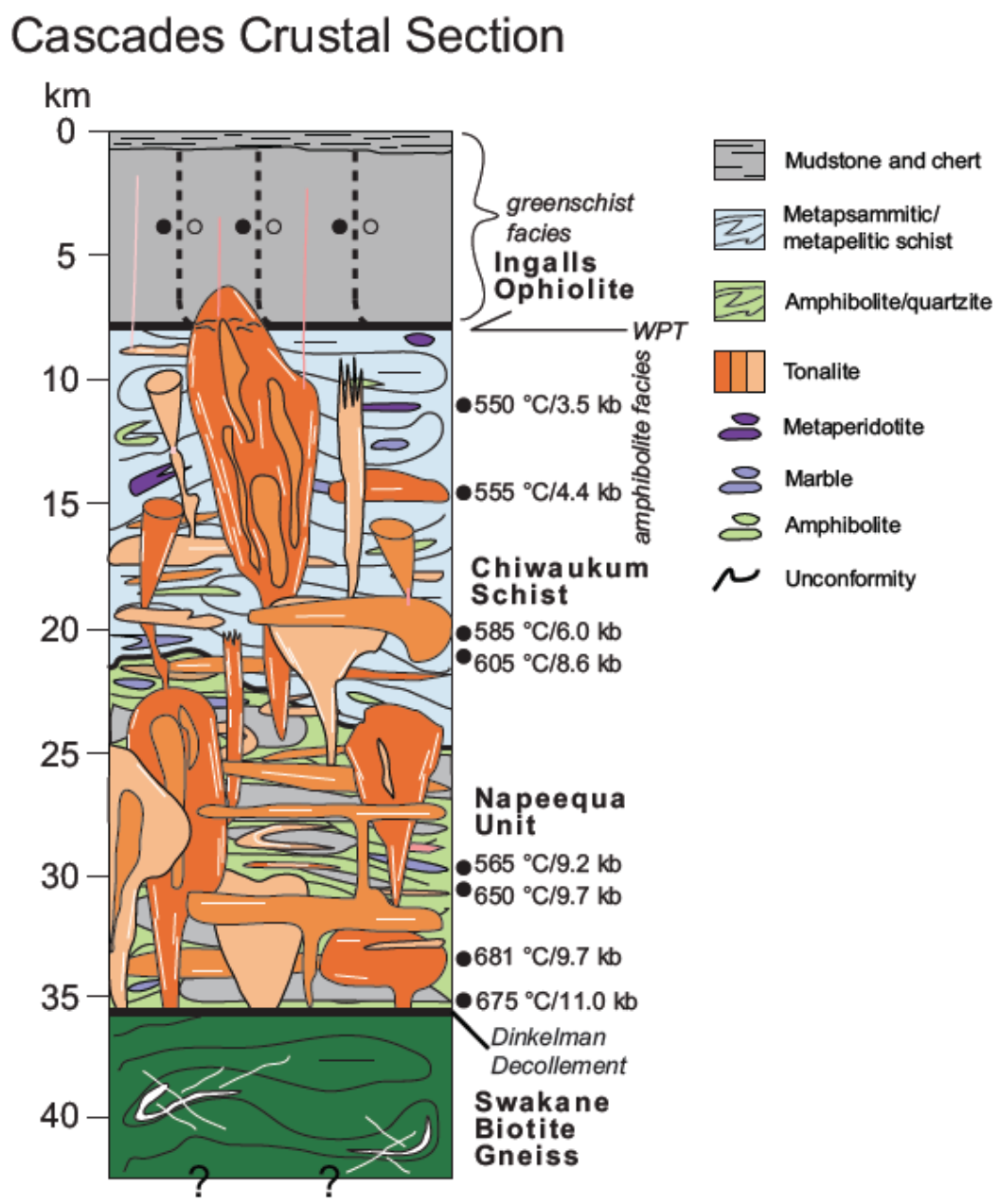

Figure 2. Possible crustal section of the NCCC from Miller et al. (2009) showing plutons and important rock units with respective crystallization temperatures and pressures.

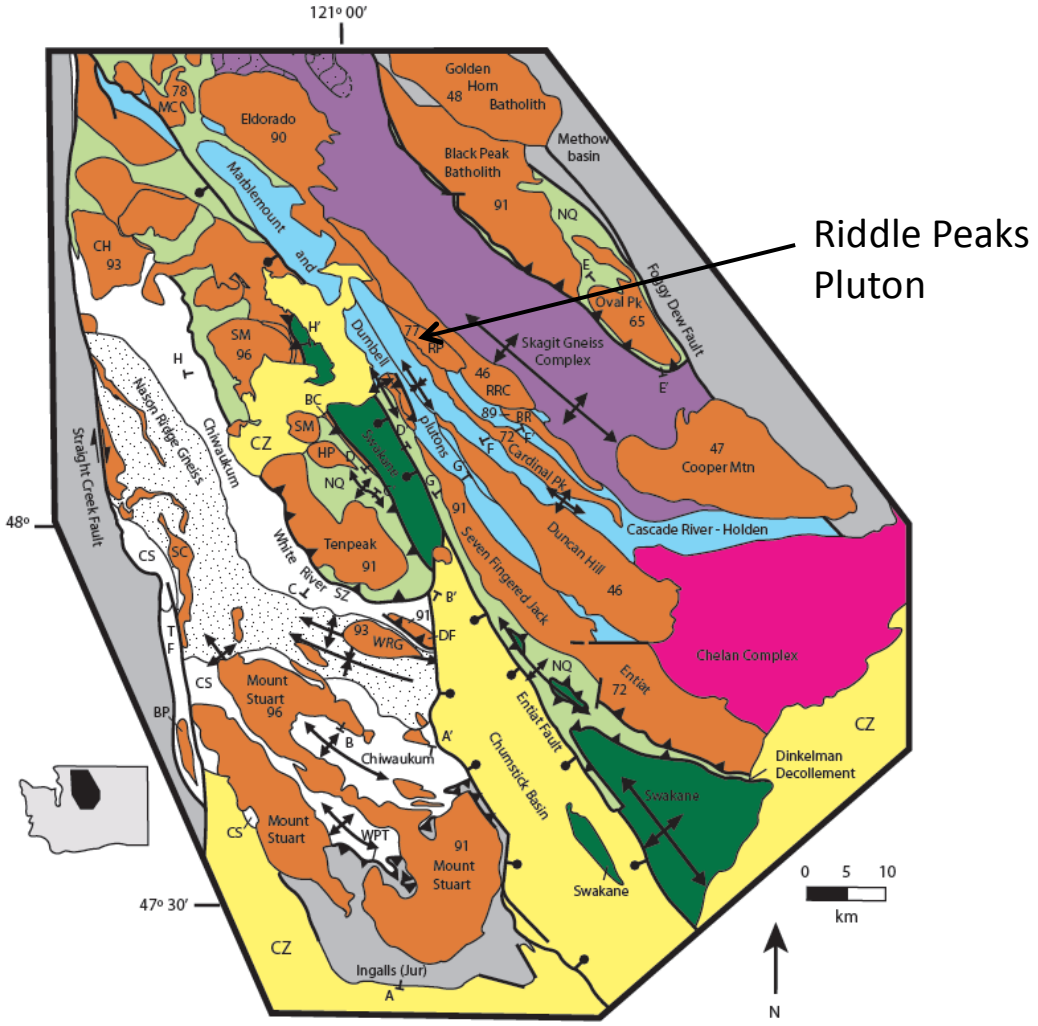

Figure 3. Plutons (shown in orange) are distributed throughout the North Cascades crystalline core. Ages are given with plutons. Many of the 96-88 Ma plutons exist in the SW part of the map in the Wenatchee block. The Riddle Peaks pluton, abbreviated RP, is part of a younger group that exists mostly within the Chelan block. (Miller et al., 2009).

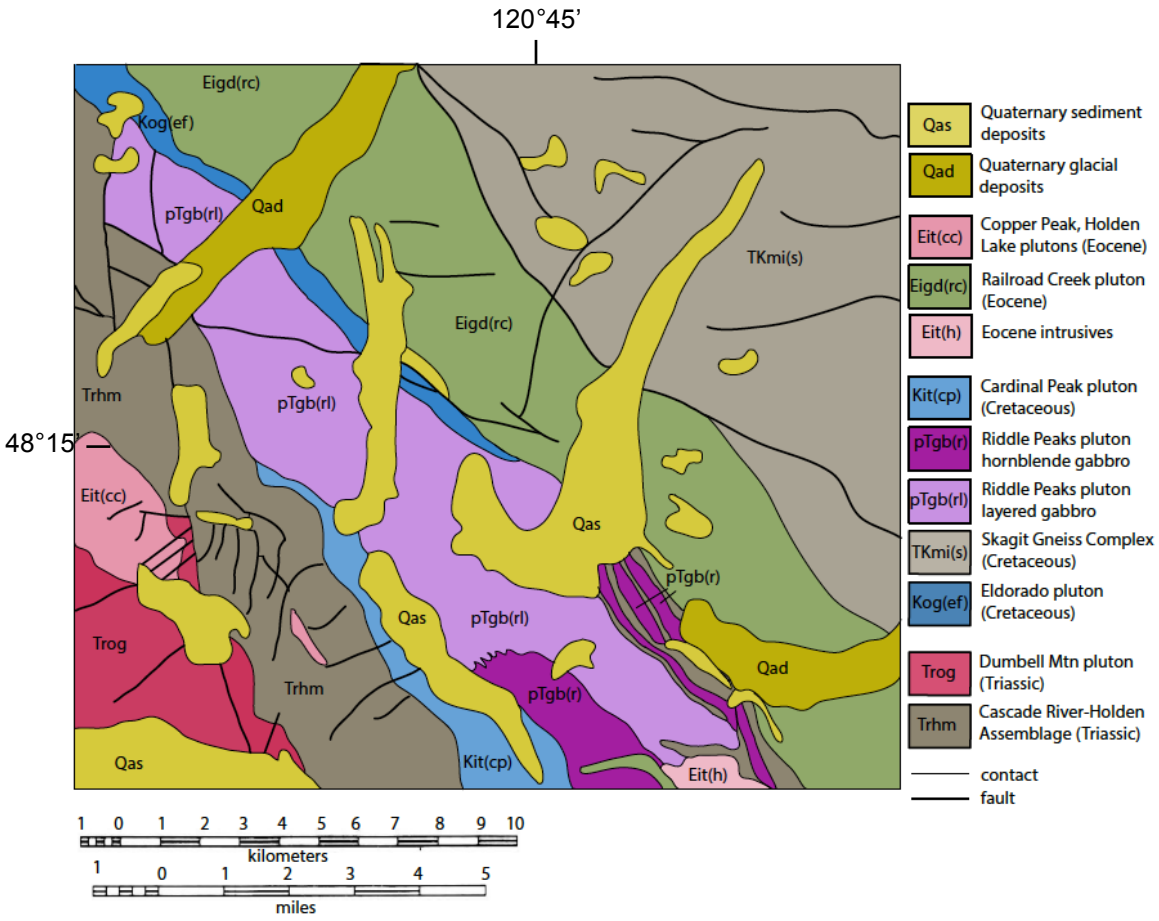

Figure 4. Geologic map of the Riddle Peaks pluton. Symbol pTigb(r) represents areas of massive gabbro; pTigb(rl) denotes layered gabbro. Modified from Cater and Wright (1967) and Cater and Crowder (1967).

Figure 5. Field photograph of layered gabbro. Plagioclase-rich layers are on the cm-scale, with sharp contacts between plagioclase and hornblende-rich layers.

Figure 6. Field photograph of a massive portion of the Riddle Peaks Gabbro, which is light gray in color due to a higher proportion of plagioclase in the rock.

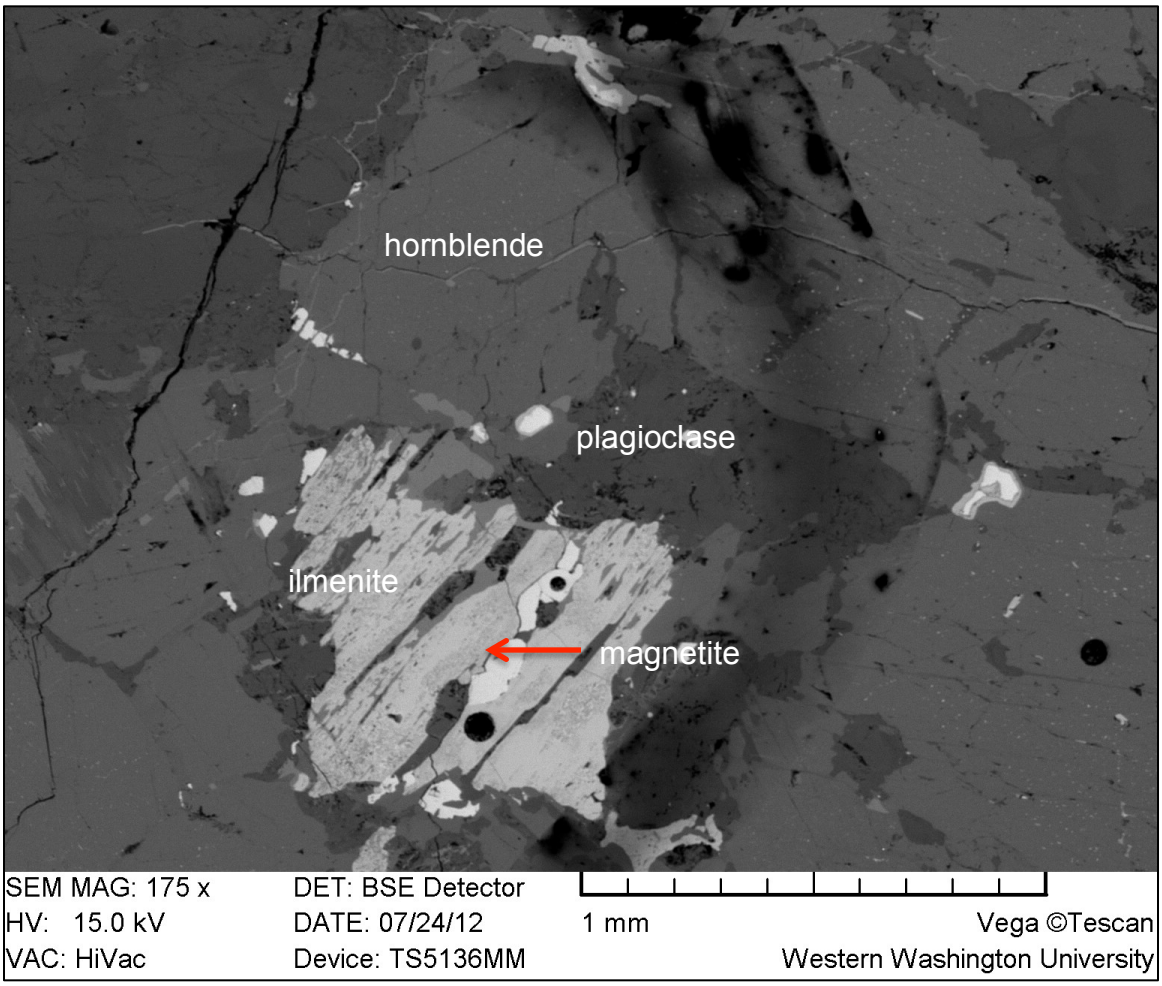

Figure 7. Back-scattered electron image of oxide textures. Ilmenite appears dissolved and grows around magnetite; both are interstitial to hornblende.

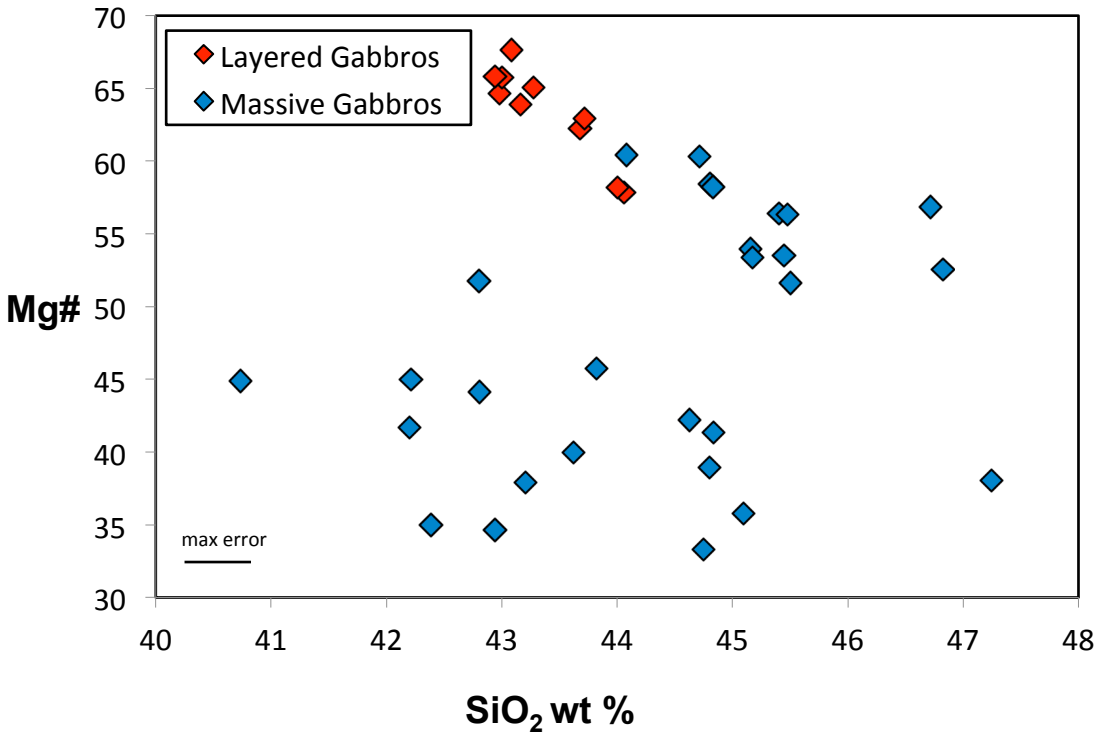

Figure 8. Plot of whole rock SiO_2 versus Mg#. Layered gabbros have the highest Mg#, but note that high Mg# doesn't correspond to the lowest SiO_2. Data are presented in table 1. Maximum error for SiO_2 is shown at bottom left. See methods for full discussion of precision and accuracy.

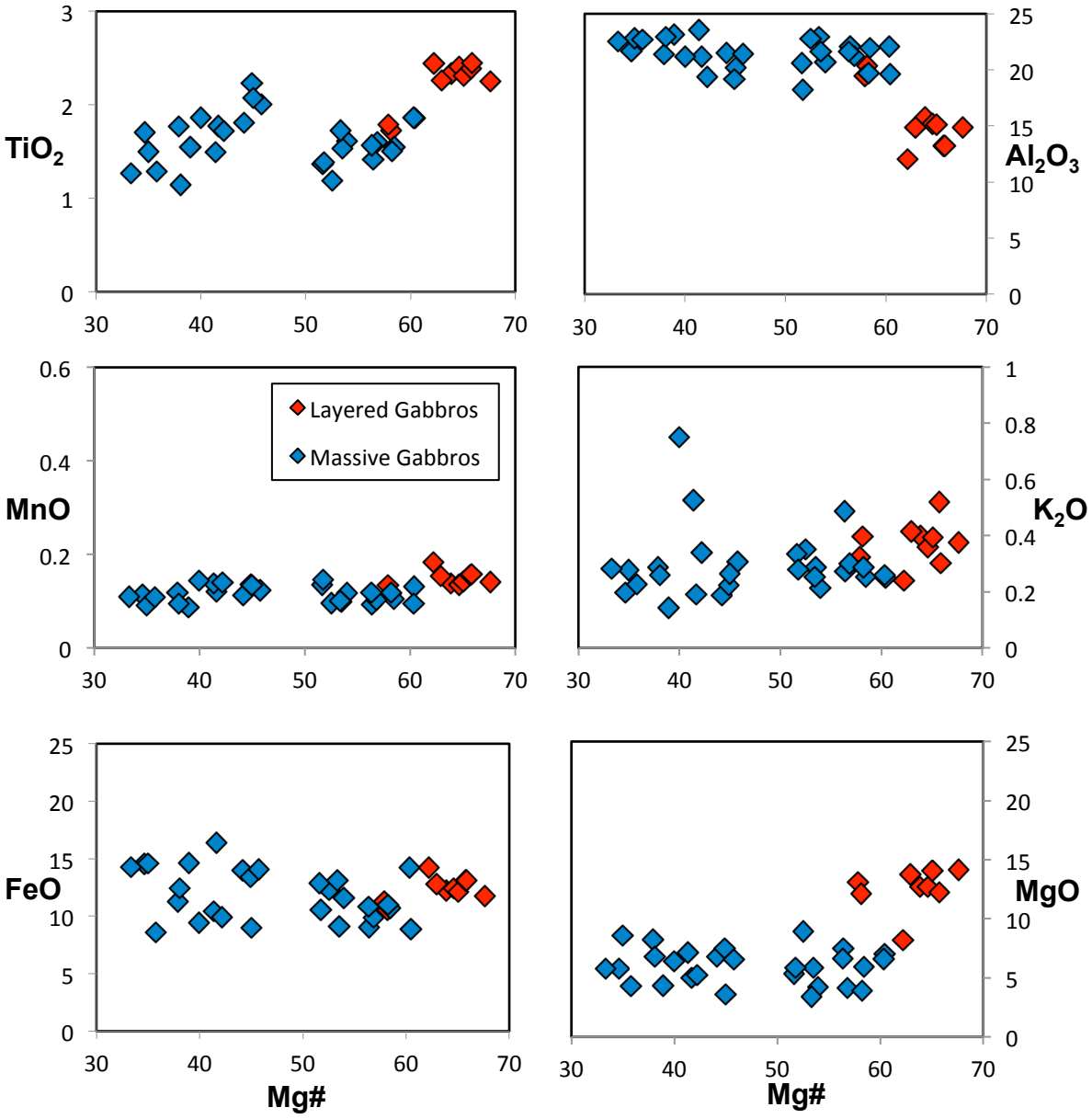

Figure 9. Whole rock oxides plotted against whole rock Mg# (100*Mg/Mg+Fe^{2+}). There is a compositional gap at ~Mg# 50. Error bars are smaller than the symbol. See methods for full discussion of precision and accuracy.

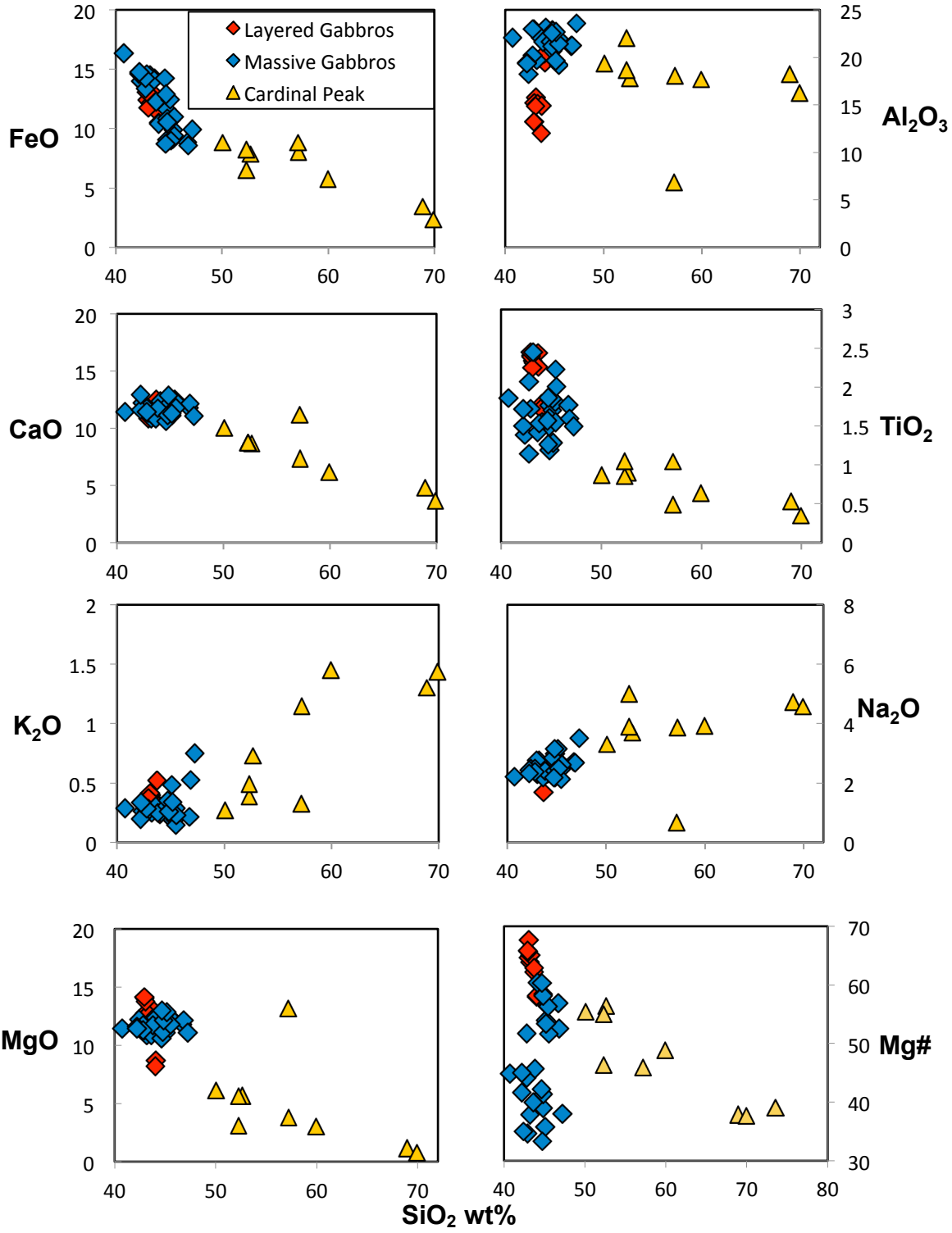

Figure 10. Harker Diagrams (oxide versus SiO_2) for Riddle Peak layered and massive gabbro, along with Cardinal Peak pluton compositions from McCrady (2013). Major elements do not vary greatly within the pluton but show trends with the Cardinal Peak compositions.

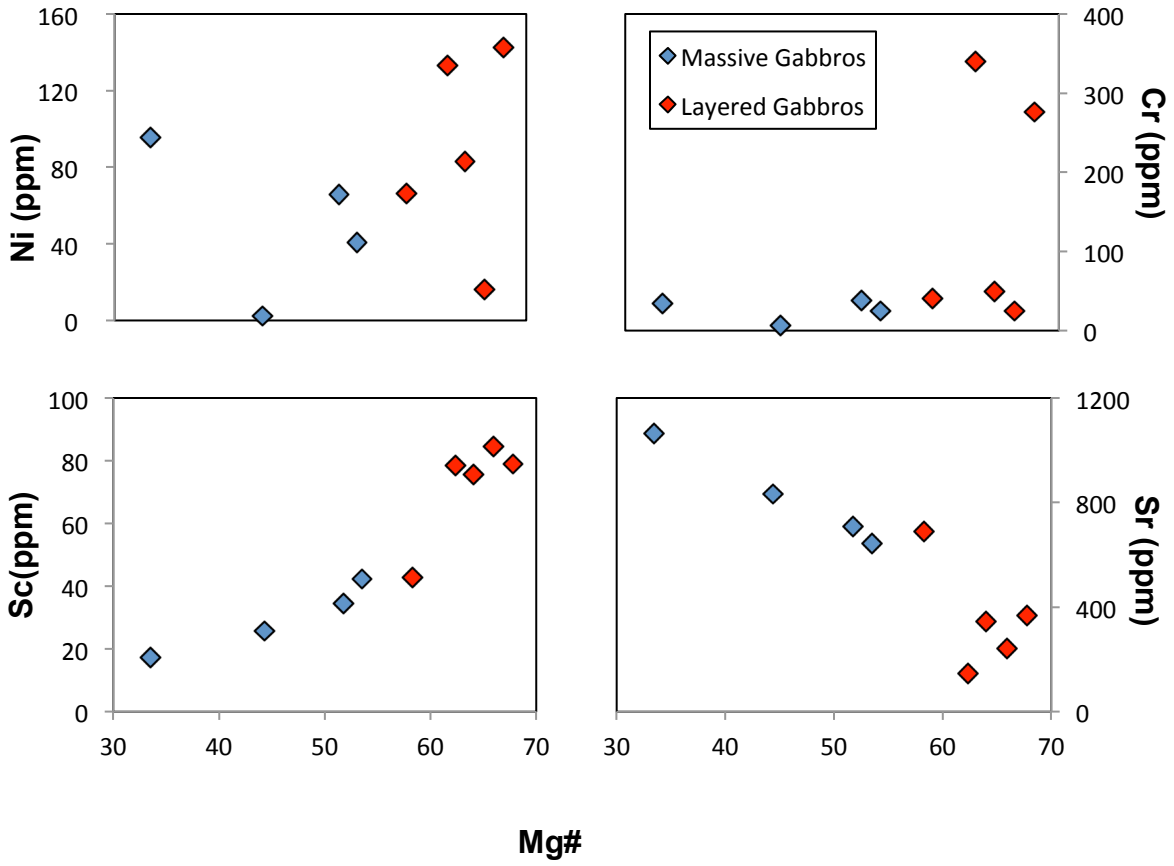

Figure 11. Mg# versus selected trace elements in the Riddle Peaks gabbro. Data are presented in table 2. Error bars are smaller than the symbol. See methods section for a full discussion of precision and accuracy.

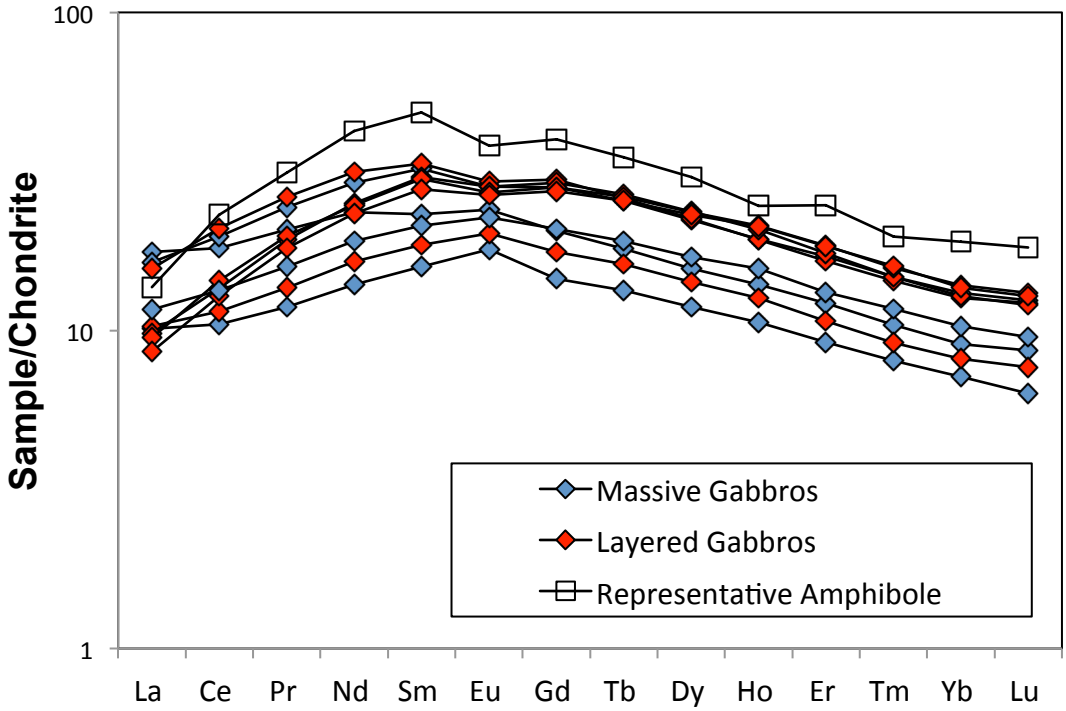

Figure 12. Rare Earth Element diagram for Riddle Peaks gabbros and one representative Riddle Peaks amphibole composition for comparison. Whole rock REE patterns are representative of amphibole accumulation. Normalization is to chondrite of McDonough and Sun (1995).

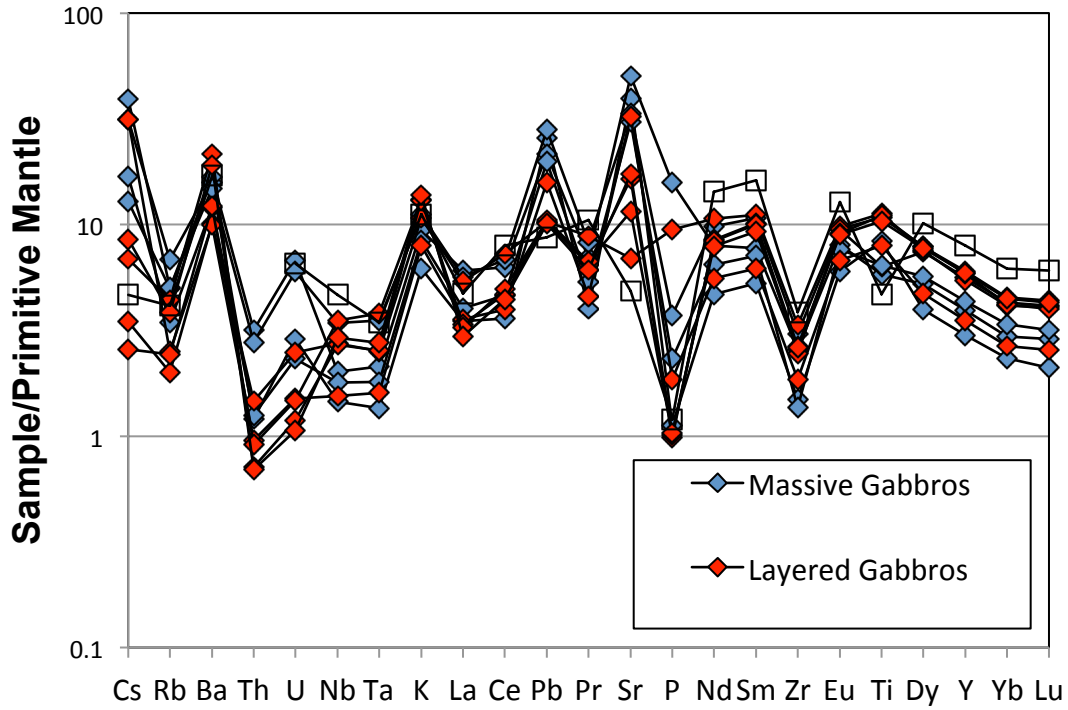

Figure 13. Trace element normalization diagram for Riddle Peak gabbro, plotted with one representative Riddle Peaks amphibole composition for comparison. Normalization is to primitive mantle from Sun and McDonough (1989).

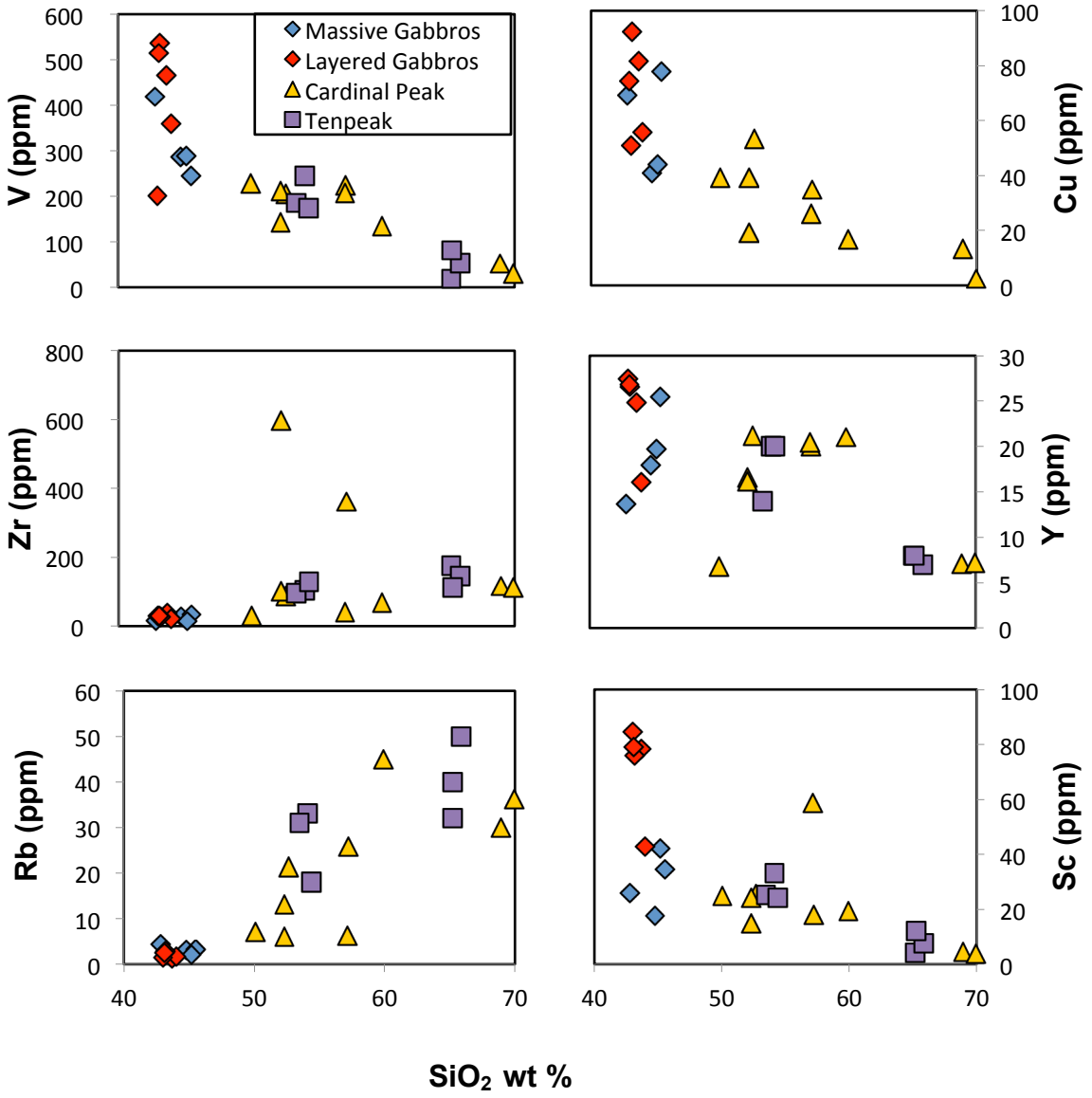

Figure 14. Selected whole rock trace elements for Riddle Peaks gabbro and nearby tonalitic plutons plotted against wt.% SiO_2. Data for the Cardinal Peak pluton is from McCrady (2013) and the Tenpeak pluton is from Miller et al (submitted manuscript). Error bars are smaller than the symbol. See methods for a full discussion of accuracy and precision.

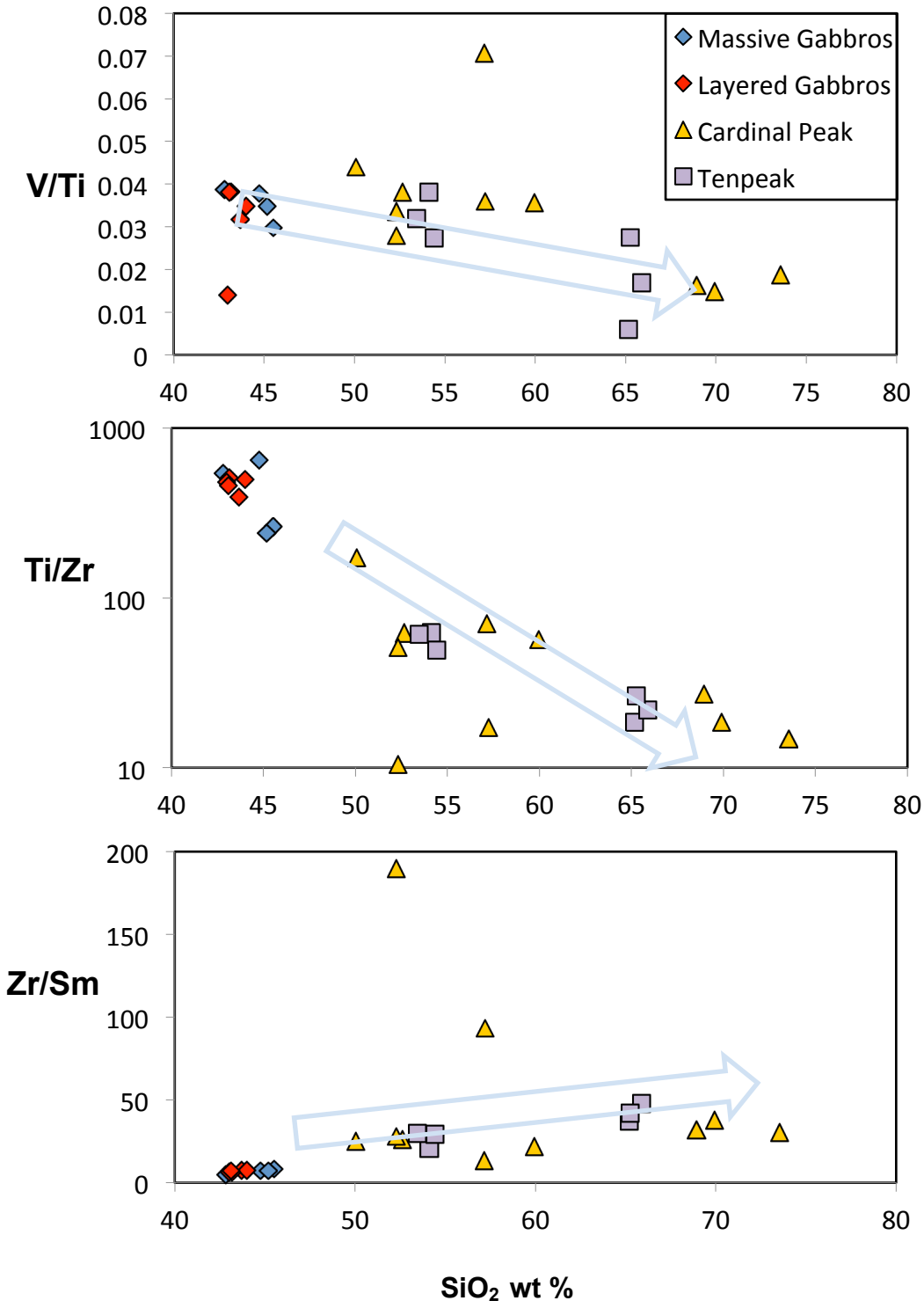

Figure 15. Trace element ratios of Ti/V, Ti/Zr, and Zr/Sm against wt% SiO_2 in the Riddle Peaks plotted with Cardinal Peak and Tenpeak compositions. Arrows denote trends indicative of amphibole fractionation.

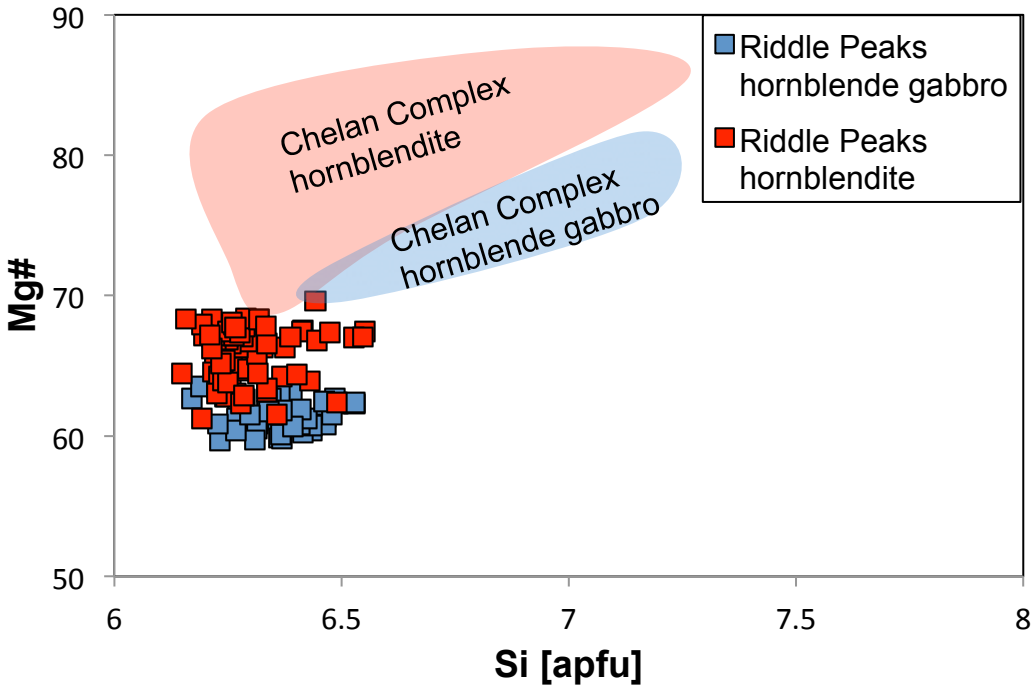

Figure 16. Plot of Mg# versus Si calculated as atoms per formula unit (apfu). Red field represents the range of Mg# versus Si (apfu) for hornblende in the Chelan Complex, while blue represents the range in hornblende gabbro in the Chelan Complex. Note the overlap with hornblende of the Riddle Peaks pluton for each lithology. However the Chelan Complex shows more variation in Si (apfu) at similar Mg#s, indicating that its hornblende experienced more subsolidus reequilibration than those in the Riddle Peaks pluton (Dessimoz et al., 2011).

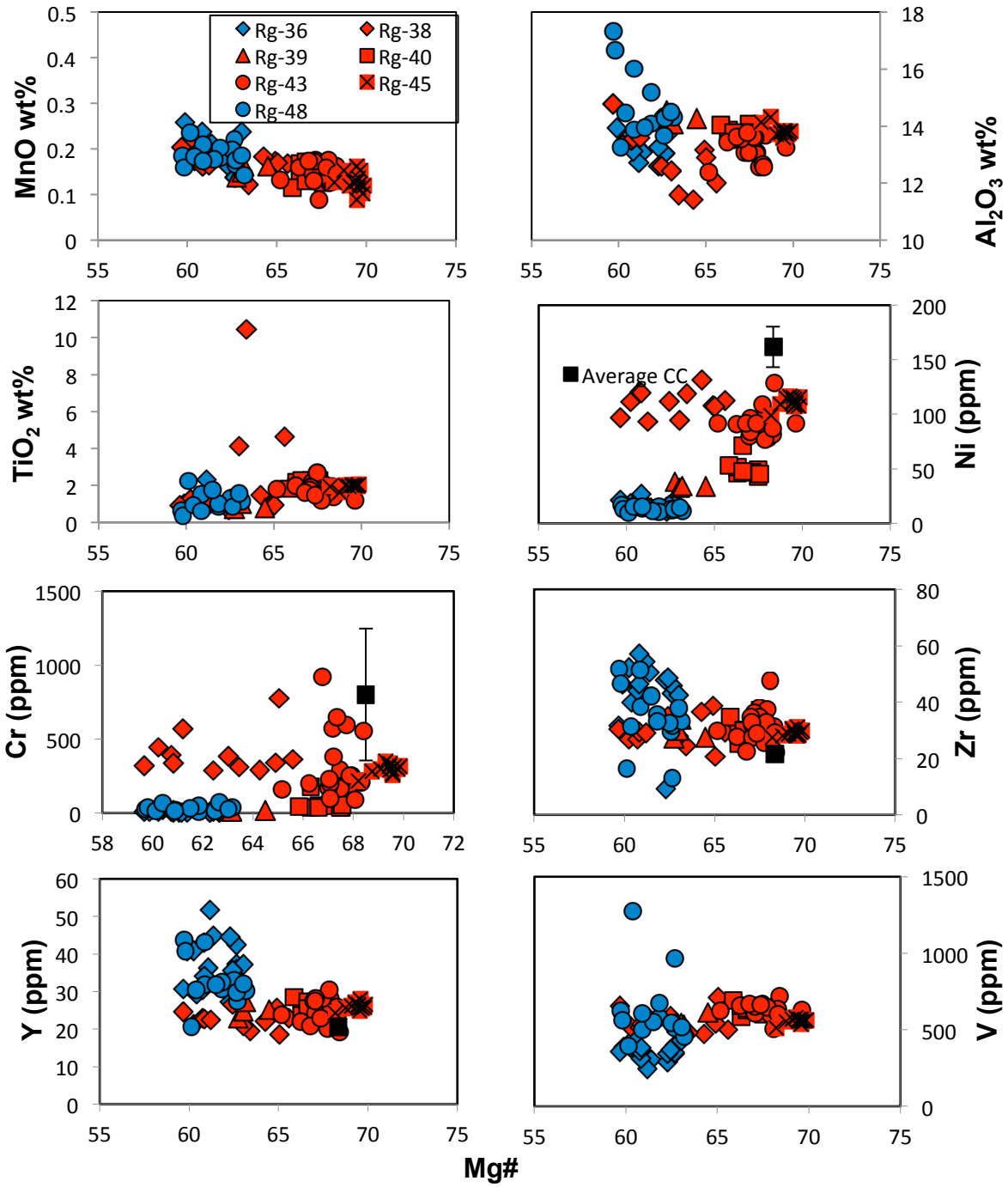

Figure 17. Select element oxides and trace elements in amphiboles plotted against their Mg#s. Amphiboles from layered samples are shown in red symbols, while amphiboles from massive samples are shown in blue symbols. Black symbols are average values (with error bars) for hornblende analyses from hornblendite and hornblende gabbro lithologies in the Chelan Complex (Average CC). Hornblendes from the Chelan Complex have higher Ni and Cr but lower Zr and Y.

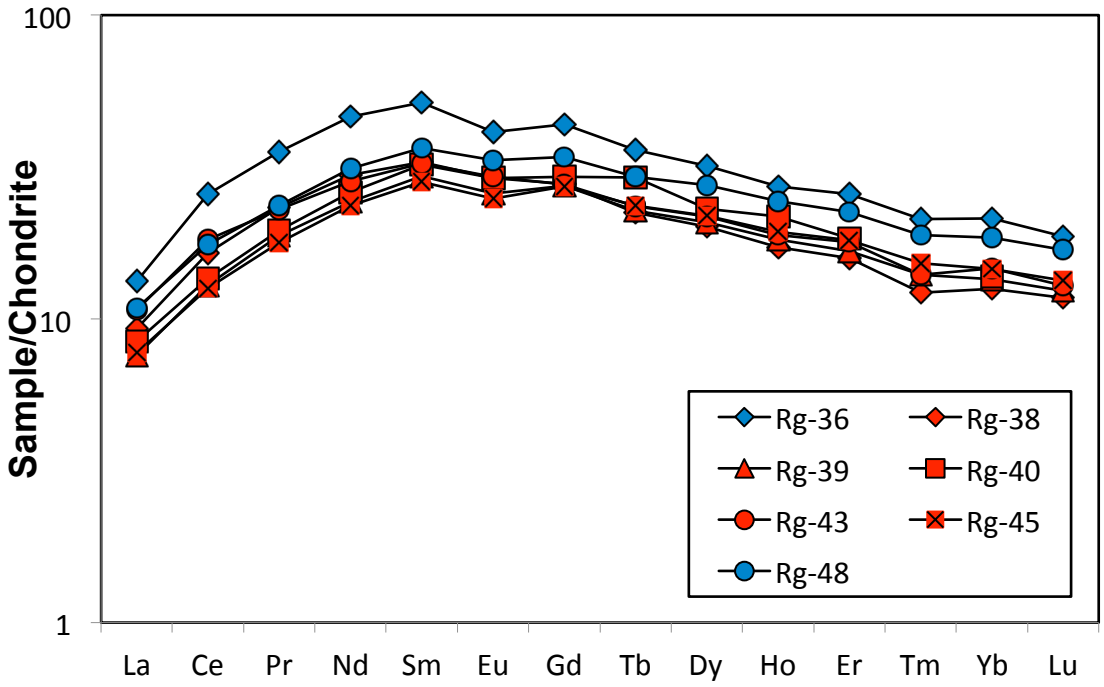

Figure 18. Chondrite-normalized REE graphs of amphibole grains. Amphiboles from layered samples have red symbols and those from massive samples have blue symbols.

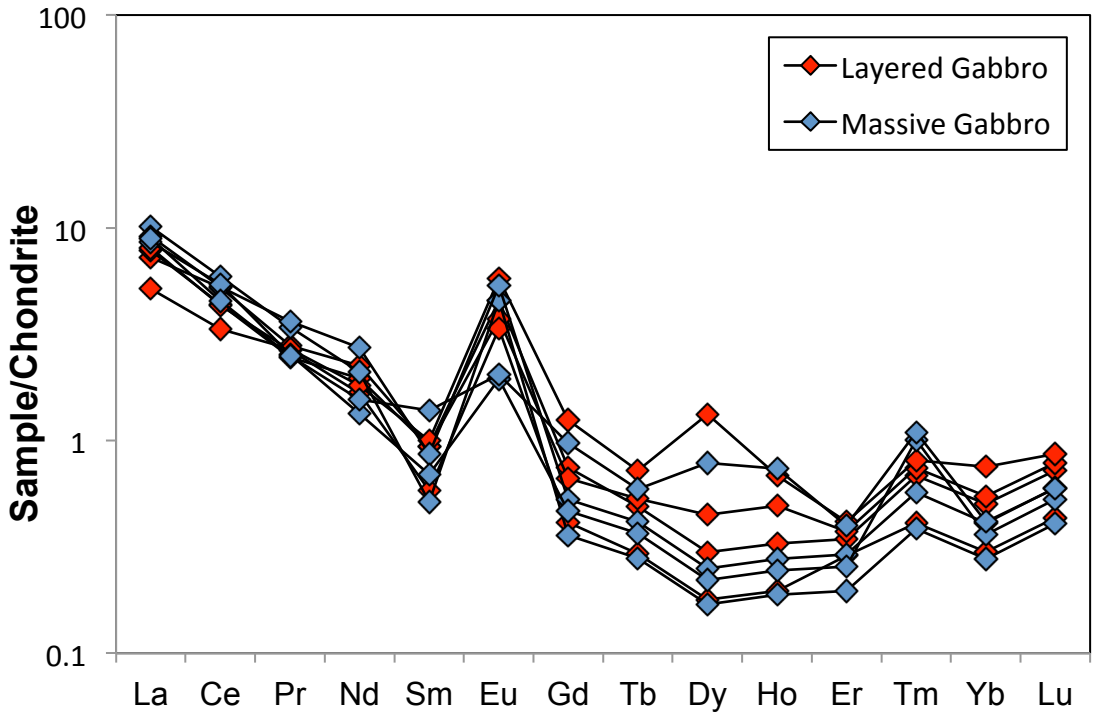

Figure 19. Chondrite-normalized REE concentrations of plagioclase grains showing large positive Eu anomalies.

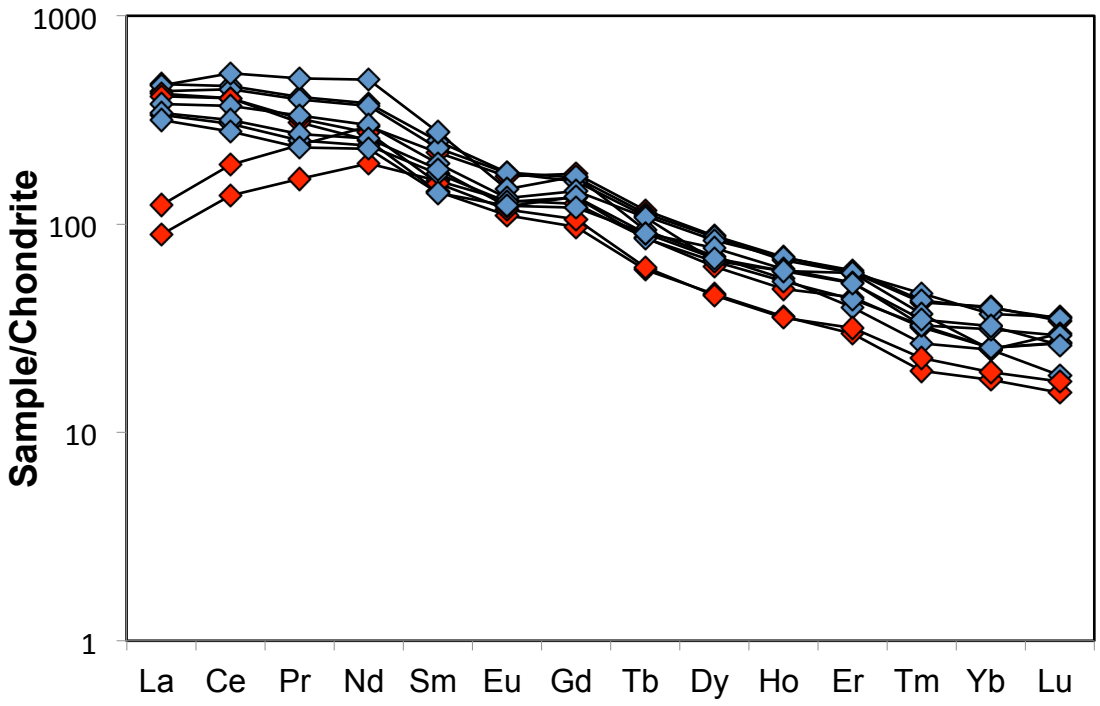

Figure 20. Chondrite-normalized REE concentrations in apatite grains.

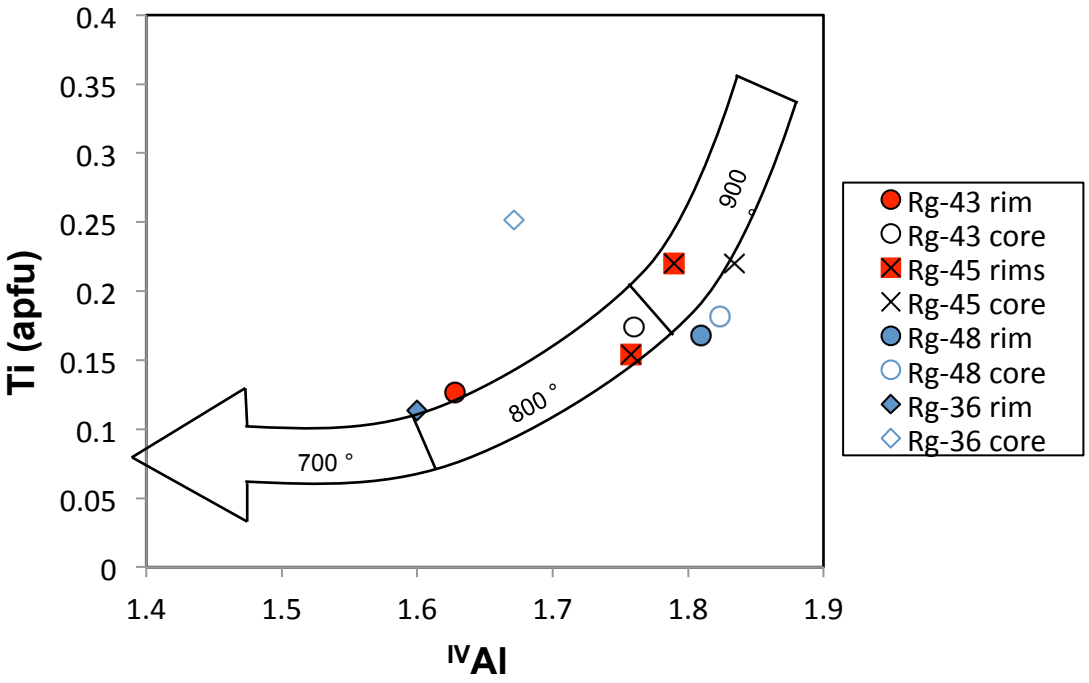

Figure 21. Results of semi-quantitative thermometry, after Ernst and Liu (1998). Where the core and rim of the same grain were measured, cores (open symbols) have higher Ti and tetrahedrally coordinated Al which corresponds to higher temperature, than rims (filled symbols).

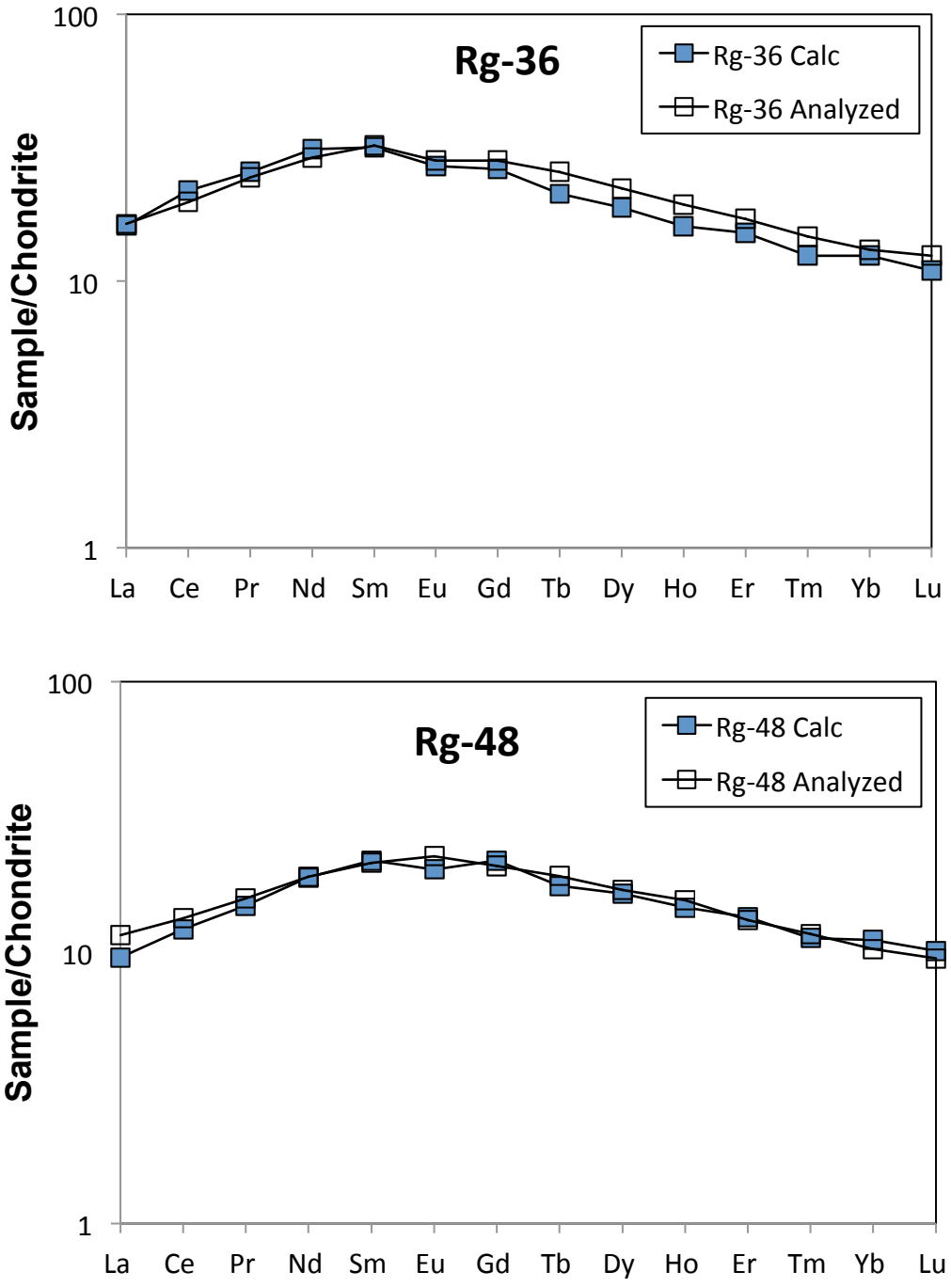

Fig 22. Calculated whole rock cumulate compositions (Calc) compared to whole rock compositions from XRF analyses.

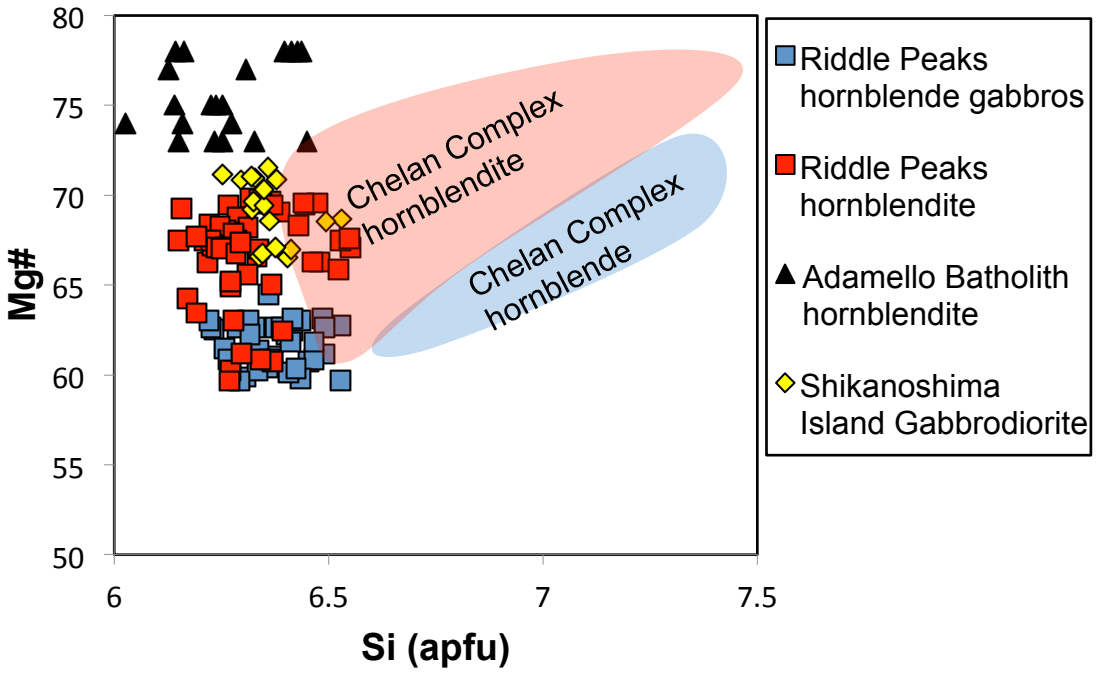

Figure 23. Amphibole Mg#s versus Si (apfu) for the Riddle Peaks pluton and several other plutons that contain amphibole in cumulate rocks (Tiepolo et al., 2011; Tiepolo et al., 2012). The red field is the range of Mg# versus Si (apfu) for the Chelan Complex hornblendite, while the blue field is the range for its hornblende gabbro.

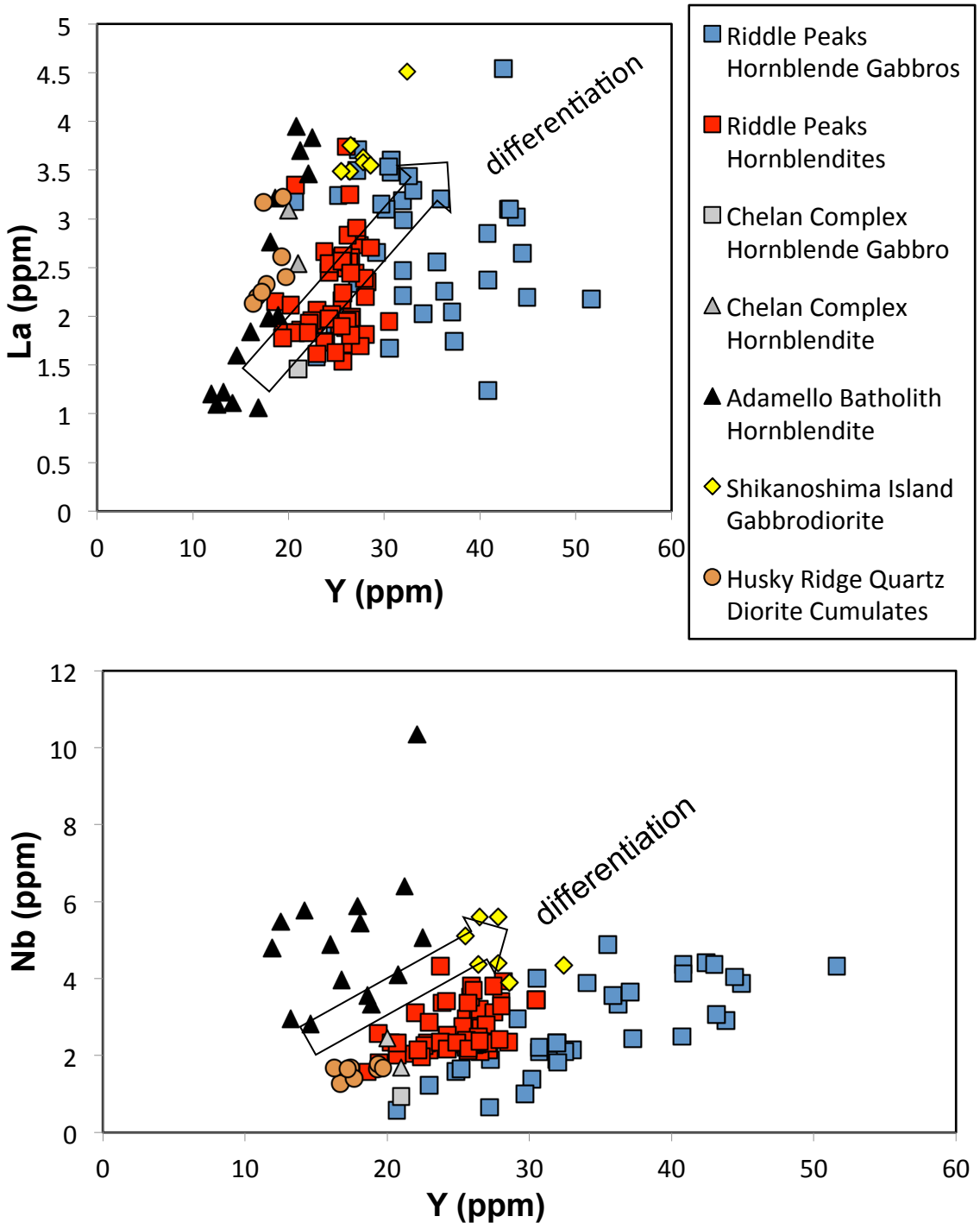

Figure 24. La and Nb versus Y plots for amphiboles in Riddle Peaks' hornblendite/hornblende gabbros compared to amphibole analyses from cumulates from other arc plutons worldwide, which regulate trace elements such as REE and Y in their respective plutonic systems (Tiepolo and Tribuzio, 2008; Tiepolo et al, 2011; Tiepolo et al, 2012).

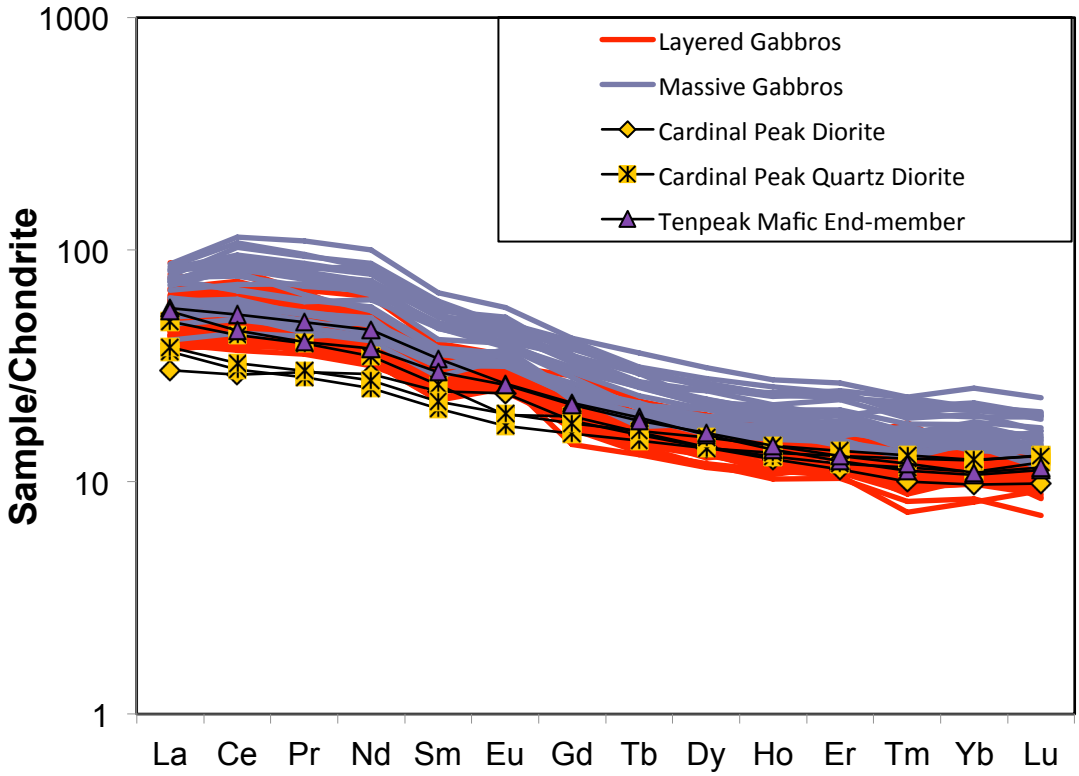

Figure 25. REE patterns for Calculated Equilibrium Liquids from the Riddle Peaks pluton. Also plotted are mafic compositional end-members from the Cardinal Peak pluton (McCrady, 2013), Tenpeak pluton (Miller et al., submitted manuscript) and average continental crust (Rudnick and Gao, 2003)

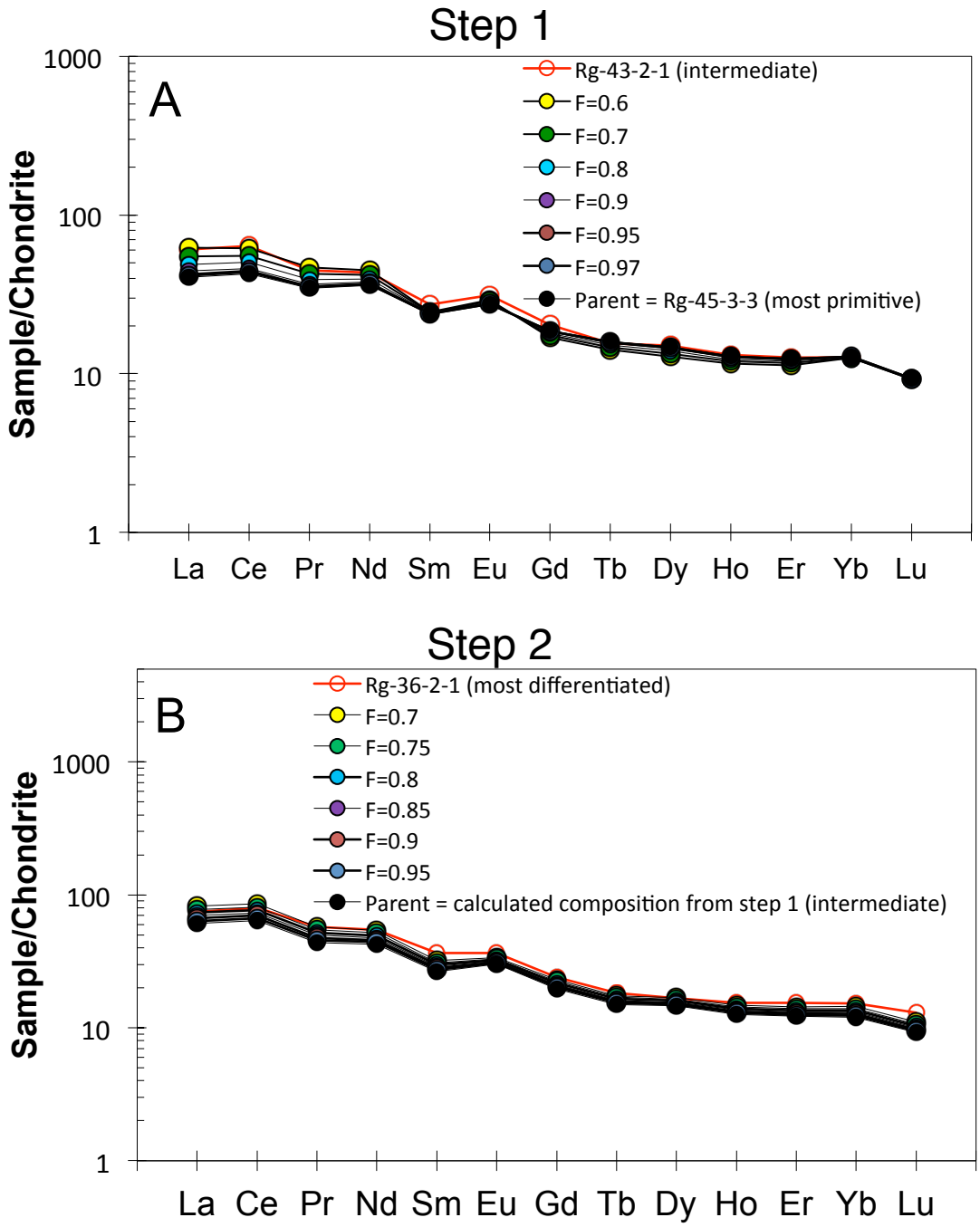

Figure 26. REE models showing concentrations of REEs in the liquid with decreasing liquid fractions. F=1.0 represents 100% liquid (0% fractional crystallization); F=0.80 represents 80% liquid (20% fractional crystallization) and so on. In Step 1, F=1.0 is the starting composition of the most primitive equilibrium liquid. Crystallizing mineral proportions approximate the mineral mode of the hornblendite/hornblende gabbro lithology from the layered part of the pluton. In Step 2, F=1.0 is the calculated result of step 1, which best matched an observed intermediate equilibrium liquid. Crystallizing mineral proportions represent the mode of massive hornblende gabbros in step 2.

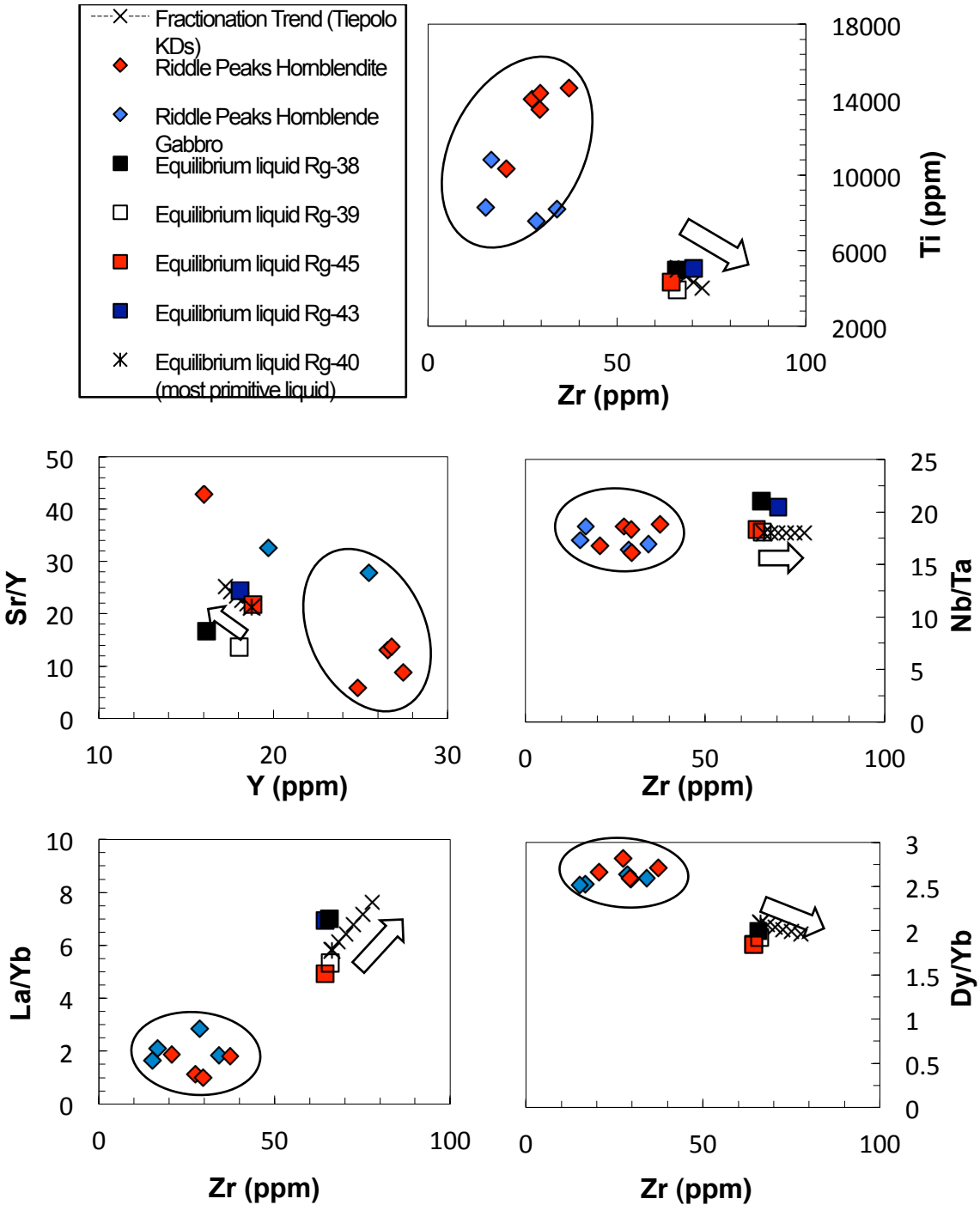

Figure 27. Trace element ratio plots for Ti/Zr, Nb/Ta, Sr/Y, La/Yb, and Dy/Yb starting with the most primitive equilibrium liquid and modeling forward to intermediate compositions using Rayleigh fractionation models for fractional crystallization. The Xs on the trend represent increasing crystallization (decreasing F) of hornblendite, and the open arrow indicates direction of the trend, away from the cumulates. Crystallization is in 5% increments, and only 25% crystallization of hornblendites (to F=0.75) from the parental primitive equilibrium liquid is shown.

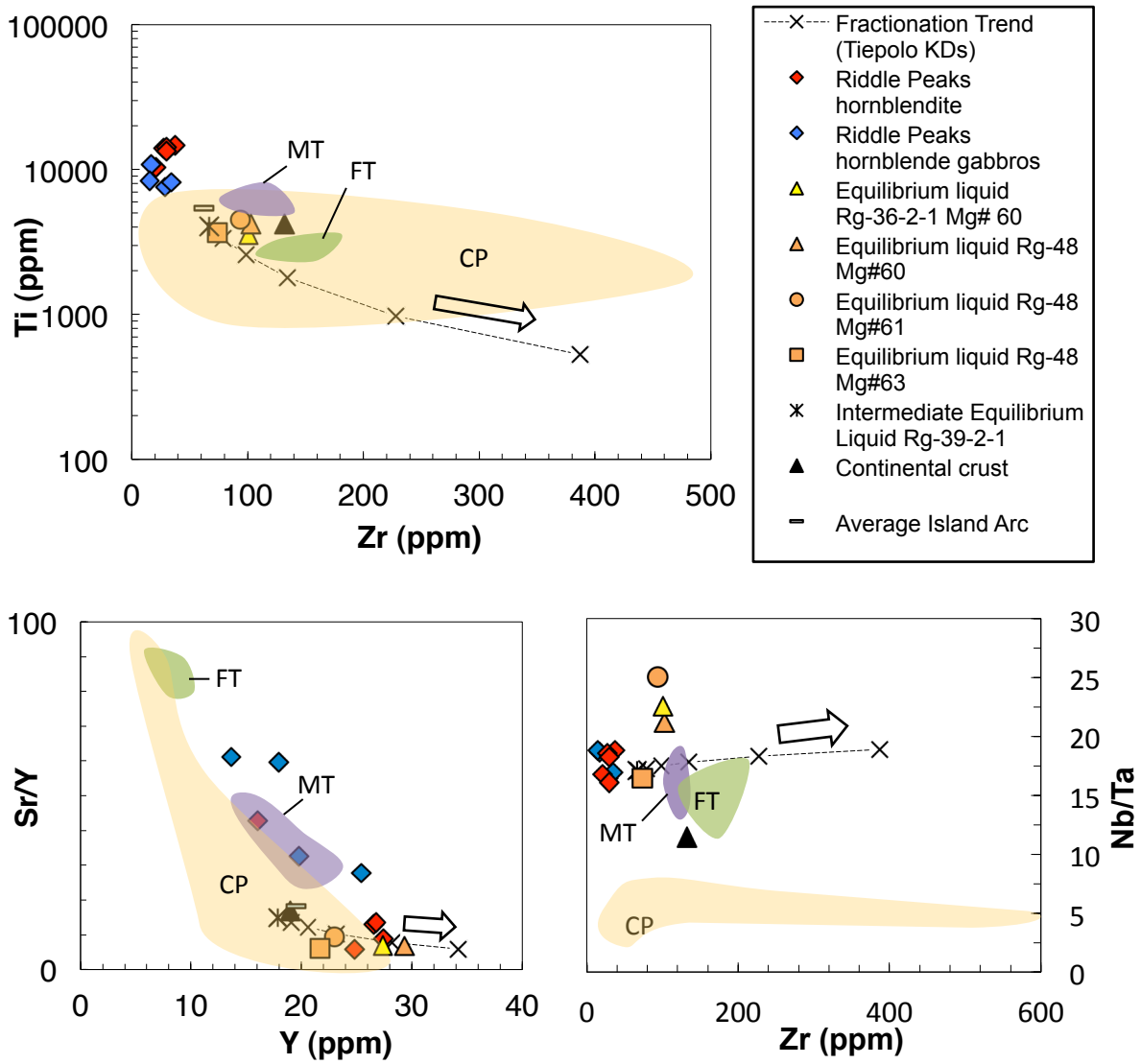

Figure 28. Same as Figure 25, but starting with an intermediate composition and modeling toward the most differentiated compositions using Rayleigh fractionation models. Arrows denote direction of fractionation trend, away from cumulate compositions. The Xs on the trend represent increasing crystallizing proportions (decreasing F, in 20% increments) of hornblende gabbro. 100% crystallization is shown and compared to continental crust (Rudnick and Gao, 2003), liquid compositions from the Cardinal Peak pluton (shown by the gold field labeled CP; McCrady, 2013), mafic (purple field labeled MT) and felsic (green field labeled FT) end-member compositions from the Tenpeak pluton (Miller et al., submitted manuscript).

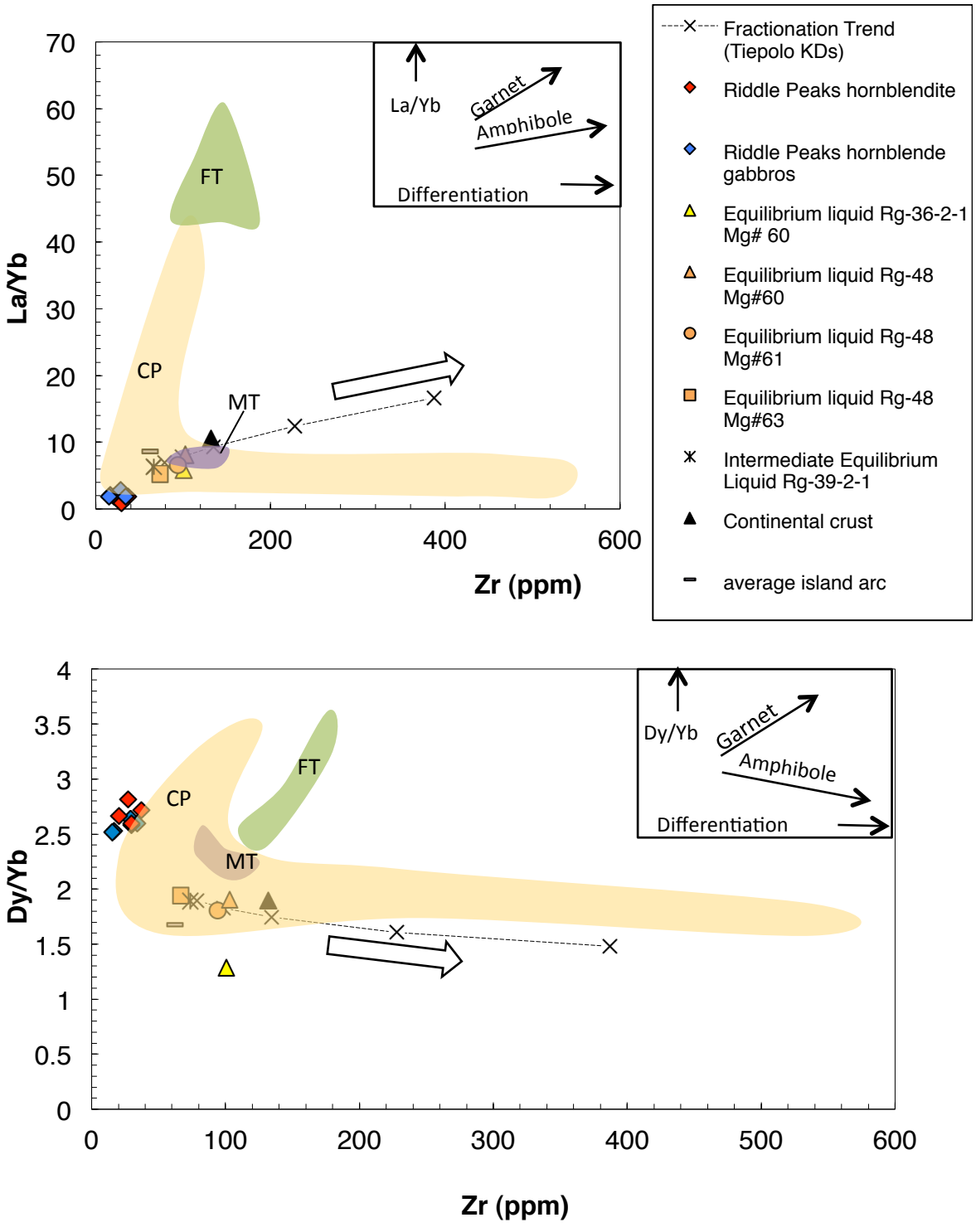

Figure 29. Same as Figure 28, but insets show trends for arc magma differentiation after Davidson et al., 2007.

Appendix A

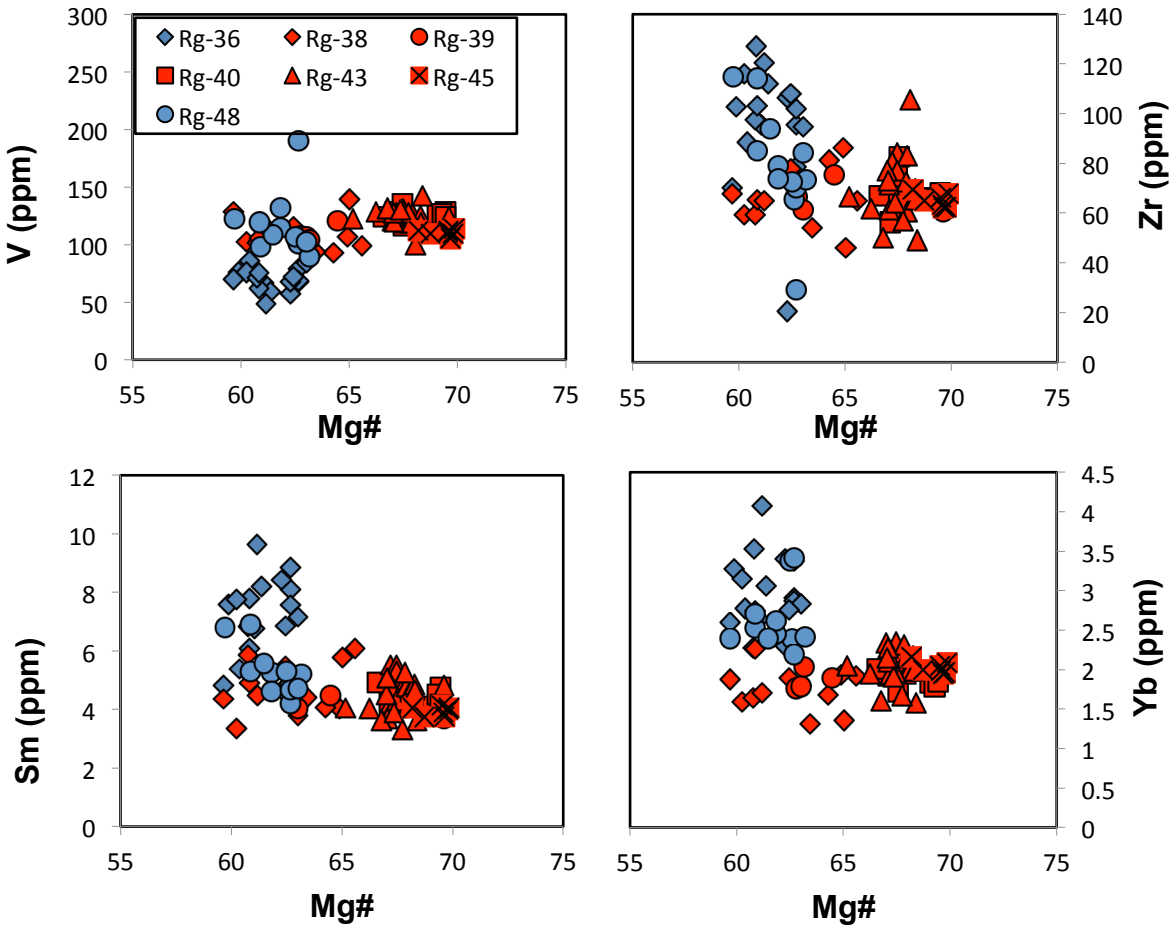

Figure 1. Mg# versus selected trace elements for equilibrium liquids to assess the validity of their magmatic trends for use in trace element ratio modeling. Mg# comes from the amphibole analysis, and trace element concentration is from the same amphibole's corresponding equilibrium liquid calculation. Blue symbols represent massive gabbros; it was determined that sample Rg-48 from the massive gabbro showed a magmatic trend based on variation in trace element concentration with Mg#.